Hordeum erectifolium, a physiological and genomic study of drought-adaptive traits

Dissertation

zur

Erlangung des Doktorgrades (Dr. rer. nat.)

der

Mathematisch-Naturwissenschaftlichen Fakultät

der

Rheinischen Friedrich-Wilhelms-Universität Bonn

vorgelegt von

Einar Baldvin Haraldsson

geboren in

Oregon, USA

Bonn, November, 2024

Angefertigt mit Genehmigung der Mathematisch-Naturwissenschaftlichen Fakultät
der Rheinischen Friedrich-Wilhelms-Universität Bonn

Gutachterin / Betreuerin: Prof. Dr. Maria von Korff Schmising
Gutachter: Prof. Dr. Peter Dörmann

Tag der Promotion: 18. Dezember 2024
Erscheinungsjahr: 2025

Table of contents

1. Summary 1
2. Introduction 2
3. Results 4
Leaf morphology of *H. erectifolium*, cultivated and wild barley 4
Assembly of the *H. erectifolium* genome 5
Raw data: Sequencing and optical mapping 5
Assembly and assembly benchmarking 5
RNA sampling, PacBio IsoSeq sequencing, structural and functional annotation 6
Tissue-and time point specific expression in vegetative and developmental tissues 8
Comparative analysis of *H. erectifolium* genome 8
Transposable element landscape in *H. erectifolium*, cultivated and wild barley 9
Shared and unique orthologs between *H. erectifolium* and across the Poaceae 11
Cross-species transcriptional drought response and recovery 13
4. Discussion 17
H. erectifolium leaf morphology has adapted to a xeric environment 17
Copy number gains in drought, saline, and cold tolerance-related gene families 18
Cross-species transcriptomic responses to drought and recovery 19
Reduced leaf RWC: *H. erectifolium* maintained leaf erectness while Morex wilted 19
Transcriptional effects were detected later and recovered faster in *H. erectifolium* 19
Differentially expressed single-copy orthologs, a direct cross-species comparison 20
The expanded gene families of ELIPs and LEAs show drought-specific expression 21
Conclusions 21
5. Figures 22
6. Materials and methods 43
Leaf transverse cutting and staining 43
H. erectifolium cultivation for DNA and RNA sampling 43
DNA extraction and Oxford Nanopore Technology (ONT) DNA sequencing 43
Germinating seeds and seedling growth for RNAseq 44
RNA sampling, extraction and PacBio IsoSeq sequencing 44
10x Genomics and Illumina sequencing 44
Genome size estimation with jellyfish and findGSE 44
ONT long-read data processing and assembly with Flye 44
Assembly polishing with ONT long-read and Illumina short-read data 45
Scaffolding of the assembled and polished contigs 45
Assembly quality benchmarks 45
PacBio IsoSeq data processing and gene structural annotation 46
lncRNA annotation pipeline 46

Functional gene annotation 46
Representative gene sequence and representative isoform per gene 46
Transposable element annotation with EDTA 47
Estimating telomeric ends and predicting centromeric positions 47
Chromosomal synteny analyzed with SyRI and plotsr 47
Quantitatification of PacBio IsoSeq data and tissue specific expression with IsoQuant 47
Gene family evolution analysis with Orthofinder and CAFE5 48
Annotation of SWEETs and phylogenetic reconstruction 48
Experimental setup for cross-species dry-down experiment 48
Dry-down experiment RNAseq and differential gene expression with maSigPro and edgeR 49
7. Supplemental data 51
8. References 52
9. Abbreviations 68
10. Acknowledgments 70

1. Summary

Drought stresses plants at multiple levels, affecting water uptake, stomatal evaporation, and intracellular stability, which in turn impacts plant fitness and yield. To develop climate-resilient crops, I investigated barley's tertiary gene pool, focusing on the crop wild relative *Hordeum erectifolium*.

First, I explored the transverse cut leaf anatomy of *H. erectifolium*, *H. vulgare cv.* Morex, a modern cultivar and the reference genome, and a wild accession of barley *H. vulgare spontaneum* B1K-04-12. I found anatomical characteristics only in the leaves of *H. erectifolium* which have been described as adaptive to xeric conditions, such as leaf rolling, increased vein and trichome density, and conversion of minor to major veins with increased bundle sheath extensions.

Next, I generated a complete chromosomal scale reference genome of *H. erectifolium* using Oxford Nanopore Technology long-read sequencing, and structural gene annotation was aided by tissue-specific PacBio IsoSeq full-length transcript sequencing. Comparing the three genomes, I investigated chromosomal structural rearrangements and the composition of long terminal repeats (LTR) retrotransposons. I discovered historical genomic signatures and clade-specific insertions of LTR retrotransposons in the genome coinciding with geological periods. One example was an insertion peak seen at ~1.8 Mya of Athila clade LTRs in both barley accessions but not in *H. erectifolium*.

Further, I compared the hierarchical phylogenetic orthologs of seven monocot species and one dicot for genetic signatures for gene gain or loss of abiotic stress-related gene families on the phylogenetic branch of *H. erectifolium*. I uncovered five gene family expansions related to adaptation to drought, saline, and cold tolerance, e.g., EARLY LIGHT-INDUCIBLE PROTEINS (ELIP), OMEGA-6 FATTY ACID DESATURASE, and CASP-LIKE PROTEIN 4.

To study the molecular responses to drought, I investigated the transcriptional response of *H. erectifolium* and Morex during a controlled dry-down drought and recovery experiment in which water was withheld for six days, and on the sixth day plants were rewatered to control levels. Interestingly, leaves of *H. erectifolium* rolled up and maintained erectness, while leaves of Morex wilted. Leaf samples were taken throughout the experiment. Transcriptional changes were detected on the second day of dry-down in Morex but not in *H.* erectifolium. Drought-induced genes in *H. erectifolium* were most at control expression 24 hours after rewatering, while Morex had not yet reached base level of drought-induced genes. During drought stress, *H. erectifolium* showed responses in photosynthesis, reactive oxygen species, detoxification, and various localizations and transport. Morex, on the other hand, was mainly enriched in the biosynthesis of small molecules and proteins. The enriched pathways in *H. erectifolium* hinted at the capacity for drought tolerance.

This work thus demonstrates the potential of *H. erectifolium* as a model species for extensive drought adaptation. It shows the morphological and genetic complexities for adaptations to xeric environments and illustrates how the tertiary gene pool of barley can be used to study anatomical, physiological, and genetic features that can aid in producing stress-resilient crops.

2. Introduction

Barley or *Hordeum vulgare* has followed humans since the beginning of agriculture over 12,000 years ago; it is considered one of the hardier cereal crops and a model for cereal (Dawson et al., 2015; Feuillet et al., 2008; Pourkheirandish & Komatsuda, 2007). Barley is the fourth most important cereal crops, trailing corn, wheat, and rice, with 155 Mt produced in 2022 (*FAOSTAT*, 2024). Over the past 20 years, extreme weather events have rapidly increased in severity and frequency, pushing the limits of crop survival/yield with compounding biotic and abiotic stresses (Lesk et al., 2022; Rezaei et al., 2023). Reduced barley production will have far-reaching and unforeseen multicultural and economic impacts due to the inaccessibility of beer with no adequate replacement (Xie et al., 2018). Due to a rapidly changing climate with increasing extreme events, we are in dire need of novel approaches and shifts to crop adaptation strategies to secure our most important food sources.

Climate change is a strong, multidimensional stressor and has already had a significant impact on plant evolution in only two to three decades and evidence for drought adaptation being a key factor (Franks et al., 2007; Karitter et al., 2024; Rauschkolb et al., 2022). Drought is a highly multifaceted and complex stressor as it touches upon all physiological and metabolic activity. Plants have developed multiple strategies to overcome drought. A first response to drought survival is by "drought escape" with shorter life cycles, via earlier flowering and faster germination; it is an early convergent evolutionary strategy across global plant clades (Groen et al., 2020; Metz et al., 2020; Whiting et al., 2024). In addition to escape, there are avoidance and tolerance, which require more extensive and persistent genetic fixations that change multiple pathways and a plant´s morphology and physiology. A few of the "long-term" strategies include stomatal density and regulation, photosynthesis, source-sink relations, hormonal regulation, root morphology, and osmotic adjustment (Basu et al., 2016).

The "long-term" survival of shorter or longer periods of drought or disadvantageous environments can require genomic restructuring to provide new genetic material for adaptive evolution. Speciation through ecological adaption is the driver of genetic and subsequent physiological changes to a new environment, where a harsher environment and a greater number of stressors accelerate the process (Butlin & Faria, 2024; White et al., 2022). The main driving force of genome evolution in eukaryotes is transposable elements (TEs), which are mobile DNA sequences that are able to replicate and insert themselves at locations across their host genome (Akakpo et al., 2020; Bariah et al., 2020; Senft & Macfarlan, 2021). TEs play a critical role in rapid adaptation and speciation, as generally, TEs are under tight repression, but during periods of high biotic or abiotic stress, they can become active (Deneweth et al., 2022; Sun et al., 2023). Active TEs will move around in the genome and can activate, modulate expression, or silence genes, and they are capable of moving or copying genomic segments with them, and rearrange them as they become active and jump to another location within their host genome (Hassan et al., 2024; Wells & Feschotte, 2020; Yang et al., 2013).

One strategy to battle the adverse and rapid effects of climate change is the use of crop wild relatives (CWR) to provide new genetic material or novel adaptations, which can then be explored within the target crop (Feuillet et al., 2008; Zsögön et al., 2018). Another aspect of modern cereal crops is that all of them are annual species. Annual species have adapted to avoid adverse weather conditions by completing their seed-to-seed life cycle, whereas perennial species have evolved strategies to thrive in their environments and withstand temporary drought or temperature fluctuation. Perennials provide

additional benefits of requiring lower manual labor, pesticide, water, and nutrient input, supporting a more sustainable agriculture (Chapman et al., 2022; Poppenwimer et al., 2023; Zhang et al., 2023).

Here, we explore the potential of *Hordeum erectifolium*, a perennial sister species of the annual crop barley. *H. erectifolium* is one of the younger species to have appeared within the *Hordeum* genus dated at ~1.3 Mya, appearing at the center of a recent speciation burst that followed after the arrival of the *Hordeum* genus in South America (Blattner, 2006; Bothmer et al., 1985, 1995). It is endemic to only a single location in the semiarid Pampas area in Argentina, where it grew among halophytes near a salt lake. The Pampas region is impacted by frequent irregular periods of drought, which can extend up to a year, while most are under three months (Bothmer et al., 1985; Cai et al., 2020; Sgroi et al., 2021). Coinciding with the driest months are the coldest, with a mean temperature of 7 °C (WMO, 2020). Additionally, due to its small distribution area, it is considered a NEAR THREATENED species by IUCN (2024). *H. erectifolium* was described as a unique species owing little resemblance to other *Hordeum* species in South America, with very glaucous erect basal leaves and pubescent on the leaf abaxial side, a thick wax coating, and large suberized silica cells (Bothmer et al., 1985, 1995). Being a perennial species, *H. erectifolium* has had to evolve to persist through long and unpredictable periods of drought. *H. erectifolium* is thus an interesting genetic resource to explore the physiological and genetic underpinnings of stress adaptation in comparison to the closely related cultivated crop barley.

In this study, we aimed to explore morphological, physiological, and genetic differences between the perennial wild crop relative *H. erectifolium* and the annual crop *H. vulgare*. For this purpose, we assembled a complete and annotated reference genome of *H. erectifolium*. We described genomic differences, including structural rearrangements and transposon composition, and explored signatures of gene family evolution potentially underlying differences in stress responses. Furthermore, we characterized the unique leaf anatomy of *H. erectifolium* and physiological and transcriptomic responses to limited water availability and recovery in comparison to *H. vulgare.*

Leaf morphology in *H. erectifolium* has undergone substantial restructuring in relation to *H. vulgare* as a potential adaptation to reduced water availability. We have assembled a near telomere-to-telomere assembly of the genome and its centromeric regions. We generated a gene expression atlas of tissue-specific full-length transcripts, characterized recent insertions of LTR retrotransposons in *H. erectifolium* and *H. vulgare,* and connected their insertion ages to geological events. We found expansions of two groups of desiccation-responsive gene families and three additional expansions of possible targets of adaptations to limited water availability and abiotic stress. *H. erectifolium,* in comparison to *H. vulgare* at the same leaf and soil relative water contents, showed more resistance to mild desiccation and a rapid and strong response of gene regulation during increased stress. Transcriptomic changes returned faster to control levels after rewatering in *H. erectifolium* versus *H. vulgare*. Our results show the potential of *H. erectifolium* as a valuable genetic and physiological resource for drought and abiotic stress adaptations, which could be explored in *H. vulgare* or to generate a new perennial crop species.

3. Results

Leaf morphology of *H. erectifolium*, cultivated and wild barley

H. erectifolium is a perennial sister species to the crop and model grass species *H. vulgare,* and it represents a unique new resource displaying potential adaptive traits to limited water availability. We sought to study the morphological, physiological, and molecular responses to drought in *H. erectifolium* compared to *H. vulgare*. We compared leaf characteristics and responses to reduced water availability for *H. erectifolium* acc. NGB6816 and the barley *H. vulgare* cv. Morex with an average drought resistance (Paul et al., 2023) and a well-annotated genome assembly. For some selected traits, we also included the wild barley *H. v. spontaneum* acc. B1K-04-12 (ecotype from Ein Prat, Israel) (Hübner et al., 2009), putatively adapted to stress-prone environments and with an available genome assembly. We concentrated on differences that were consistently observed between *H. erectifolium* and both the elite cultivated barley variety and wild barley accession.

H. erectifolium has a glaucous appearance of the leaf, and leaves stand erect (Fig. 1A) (Bothmer et al., 1985, 1995). Upon reduced water availability, *H. erectifolium* showed leaf rolling while maintaining an erect leaf structure, whereas leaves of barley lost their leaf structure and wilted (Fig. 1A-C). Leaf rolling is typically supported by specific leaf anatomies such as reduced or lack of bulliform cells that provide structural support to keep the leaf flat (Redmann, 1985). We therefore compared the leaf anatomy of the flag leaf and the first leaf below the flag leaf among *H. erectifolium*, Morex, and wild barley. The leaves of *H. erectifolium* had no bulliform cells, and on the adaxial side, they had a prominent ribbed leaf structure with short and long trichomes (Fig.). In contrast, the leaves of cultivated and wild barley both had a flat leaf surface, reduced trichomes to absent, and showed pronounced bulliform cells (Fig. 1D). We examined further the leaf structure and venation, as a main structural component of leaves are the bundle sheath extensions or sclerenchyma cells and bundle sheath extensions (BSE) is one feature classifying major veins from minor veins (Perico et al., 2022). The total number of veins per mm was ~5.9 in *H. erectifolium* and ~3.5 in barley (Fig. 2A). The cultivated and wild barley had three minor veins interspaced between each major vein, while *H. erectifolium* had on average only one minor vein between major veins but the new "central" major vein appeared sometimes underdeveloped (Fig. 1D). Consequently, the minor/major vein ratio in *H. erectifolium* was significantly reduced compared to barley, ~1.2 vs. ~3.1 (Fig. 2A). Additionally, *H. erectifolium* had a much more extensive sclerenchyma cells overall and on the adaxial side of the veins compared to barley. Sclerenchyma cells are connected with increased photosynthetic activity, water transport, and more rapid stomatal closure in addition to structural support (Jarvis, 2012; Nikolopoulos et al., 2002; Palermo et al., 2023; Sack et al., 2013a). A couple of indicators of investment in leaf growth and photosynthesis are Specific Leaf Area (SLA) and elemental Carbon-to-Nitrogen (C:N) ratio. We found that *H. erectifolium* had significantly lower SLA, 1.5 mm^2/mg, and significantly higher C:N ratio, 13, than cultivated barley, 2.4 vs. 2.2 mm^2/mg and C:N ratio 7 vs. 8, respectively (Fig. 2B, C).

In short, *H. erectifolium* leaves were significantly different in all quantified traits (except width and thickness) (Fig. 2A); it had a three times higher ratio of major veins and twice the number of veins per mm, it had a greater abundance of sclerenchyma cells ab-/adaxial of the vascular bundle than barley and extensive trichomes on the adaxial side.

Assembly of the *H. erectifolium* genome

Due to the unique leaf morphology and response to reduced water availability in *H. erectifolium*, we wanted to explore in more detail the genomic and cross-species transcriptional responses to drought in relation to the cultivated barley representative Morex, as cultivated barley and wild barley presented leaf curling but not rolling in response to drought. To that end, we first created a reference genome for *H. erectifolium*. *H. erectifolium,* like barley, has a large diploid (2n=14) genome, reported with a haploid size of ~4.6 Gbp by flow cytometry, while *H. vulgare* is ~5.2 Gbp (Jakob et al., 2004). Therefore, we assembled the genome of the only available *H. erectifolium* acc. NGB 6816 from Nordgen (Nordic Genetic Resource Center, Sweden).

Raw data: Sequencing and optical mapping

The *H. erectifolium* genome was sequenced on 27 ONT R9.4.1 flowcells, with 24 GridION flowcells sequenced at The Max Planck-Genome-Centre Cologne (MP-GC) (Cologne, Germany) and 3 PromethION flowcells sequenced at the Genomics & Transcriptomics Laboratory, HHU (Düsseldorf, Germany). The raw sequencing signal was then basecalled with Guppy 5.0.7 (ONT) using the Super accuracy model, yielding basecalled reads in a total of 321 Gb, ~72-fold coverage, of Q-score above Q7, with a read N50 of 41,923 and mean read quality score of Q11.7.

The 10x Genomics linked reads were sequenced at Novogene (Beijing, China), yielding 244.6 Gb of raw reads, representing ~55.6-fold coverage of the *H. erectifolium* genome with linked Illumina reads. These reads were used for k-mer analyses of the genome, short-read polishing of the draft genome, consensus-completeness analyses with Merqury (Rhie et al., 2020), and the first round of assembly correction and scaffolding. We also generated 510 Bionano optical maps of *H. erectifolium* (NGB 6816) with an N50 of 20.9 Mbp and a total genome map length of 4.04 Gbp (Hana Šimková, Centre of Plant Structural and Functional Genomics, Olomouc, Czech Republic). In addition, using selfed seeds of the sequenced *H. erectifolium,* we generated Hi-C libraries and sequencing data yielding 328.3 million PE150 Hi-C chromosomal conformation capture reads, a total of 72.2 Gb representing ~16.4-fold coverage. The summary of the raw sequencing data is in Table S1.

Assembly and assembly benchmarking

Initial genome characterization of *H. erectifolium* was made with the linked-read 10x Genomics Illumina sequencing data using k-mer frequency analysis. A 21-mer frequency table was generated with Jellyfish, and then findGSE was used to calculate genome size and repetitive ratio and to estimate heterozygosity (Marçais & Kingsford, 2011; Sun et al., 2018). The haploid genome was calculated at 4.4 Gbp, a repeat ratio of 75 %, and no heterozygosity was observed (Fig. 3A). The calculated genome size was in the range of previously published flow-cytometry data, 2n = 9.49 ±0.05 pg, or ~4.64 Gbp (Jakob et al., 2004).

The draft genome was assembled with Flye using only ONT long-read sequences with ≥Q7; Flye also performed the first ONT long-read polishing step as part of its pipeline (Kolmogorov et al., 2019). The draft genome assembly size was 3.93 Gbp and consisted of 3,170 contigs, with an N50 of 14.1 Mbp and L90 of 302 contigs (Table S2).

Due to the high error rate in ONT long-read sequences, polishing of the draft genome assembly was required. After the first polishing with Flye and following ONT recommendations, the assembly was subsequently polished using Racon followed by polishing with Medaka (ONT), both using only the ONT long-read sequences (Vaser et al., 2017). Lastly, two rounds of polishing with high accuracy short-read Illumina sequences using Hapo-G were performed (Aury & Istace, 2021). Each step incrementally increased the consensus-completeness score of the draft genome; it was estimated by k-mer analysis in Merqury using the Illumina short-read data as k-mer baseline. From the initial draft assembly to the final pseudomolecules, the k-mer completeness and QV estimate score went from 76 % and 21.3 (99.3 % correct) up to 94 % and 34.6 (99.97 % correct), respectively (Rhie et al., 2020) (Table S3).

The polished draft genome was then incrementally scaffolded, starting by correcting for misassembly, and then scaffolded with the ARCS-Tigmint pipeline using 10x Genomics linked-read sequencing data (Jackman et al., 2018). The assembly N50 went from 14.2 Mbp to 26.3 Mbp, and L90 went from 302 to 186 scaffolds. Then, it was further scaffolded using hybrid-scaffolding with Bionano optical mapping, bringing the N50 to 67.7 Mbp and an L90 of 76 scaffolds. Construction of the final pseudomolecules was completed using the TRITEX pipeline and Hi-C chromosomal conformation capture sequencing data (Monat et al., 2019), resulting in 97.7 % of the assembly being anchored into 7 pseudomolecules with 3.85 Gbp, while only 88.6 Mbp in 2,686 contigs remained unanchored. The final completed assembly size was 3.94 Gbp (Fig. 3B, C) (Table S2).

To estimate gene space completeness of the assembled genome, BUSCO was used with the Poales database (poales_odb10), consisting of 4,896 conserved single-copy orthologs (Manni et al., 2021). The genome contained a total of 98.2 % (n = 4,806) complete BUSCOs, thereof 93.4 % (n = 4,572) were single-copy and 4.8 % (n = 234) were duplicated, with 12 fragmented and 78 missing BUSCOs.

In brief, high molecular weight (HMW) DNA was isolated from young leaf tissue of a single plant, and the HMW-DNA was sequenced using long-read Oxford Nanopore Technologies (ONT) and assembled using Flye long-read assembler. This was followed by hybrid polishing first with ONT long-reads and then by short-read Illumina sequences. Scaffolding was done incrementally, first with 10x Genomics data (linked short-read Illumina reads), then hybrid-scaffolding with Bionano optical mapping, and finally brought to pseudomolecules with Hi-C sequencing data.

Taken together, we assembled a chromosomal-scale reference genome of *H. erectifolium* with ONT long-reads after polishing with Illumina short-reads and an average base error rate of 1 error per 3000 bases. The final genome consisted of 3.85 Gbp assigned to 7 pseudomolecules with 88.6 Mbp unassigned contigs.

RNA sampling, PacBio IsoSeq sequencing, structural and functional annotation

To establish a good structural gene annotation, we conducted a comprehensive transcriptome profiling of *H. erectifolium*. We sampled twelve independent tissues over development at two time points during the day, Zeitgeber Time (ZT) 1-3 (MOR) and ZT 13-15 (EVE). The samples included reproductive and vegetative tissues. The vegetative tissue contained three-day-old germinating seeds (GS3, only time point ZT 13-15), whole roots (RO8, 8 days post germination), and whole shoots (LS8, 8 days post germination). The reproductive tissues consisted of pools of developing spikes that

were pooled by their developmental Waddington stage (Waddington et al., 1983), early reproductive stage (ESP, W3.0-4.5), at floral development (MSP, W5.0-6.5), and during rapid spike and floret growth (W7.0-8.0, LSP). In addition, anthers (ANT) and ovules (OVU) were individually dissected at W10.0 and caryopses (CAR, 10 days post anthesis, at time point ZT 1-3). At anthesis, the 3rd nodes (NOD), 4th internodes (INT), and flag leaves (FLF] were collected. The 22 samples were individually barcoded and sequenced with PacBio IsoSeq and Teloprime (Lexogen GmbH, Vienna, Austria) 3'-prime and 5'-prime full-length library preparation. The total sequenced read number was 6,405,982 reads, with reads per sample ranging from 94,465 to 477,754 reads, an average of 291,181 reads per sample. Filtering out reads that did not have both a 3'-prime and a 5'-prime cap primers resulted in 3,645,621 full-length non-chimeric complete reads for annotation and analyses (Table S1).

The filtered reads were mapped to the genome, 861 (0.02 %) reads remained unmapped, and identical redundant transcripts were collapsed with the Isoseq3 pipeline, producing 38,191 unique genes and 191,171 isoforms, and Open Read Frames (ORFs) were predicted with TransDecoder. Given the high-quality transcripts of the IsoSeq dataset, we could explore the presence of lncRNA in the sequenced transcriptome. This yielded 29,099 protein-coding IsoSeq genes with ORFs and 8,993 putative lncRNAs.

Isoforms of a gene captured by IsoSeq sequencing often had alternative transcription start sites (TSSs) and transcription termination sites (TTSs) but identical CDSs. Therefore, we retained only one unique CDS for each isoform per gene, which resulted in 98,238 unique CDSs. Mean gene and isoform CDS lengths were 5,835 bp and 786 bp, respectively. The mean number of isoforms per gene was 3.4, and the mean number of exons per mRNA and CDS was 5.9 and 4.5, respectively. The mean gene length of lncRNA genes was 1,857 bp, and they showed fewer isoforms per gene in comparison with protein-coding genes, 1.8 vs. 3.4, exon length 472 bp vs. 272 bp, and exons per isoform 2.0 vs. 5.9, respectively (Table S4).

As not all genes were captured by sequencing, *de novo* annotation was performed with Helixer, predicting 55,287 protein-coding genes (Holst et al., 2023). However, if a Helixer transcript prediction had the same CDS as IsoSeq but different 3'- and 5'-UTRs (TSS and TTS) lengths, the IsoSeq transcript was kept. A total of 11,327 Helixer predictions were discarded, and only 9,548 genes had further overlapped with Isoseq predictions, which were then merged together as isoforms. For the final gene annotation, we produced 71,475 genes with 157,682 isoforms (210,732 with their UTR variations included) after merging the structural gene annotations from both IsoSeq and Helixer. Thereof, 62,482 were protein-coding genes with 141,631 isoforms, and 8,993 were putative lncRNA genes with 16,051 isoforms (Table S4).

A representative protein-coding isoform per gene was chosen by alignment score to the UniRef90 (2023_02) protein database (The UniProt Consortium et al., 2023); otherwise, if there was no alignment, the longest isoform was chosen. This resulted in a selection of 54,970 representative isoforms by alignment.

Protein-coding genes were classified as high or low confidence based on a similarity threshold of 80 % similarity between a predicted protein and database, Uniref100 (2024_04) (The UniProt Consortium et al., 2023). Accordingly, 45,282 genes and 112,886 isoforms were classified as High-Confidence, and 17,200 genes and 28,745 isoforms as Low-Confidence. Functional annotations of

protein-coding genes were made with InterProScan (Blum et al., 2021; Jones et al., 2014). InterProScan assigned functional or domain annotations to 52,966 genes (39,369 with an InterPro entry). Additional gene names were assigned with SPROT (The UniProt Consortium et al., 2023).

In summary, with the tissue and time point-specific IsoSeq sequencing, we could generate high-accuracy gene predictions with UTR and isoform information, as well as lncRNA predictions. Complemented with *de novo* gene prediction, we had a final set of 71,475 genes and 157,682 isoforms.

Tissue-and time point specific expression in vegetative and developmental tissues

We wanted to explore the characteristics of the tissue, development, and time of day-specific expression IsoSeq dataset that was generated above. To that purpose, we quantified the IsoSeq sample gene expression and defined the trajectories of tissue/developmental/time-of-day profiles. We clustered the IsoSeq expression data of the 22 samples with principal component analyses (PCA) and found that the caryopsis, 10 days post anthesis (CAR) sample explained 53 % of PC1 (Fig. 4A). The variance of vegetative and reproductive tissue was explained along PC2 at 16 %, with roots (RO8), stem nodes (NOD), and anthers (ANT) at the center (Fig. 4 A, B). All sampled morning (MOR, ZT 1-3) and evening (EVE, ZT 13-15) tissue pairs grouped closely together except the morning/evening stem node (NOD), in which the morning stem node (NOD) clustered consistently closer to the developing shoot apical meristem (ESP, MSP, LSP) samples.

We selected the top 20 genes that contributed the most to PC1 and PC2 and found that high expression of multiple Gliadin genes in caryopsis (CAR) caused the high variance in PC1; gliadin is the main storage protein in cereal seeds (Fig. 4A) (Ribeiro et al., 2013). The trajectory of developing shoot apical meristem and ovules was most influenced by TIM23 (Translocase of the Inner Mitochondrial Membrane 23), histones (H2A and H3/CENP-A), and photosynthesis-related genes like CAB (CHLOROPHYLL A-B BINDING PROTEIN) proteins and RuBisCo (RIBULOSE BISPHOSPHATE CARBOXYLASE/OXYGENASE) were associated to the above-ground vegetative tissues (Fig. 4A, B). TIM23 is a mitochondrial preprotein transporter and potential regulator of mitochondrial biogenesis and respiratory demand, which is needed in a rapidly dividing and developing spike (Wang et al., 2012). Histones are at the center of chromatin remodeling and regulation of plant development, growth, and environmental response (Wu et al., 2023; You et al., 2017).

In short, we have obtained a first glance into the tissue/developmental/time-of-day expression profiles, which genes potentially influence a given developmental or time-of-day trajectory, as well as a first insight into tissue and time-specific gene expression.

Comparative analysis of *H. erectifolium* genome

We aimed to further characterize the genome of *H. erectifolium* and compare it to the genomes of the spring barley cultivar Morex and the wild barley accession B1K-04-12. First, we described the chromosome organization and structure by mapping the genic and intergenic space and repeat content and by identifying telomeric sequences, centromere locations, and transposable element (TE) composition. However, we did this with consideration that Morex was assembled with PacBio HiFi long-read sequencing while B1K-04-12 was assembled using short-read Illumina sequences, which

could increase the number of small inversions in comparison with long-read assemblies and impact the TE analysis (Jayakodi et al., 2020). We also established orthogroups across eight Poaceae species along with *Arabidopsis thaliana*, with the purpose of exploring gene families unique to or shared with *H. erectifolium* and gene family expansions or contractions.

Due to their length and high degree of repetitive sequences, assembly through telomeres and centromeres is one of the remaining challenges in gapless genome assemblies (Navrátilová et al., 2022). By aligning the telomeric sequence "TTTAGGGn" to the genomes, we found that telomeric ends had been assembled in *H. erectifolium* on the short arms on five out of seven chromosomes but not on any of the long arms. However, they were neither found on chromosomes 4H and 5H, nor in barley genome. Centromeres were mapped by aligning the Gypsy long terminal repeats (LTR) CRM sequences, annotated with "The Extensive de novo TE Annotator" (EDTA), to the assembly, as CRMs have been shown to be highly enriched in the centromeric regions (Neumann et al., 2011). Centromeres were located on all chromosomes in *H. erectifolium* (Fig. 5), and the predicted centromeric locations line up with the Hi-C contact map in Fig. 3B. Size estimation of the centromeric space for each chromosome ranged from 20 to 49 Mbp or ~3.8 to 8.5 % of the respective chromosomal length. In the published assembly of Morex, they note that the centromeres were not properly assembled, but they could predict their size with Hi-C sequencing data at ~5 Mbp, while we predicted the *H. erectifolium* centromeres to be four to ten times larger (Mascher et al., 2017, 2021). By using the same method as for centromere prediction in *H. erectifolium*, aligning CRM sequences to the assembly, we could confirm their location but not improve the size prediction of the centromeres as these were not well assembled.

The overall chromosomal synteny between *H. erectifolium*, Morex, and B1K-04-12 was well preserved, but with many structural rearrangements. Most notable was a complete chromosomal inversion of chromosome 3H that spanned 471 Mbp or 81.4 % of the chromosome in *H. erectifolium* and 570 Mbp or 91.7 % in Morex (Fig. 3C). The second largest inversion was found around the centromere of 4H, where the breakpoints spanned a region of 56 Mbp or 10.2 % of the chromosome in *H. erectifolium* and 109 Mbp or 17.9 % in Morex. Between *H. erectifolium* and Morex, there were 59 inversions over 1 Mbp, and 17 over 10 Mbp. Between Morex and B1K-04-12, they were 32 and 1, respectively.

In summary, the short arms of five chromosomes were assembled to their telomeric ends. We were also able to identify centromeric locations and predict their potential sizes in *H. erectifolium*. A near complete chromosomal inversion was found on chromosome 3, and a large centromeric inversion on chromosome 4.

Transposable element landscape in *H. erectifolium*, cultivated and wild barley

The split between *H. erectifolium* and *H. vulgare* happened 9.2 Mya ago, and the last common ancestor of *H. erectifolium* and its sister species *H. stenostachys* was ~1.3 Mya (Brassac & Blattner, 2015). Transposable elements (TE) are considered one of the main drivers of evolution as they can influence genome size variation and structure, silence, activate, or duplicate genes (Bennetzen et al., 2005; Vitte et al., 2007; Wells & Feschotte, 2020). TEs are normally under tight control, but during times of stress, such as drought, cold, or heat, their repression falters, and they become active, often corresponding to geological events (Belyayev et al., 2014). Therefore, we *de novo* annotated TEs in

the newly assembled *H. erectifolium* genome with EDTA (Ou et al., 2019). EDTA reported that in *H. erectifolium,* 85.7 % of the genome was composed of interspersed TE repeats, thereof 68.2 % were LTR retrotransposons, with more abundant Gypsy LTR superfamily at 20.1 %, Copia at 11.5 %, and the remaining 37.6 % were classified as unknown LTRs (either Copia or Gypsy). The remaining major groups of nonLTRs were Terminal Inverted Repeats (TIRs) at 11.3 % and nonTIR (Helitron) at 5.3 %. We wanted to further explore differentiation in the TE landscape between *H. erectifolium* and Morex, and B1K-04-12, therefore, we re-annotated the barley genomes using the same pipeline. The total TE base pair coverage ratio per genome was relatively stable at 85.7 %, 87.5 %, and 86.9 % for *H. erectifolium*, Morex, and B1K-04-12, respectively. Other enriched transposons in *H. erectifolium* were TIR-CACTA elements, which represented 7.2 % of the overall repeats, while in Morex and B1K-04-12, they were 1.3 % and 2.2 %, respectively (Table S5).

The insertion times of intact LTRs were calculated using the nucleotide substitution rate in rice, $1.3x10^{-8}$, to assess TE insertion age and utilize them as an indicator of their activation time (Ma and Bennetzen, 2004; Ou and Jiang, 2018). We found two pronounced peaks of Gypsy element insertions at ~0.5 Mya in *H. erectifolium* and at ~1.8 Mya in Morex and B1K-04-12, while there was a concurrent insertion of Copia elements in all three accessions during the Chibanian period ~0.5 Mya (Fig. 6A); this period saw an increase in the magnitude and asynchronicity of global glacial cycles (Sun et al, 2021). The burst of TE insertions was occurring concurrently with the end of Gelasian and the start of the Calabrian period at 1.8 Mya and was first marked by northern glacial expansion and later oceanic events in the Mediterranean (Cita et al., 2012; Gibbard et al., 2010). While the total TE amount was consistent between genomes, there was variation in the number of intact (complete/whole) LTRs by clade (Fig. 6B). Three LTR clades contributed the most to the composition in each genome; in *H. erectifolium,* Retand (39 %), Angela (23 %), Tekay (15 %), and SIRE (8 %) representing 85 % of all LTRs, while in Morex and B1K-04-12, Angela (39 %, 35 %), Athila (29 %, 35 %), Tekay (10 %, 8 %), and SIRE (7 %, 9 %) representing 85 % and 87 % of all LTRs, respectively.

Interestingly, the insertions of Copia LTRs at ~0.5 Mya in all three genomes were driven mainly by Angela and, to a minor extent, SIRE, while additional insertions of Tekay in *H. erectifolium* contributed to a sharper peak of LTR insertions at 0.5 Mya (Fig. 6C). The insertion time peak at ~1.8 Mya was due to the clades Retand in *H. erectifolium* and Athila in Morex and B1K-04-12, respectively. Insertion times of Copia and Gypsy were normalized to the oldest insertion found at ~6.4 Mya and a heatmap corresponding to the age of insertion along the chromosomes, <0.6 Mya (red) and >0.6 Mya (blue) (Fig. 6D). While new insertions of Copia elements were more frequent towards chromosomal ends in all genomes, they were also found across the entire chromosome, and in *H. erectifolium* there was as well extensive insertion of Gypsy elements with the same pattern. There were recent, ≤0.6 Mya, but minimal insertions of Gypsy elements towards the chromosomal ends in Morex and B1K-04-12.

In short, TEs have contributed to genome evolution/structure between these accessions. Even though the total nucleotide ratio was similar at 85.7 % to 86.9 %, the species had unique LTR profiles. The two major bursts of LTRs in the *Hordeum* genus at ~0.5 and ~1.8 Mya correspond to major climatic transitions, the more recent during Chibanian and the older seen only in barley during the transition of Gelasian to the Calabrian period. For example, the Copia element Angela became active in both species ~0.5 Mya while separated over 9.2 Mya and separated by the Atlantic on different continents. Whereas Gypsy elements Tekay and Retand had a peak of insertions at similar times, ~0.5 Mya, in

H. erectifolium, Athila had a burst of activity around ~1.8 Mya in *H. vulgare* coinciding with geological events in the Mediterranean at the start of Calabrian.

Shared and unique orthologs between *H. erectifolium* and across the Poaceae

We wanted to identify shared and unique orthogroups for *H. erectifolium* genes across the Poaceae family. Therefore, we selected six monocots and one eudicot in addition to *H. erectifolium*. The species selected were *Arabidopsis thaliana, Sorghum bicolor (Panicoideae), Zea mays (Panicoideae), Oryza sativa (Oryzeae), Brachypodium distachyon (Brachypodieae), Triticum aestivum (Triticeae),* and *Hordeum vulgare cv.* Morex *(Triticeae)*. We also added the proteome of *H. v. spontaneum acc.* B1K-04-12 *(Triticeae)* to the orthogroups analysis with Orthofinder (Emms & Kelly, 2019). *A. thaliana* was selected as an outgroup species, and the wheat (*T. aestivum*) genome was divided into its A, B, and D subgenomes and unassigned contigs. We identified a total of 38,313 phylogenetic hierarchical orthogroups (HOGs). There were 9,564 HOGs shared between all eight species, thereof 3,656 HOGs shared within *Poaceae* but not within *A. thaliana,* and 1,495 HOGs were unique to *H. erectifolium*. (Fig. 7). HOGs exclusive to *H. erectifolium* were enriched for genes with biological process (GO) functions in post-transcriptional modification of RNA, such as methylation and ncRNA/rRNA processing, icosanoid transport, cell redox homeostasis and peptide signaling.

We further analyzed the HOGs for gene family expansion/contraction with CAFE5 (Mendes et al., 2021). CAFE5 tested a total of 11,851 gene families and reported 558 gene family expansions/contractions, $p < 0.05$, thereof 125 expansions and 13 contractions branch-specific for *H. erectifolium* (Table S7). Of those, we focused on families with putative functions in abiotic stress resistances, where we found six gene families that had undergone expansions in *H. erectifolium*.

The first family contained a HOG of early light-inducible proteins (ELIPs) (N0.HOG0000126), where *H. erectifolium* had 25 copies while barley had 18-20 ELIPs. This was caused by an extension of tandem duplications on chromosome 5, with 18 copies in *H. erectifolium,* while 11-12 tandem copies in barley. Expanded tandem repeat arrays of ELIPs have been identified as a sign of desiccation tolerant plants, where their rapid expression protects against photooxidative damage during dehydration (Marks et al., 2024; VanBuren et al., 2019; Zhuo et al., 2013).

A second expansion of desiccation-related gene families was late embryogenesis abundant (LEA) proteins, LEA_1, (N0.HOG0001297); here, *H. erectifolium* had eight copies on chromosome 7 while barley had two to four. LEA proteins are intrinsically disordered and highly hydrophilic; in simple terms, they substitute water molecules to stabilize proteins and membranes during drying (Candat et al., 2014; Garay-Arroyo et al., 2000; Hand et al., 2011).

The third expansion of note was Casparian strip membrane protein (CASP), (N0.HOG0001008), namely CASP-like protein 4, where *H. erectifolium* had 12 homologues, In contrast, other species had two to three copies except for the *Panicoideae* subfamily, for example, maize and sorghum had five to six copies. This increase in *H. erectifolium* was gained by ten tandem duplicated copies of CASPs on chromosome 2. CASPs are part of the Casparian strip formation, which is a tight water and nutrient diffusion barrier in roots, which impacts root morphology, helping in adaption to drought and salt stress (Grünhofer et al., 2021; Kreszies et al., 2020; Naseer et al., 2012; Roppolo et al., 2014).

The fourth gene family belonged to fatty acid desaturase (FAD2) (delta-12/delta-15 fatty acid desaturase), (N0.HOG0001457), and had seven copies, whereas other genomes had one to four copies. FAD2 converts the monounsaturated oleic acid (18:1) to the polyunsaturated linoleic acid (18:2) and has been shown to contribute to cold and salt stress by increasing cell membrane integrity (Dar et al., 2017; Nguyen et al., 2019; Zhang et al., 2012).

The fifth expansion was of the zinc/iron transport family (ZIP) (N0.HOG0002647); here, *H. erectifolium* had a total of seven copies, four copies on chromosomes 2H and three copies on 7H, while all other genomes had a maximum of three copies. Other species of the *Triticeae* had no copies on chromosome 7H. The ZIP family are transmembrane transporters, providing uptake and maintaining homeostasis of Zn, Fe, Mn, Cu, and Cd; these are essential micronutrients but toxic in excess except for the nonessential toxic heavy metal Cd (Li et al., 2022; Milner et al., 2013; Song et al., 2019; Zheng et al., 2018).

The sixth and final expanded gene family were two expansions in the Sugars Will Eventually be Exported Transporters (SWEET) gene family; each of the two HOGs contained ten SWEET genes in *H. erectifolium* while most other species had four to six copies, and wheat had 16 on the B genome. The two SWEET groups were composed of HvSWEET5 (4), HvSWEET6a,b (5), and HvSWEET7a (1), indicted numbers in brackets are for number of homologes in the HOG the belonged to *H. erectifolium.* Cultivated and wild barley had only one of each orthologe, (N0.HOG0000496), while the other HOG contained HvSWEET14a,b (6) and HvSWEET13a,b (4), (N0.HOG0000585). However, wheat contains a combined HvSWEET14a,b (12) and HvSWEET13a,b (10) in the same HOGs (Table S7).

The SWEET family is involved in diverse functions within plants, such as source-to-sink sugar transport, pathogen defense, and abiotic stress resistance, for example, mobilization of sugar during water scarcity can maintain osmotic pressure (Q. Chen et al., 2022). SWEET13 and SWEET14 have been described as important to pollen viability in *A. thaliana*, to lower accumulation of cadmium in wheat through increased root lignification thus more efficient phloem loading of sucrose in C4 grasses (Gautam et al., 2019; Isoda et al., 2022; Liu et al., 2022). We searched for additional genes annotated as belonging to the SWEET family and found, for example, in total 37 in *H. erectifolium*, 100 in wheat within three subgenomes, and 23 in barley cv. Morex (Fig. 8).

We additionally explored if any of the 37 annotated SWEETs were tissue-specific in *H. erectifolium*. We analyzed the 22 PacBio IsoSeq samples, 12 individual tissues with 10 tissues sampled both in the morning (MOR, ZT 1-3) and evening (EVE, ZT 13-15) (Fig. 9). There, we found HvSWEET4 (Herectifolium_NGB6816_ONT-6HG53985) ubiquitously expressed in every sample, in agreement with previous published data on HvSWEET4 in barley (Yue et al., 2023). We found a homologue of HvSWEET3 (Herectifolium_NGB6816_ONT-3HG9439) and of HvSWEET5 (Herectifolium_NGB6816_ONT-1HG46935) were only found in the shoot apical meristems (ESP, MSP, LSP) and anthers (ANT). Of the tandem duplicated HvSWEET13b in *H. erectifolium,* it appears to have undergone neofunctionalization as they showed differential tissue-specific expressions, for example, one copy of HvSWEET13b (Herectifolium_NGB6816_ONT-6HG56972) was only expressed in the flag leaf (FLF). Another homologue of HvSWEET7a (Herectifolium_NGB6816_ONT-7HG38920) was only found in vegetative tissues during evenings (EVE) but found in reproductive tissue during both morning (MOR) and evening (EVE).

In summary, we found a set of genes unique to *H. erectifolium* with an enrichment of terms associated with post-transcriptional modification of RNA, plant signaling, and cell redox homeostasis. Further,we found expansions of genes related to abiotic stress adaption. These were duplications of CASP genes, which regulate the formation of the Casparian strip, expansions of desiccation-related gene families ELIPs and LEA, and an expansion of FAD2 with connections of salt and cold adaptation. Lastly, we found expansions/retention of two subclades of SWEET-related genes.

Cross-species transcriptional drought response and recovery

Since *H. erectifolium* exhibited different morphological responses to drought compared to barley, we further explored (physiological) and transcriptional responses to drought in *H. erectifolium* compared to Morex. We wanted to explore similarities and differences in the transcriptional responses to drought between *H. erectifolium* and barley, *cv.* Morex. For that purpose, we set up a dry-down drought and recovery experiment. We established a growth assay to account for the different growth and developmental rates of both species at the vegetative stage when they have developed a comparable amount of biomass. With this approach, we wanted to ensure that the reduction in leaf relative water content (RWC) was comparable between plants of the two species during the dry-down assay. Soil field capacity (FC) was adjusted to 50 % before withholding water for six days for the dry-down treatment, while control plants were maintained at 50 % soil FC. On the sixth day of treatment (DOT6), drought-treated plants were re-watered to 50 % soil FC. Replicate samples were collected from both control and drought treatments at three time points during dry-down on DOT 2, 5, and 6, and the final sample was taken on DOT 7, 24 hours after re-watering. At each time point, four replicate samples were collected from the second leaf at ZT 8 for transcriptomic analyses per treatment consisting of a pool of two plants per sample.

During dry-down, both leaf RWC and soil FC decreased at comparable rates for both species with no significant differences between plants of species at each respective DOT (Fig. 10A). On the last day of dry-down, DOT6, average leaf RWC and soil FC for *H. erectifolium* were at 42 % ± 9 and 11 % ± 2, and for Morex at 51 % ± 9, and 13 % ± 0.6, respectively. Strong phenotypic differences at DOT5 were observed; leaves of *H. erectifolium* had rolled inward and remained erect, whereas the leaves of Morex had wilted and needed to be supported by sticks throughout the experiment (Fig. 10C, D). Both species recovered leaf turgor and the leaf RWC was back to control level, and regained leaf structure 24 hours after re-watering on DOT7. No visible symptoms of senescence, i.e., no visible yellowing of leaves, were observed at DOT7 nor seven days after re-watering, DOT13.

In total, 64 samples were collected and sequenced with an average count of 21 million paired-end (PE150) reads per sample. The RNAseq data of *H. erectifolium* was mapped to the genome generated in this study, and the RNAseq data of Morex was mapped to the Morex V3 reference (Mascher et al., 2021). Mapping rates for both genomes had the same percentage,89 % of uniquely mapped and 7.7 % of unmapped reads due to being too short. Mapped RNAseq reads were then quantified with featureCounts and their respective gene annotations, resulting in 85 % and 91 % being assigned to an annotated gene in *H. erectifolium* and Morex, respectively.

We applied two approaches for the identification and characterization of the transcriptomic changes in response to drought. For the temporal analysis, taking into account time, day of sampling, and treatment variables, we used maSigPro, which generated a regression model for each gene using the

global gene expression profiles. Then, differentially expressed genes (DEGs) were selected by a threshold of an $R^2 >= 0.7$ fit to the regression model (Nueda et al., 2014). This allowed us to identify differentially expressed genes (DEGs) regulated by reduced water availability during the experiment while considering the different DOTs as dependent variables.

Because the regression model only identified DEGs for transcripts that were expressed over several DOTs, we also conducted pairwise expression at each DOT between control and drought in both species to identify transient DEGs that were only expressed at a specific DOT. We thus retained all the DEGs from maSigPro and captured the transiently expressed genes with edgeR, which had an FDR < 0.01 at a specific DOT. The edgeR analysis also provided logFC and information on up- and downregulation. With this approach, we identified 15,036 DEGs in *H. erectifolium* and 13,119 DEGs in Morex. However, no DEGs were detected in *H. erectifolium* at DOT2, whereas 261 were detected in Morex.

In *H. erectifolium*, 7,562 (50 %) of the DEGs overlapped with the DEGs identified with the regression model, and 7,095 DEGs were specifically identified with the pairwise expression analysis. No DEGs were detected at DOT2. The majority of DEGs (7,095) were only detected in the pairwise analysis and were specifically up or downregulated at DOT5 and 6 (5,600), or at DOT7 (1,116) in the drought treatment. The transient DEGs at DOT5 and 6 were enriched for photosynthesis and reactive oxygen species metabolism, and DEGs at DOT7 for processes involved in hormone responses, RNA modifications, and reactive oxygen species metabolism (Fig. 11A).

In Morex, 6,948 (55 %) of the transient DEGs overlapped with the DEGs identified with the regression model, and 5,737 DEGs were specifically identified with the pairwise expression analysis. The majority of DEGs (5,737) were only detected in the pairwise analysis and were specifically up or downregulated at DOT5 and 6 (2,813) or at DOT7 (1,861) in the drought treatment. The DEGs at DOT2, 5, and 6 were enriched for cell signaling, upregulation of cyclins, and RNA modification-related pathways. At DOT7 for processes involved in RNA modifications, DNA replication and conformation change were enriched (Fig. 11B).

The maSigPro-identified DEGs were clustered with hclust into nine expression profile clusters using their TMM normalized read counts (CPMs) from edgeR (Y. Chen et al., 2024; Nueda et al., 2014). Overall, we detected 7,941 DEGs in *H. erectifolium* (Fig. 12A), and 7,382 DEGs were identified in Morex (Fig. 12B). We classified the clusters based on their expression profiles before further classifying them by functional enrichment analysis with Clusterprofiler (Fig. 13) (Xu et al., 2024). For each species, we identified nine clusters, which could be summarized into four major patterns: the first group, A (red), included clusters 1 and 2 from both species; these comprised 2,694 DEGs in *H. erectifolium* and 1,690 in Morex and did not show strong expression changes during drought treatment but increased significantly to the control samples at recovery (DOT7) (Fig. 13). The DEGs were enriched in functions related to peptide biosynthesis and translation.

A second group, B (blue), had DEGs downregulated upon drought and returned to control levels on DOT7. They counted 2,353 DEGs involved in photosynthesis and cytokinin signaling in *H. erectifolium*, and 3,396 DEGs involved in peptide transport, organic acid metabolism and photosynthesis in Morex.

The third group, C (violet), had DEGs upregulated during drought, with a peak at DOT6 and drop24 hours after re-watering (DOT7) to control levels or below control. There were 2,446 DEGs involved in intracellular reorganization, transport, response to salicylic acid, polysaccharide metabolism, and protein dephosphorylation in *H. erectifolium*, and 2,758 DEGs involved in peptide organic acid metabolism, intracellular signaling and protein synthesis in Morex.

The fourth and final group, D (black), had only a single cluster. The pattern was down-regulation under drought, but no recovery on DOT7. The 448 DEGs in *H. erectifolium* were only enriched for vesicle-mediated transport, and for the 471 DEGs in Morex, no terms reached the significance threshold in the cluster.

We further looked at the overlap of DEGs which were identified as single copy (SC) orthologs with Orthofinder, totaling 19,049 orthologs between *H. erectifolium* and Morex (Table S8). Of those, there were 8,951 SC DEGs in *H. erectifolium* and 9,319 in Morex; however, only 25 % were shared between both species. Broken further down, there was a higher share of 33 % of SC DEGs that were part of the regression fit while only 15 % shared with the transiently expressed DEGs.

From the SC orthologs identified by time series regression fit, we found common functional enrichments of amide and small molecule biosynthesis, carboxylic acid metabolism, and photosynthesis. No enrichments were found in the transiently expressed SC orthologs overlap. Of the regression fit SC orthologs only in *H. erectifolium,* they were enriched for cellular and protein localization, vesicle-mediated transport and macromolecule catabolism. For Morex, carbohydrate and glucan metabolism, as well as polysaccharide metabolism and biosynthesis were enriched. In the transient SC orthologs, *H. erectifolium* had enrichment in reactive oxygen species (ROS) metabolism, cellular detoxification and response to toxic substances, and response to chemicals. In contrast, Morex only had enrichment in RNA modification-related functions.

We also used the pairwise comparison at each DOT between control and drought in both species to see a general expression profile of the top four most significantly enriched GO terms found by gene set enrichment analyses (GSEA) for each DOT. Aggregating the enriched categories resulted in nine enriched GO terms for both *H. erectifolium* and Morex. The CPMs of RNAseq reads which belonged to genes found in the GSEA analyses were averaged across replicates, and their expression profiles were represented in a heatmap (Fig. 14A, B). The three largest GO term groups were shared between *H. erectifolium* and Morex: translation, RNA modification, and vesicle-mediated transport. However, in these three groups, there was a stark difference between *H. erectifolium* and Morex in up-down regulation transitions from drought stress on DOT5 and DOT6 to recovery on DOT7, 24 hours after re-watering. In *H. erectifolium,* there was a general reversal of the stress-induced up-down regulation of gene expression levels from DOT5 and 6 to DOT7, whereas this transition back to control levels did not take place in in Morex as in *H. erectifolium*.

As there were two expansions of SWEET genes identified in *H. erectifolium*, we explored if any of the annotated SWEETs found in *H. erectifolium* or Morex were differentially expressed. We found that nine out of the 37 in *H. erectifolium* and eight out of 23 in Morex were differentially expressed (Fig. 15B). There were few common patterns of SWEETs expression except for SWEET15a, which was the most notable. It had a shared expression profile in both species, and in *H. erectifolium*, there was an additional expression of a second SWEET15a (Fig. 15C).

We further explored if the expanded gene families of LEA and ELIP were differentially expressed during drought. *H. erectifolium* had two expressed LEA copies in response to drought while Morex had only one (Fig. 15D). Of the expanded ELIPs, there was a rapid and transient expression of 13 out of the 25, homologues of ELIPs in *H. erectifolium*, whereas Morex expressed eight out of the 20 (Fig. 15E). There was a strong upregulation of both LEAs and ELIPs in *H. erectifolium*, starting at zero on DOT2 going up to 12 logFC on DOT5 and 6, and dropping to zero again on DOT7. While LEA expression in Morex had a similar profile, ELIPs had a lower and slower expression where it went from zero to at most three logFC on DOT5 with the highest reaching eight on DOT6 and none reaching zero on DOT7.

Taken together, we were able to control for both leaf and soil water content during the drought experiment and acquired an accurate estimation of cross-species responses to desiccation. *H. erectifolium* had no detectable DEGs at the onset of drought, yet it had more transient DEGs at greater drought stress (DOT5 and DOT6) and went rapidly down after re-watering. Morex appeared to be more sensitive to drought as there were transcriptomic changes at DOT2, and DEGs did not stabilize as rapidly after re-watering on DOT7 as in *H. erectifolium*. Generally, Morex showed fewer DEGs during greater drought stress than *H. erectifolium*. DEG functional enrichment in *H. erectifolium* was more coordinated and responsive than Morex, with a regulation of genes involved in response to stress, cellular localization, photosynthesis and hormone response, and metabolic and biosynthetic processes. However, Morex regulated photosynthesis, intracellular signaling, and cell cycle-related pathways, with many contradictory up-and-downregulated metabolic and biosynthetic processes at the same time. Drought-affected pathways found by regression analyses in *H. erectifolium* had returned to control levels 24 hours after re-watering, whereas in Morex, only half reached control levels. In short, *H. erectifolium* was more resistant to drought onset and showed better coordination of gene expression, with a more rapid recovery after re-watering than Morex at the same soil water availability and leaf relative water content.

4. Discussion

H. erectifolium leaf morphology has adapted to a xeric environment

In this study, we investigated *H. erectifolium,* a perennial congener of the annual barley, *H. vulgare*, as a potential model species for improved survival during limited water availability. We characterized leaf morphological features, created a fully annotated reference genome, and performed a comparative study on the transcriptomic dynamics during reduced soil water availability between *H. erectifolium* and *H. v. cv* Morex. We discovered extensive remodeling in *H. erectifolium* leaves with multiple xeromorphic features, such as leaf rolling, larger bundle sheath extensions (BSE), higher vein density, and abundant trichomes (Haworth & McElwain, 2008; Shields, 1950).

Leaf rolling is a common adaptive strategy among grasses in arid and saline areas, a mechanism to conserve water during reduced water availability, salinity, and high irradiation (Moulia, 2000; O'Toole & Cruz, 1980; Redmann, 1985). *H. erectifolium* rapidly rolls its leaves during water deficit, thereby reducing exposed leaf surface area to evaporation and likely limiting heat and photosynthetic damage from irradiance (Kadioglu & Terzi, 2007). Leaf rolling in rice has been shown to occur before stomatal closure and supports the idea that leaf rolling is mechanistically controlled by turgor pressure (Wang et al., 2023).

The adaxial side of *H. erectifolium* leaves had an extensive ribbed or grooved leaf structure covered with a high density of shorter trichomes and sparser but longer trichomes on top of major veins (Fig. 1B-D). The trichomes could potentially stabilize a microclimate with reduced vapor pressure to ensure stomatal conductance and provide UV protection (Galdon-Armero et al., 2018; Liakoura et al., 1997). The increased density of trichomes and grooved leaf structure could also be involved in water supplementation for *H. erectifolium* by capture of dew or fog (Berry et al., 2019; Hakeem et al., 2021). We also anecdotally observed that as the leaf of *H. erectifolium* develops and extends, the abaxial side appeared to be always turned upwards, and it was also covered in what appears to be a layer of cuticular wax (Bothmer et al., 1985) Both of these traits could be attributed to increased UV protection and water conservation (Lee & Suh, 2015; Xue et al., 2017).

We also observed a more uniform and compact cell structure of the epidermis compared to Morex and the wild barley accession B1K-04-12, which could contribute to a better transpiration barrier and structured cuticular layer (Fig. 1D) (Kasapligil, 1961; Shields, 1950). Bulliform cells and sclerenchymatous structures contribute to leaf rolling, as evidence from reduced bulliform cell size. The altered sclerenchyma structure phenotype mutants in rice and maize have shown, however, both of these mutants presented a fixed rolled-leaf phenotype (Nelson et al., 2002; Sun et al., 2020). *H. erectifolium* has absent or very reduced bulliform cells, yet it could quickly adjust leaf rolling based on water status. This is a very advantageous feature that has been sought after in crops for a very long time, both as a water conservation mechanism during high irradiance, temperate or low soil water availability (Chandra et al., 2022; Shi et al., 2007; Sun et al., 2020; G.-H. Zhang et al., 2009). This makes *H. erectifolium* an interesting target species to understand the underlying structural mechanisms and developmental pathways contributing to leaf rolling.

One of the more surprising findings was the ratio of major-to-minor veins in *H. erectifolium* in comparison to barley, Morex and B1K-04-12, because in *H. erectifolium,* the central of three minor

veins had become a major vein (Fig. 1D). The major veins had, in addition, what appeared to be a greater amount of BSE and sclerenchymatous tissue and increased compartmentalization of mesophyll between BSE. A higher density of BSE has been connected with increased water economy, water use efficiency and a higher rate of photosynthesis (Barbosa et al., 2019; Lynch et al., 2012; Nikolopoulos et al., 2002; Sack et al., 2013a; Sack & Scoffoni, 2013b). Additional features of increased BSE have been reported to be associated with increased light penetration, and BSE-connected stomata was more responsive to changes in water status and humidity than mesophyll-connected stomata (Buckley, 2005; Buckley et al., 2011). Thus, we found that the phenotypic observations in *H. erectifolium* imply the potential of improved water economy, photosynthetic capacity, and protection against high irradiation due to its xeromorphic adaptations.

Any of these physiological features would be a beneficial target to explore to improve barley to reduced water availability and increased photosynthesis. Some would provide long-term survival, but others could help in the shorter term. A first target could be to manipulate venation by increasing density or changing minor veins to major, as many developmental genes, such as Rolled Leaf-Dominant (RL-D), SHALLOT-LIKE1, ROLLED LEAF 9, ROC5 and ROC8, have been identified, and ratio of minor to major veins could be a matter of hormonal or a gene dosage effect (Chandra et al., 2022; Gong et al., 2022; Perico et al., 2022; Sack & Scoffoni, 2013b; Xu et al., 2021; Yan et al., 2008; G.-H. Zhang et al., 2009). Taking all these xeromorphic traits together, we believe that *H. erectifolium* would be well-adapted to water-limited areas. We believe that *H. erectifolium* could be a great candidate for barley crop improvement by studying cross-species drought tolerance and as tentative goal of generating a true leaf-rolling crop phenotype, given the current lack of a fully leaf-rolling crop species.

Copy number gains in drought, saline, and cold tolerance-related gene families

As the morphological changes in *H. erectifolium* were quite extensive, we explored phylogenetic gene gain-loss signatures of adaptations to abiotic stresses in *H. erectifolium.* We uncovered six gene families which had gained a significant number of copies to their respective HOGs on the phylogenetic branch of *H. erectifolium.* To exclude or minimize the effect of gene loss or gain due to breeding, we included the wild barley accession B1K-04-12 in the analyses. Increases in gene copy numbers were associated with adaptation to stresses either through neofunctionalization or for a rapid response to the stressor by increasing the transcriptional strength by having a tandemly duplicated gene (Dassanayake et al., 2011; Wu et al., 2012). The uncovered gene family expansions could all be attributed to the environment in which *H. erectifolium* was found, where unpredictably long droughts can occur, saline soil, and cold but not freezing temperatures in winter occur (Bothmer et al., 1985; Cai et al., 2020).

H. erectifolium gained four copies of FAD2, which enzymatically converts oleic acid (monounsaturated) to linoleic acid (polyunsaturated) and omega-6 fatty acid. Polyunsaturated fatty acids are important for cell membrane fluidity at lower temperatures, and FAD2 has been related to both seedling survival in salty soil and increased cold tolerance (Dar et al., 2017; Kargiotidou et al., 2008; J. Zhang et al., 2012). We also found that *H. erectifolium* had gained ten tandemly duplicated copies of CASP4. CASP4 is one of five members of the CASP gene family, which are essential in the formation of the Casparian strip, an impermeable barrier to water and salts (Naseer et al., 2012; Roppolo et al., 2014). These additional copies of CASP4 could potentially infer stress-activated

formation of additional Casparian strips in the root as a response to salt or osmotic stresses (Kreszies et al., 2020; Wei et al., 2021). ELIPs and LEAs are both generally mentioned in relation to desiccation tolerance, and we could verify their role in desiccation tolerance as we found high upregulation of them during drought stress and rapid downregulation at recovery (Fig. 15D). Large tandem duplications of ELIPs are associated with desiccation tolerance in plants where they stabilize and protect photosynthetic components during dehydration and help with thermal dissipation (VanBuren et al., 2019; Ye et al., 2024). LEAs play a different and more general role during desiccation by stabilizing numerous types of cell components, from DNA to proteins to cell membranes (Artur et al., 2019; Hernández-Sánchez et al., 2022). We infer from these gene expansions that *H. erectifolium,* in addition to its morphological adaptations, also carries genomic signatures of desiccation, cold, and salinity tolerance.

Cross-species transcriptomic responses to drought and recovery

As *H. erectifolium* displayed multiple xeromorphic features and gains in gene families of osmoprotective capacity, we wanted to study their transcriptomic response to reduced soil moisture and recovery after that. We carefully synced up the biomass before the start of the drought experiment and also aimed at suppressing reproductive development by keeping the lights day neutral, 12 hours day/night cycles. We did this in order to have the cross-species comparison as equal as possible. These kinds of considerations are often disregarded in many studies, both in regard to the developmental stage and starting biomass. As setting up a controlled in-soil drought experiment is challenging, many studies simply remove the plants from soil or media and let the roots air dry (Lei et al., 2024; Li et al., 2019).

Reduced leaf RWC: *H. erectifolium* maintained leaf erectness while Morex wilted

We were able to achieve a near-identical reduction in soil moisture content over the six-day dry-down between both species. Therefore, we were able to control a critical factor in the cross-species comparison to drought. *H. erectifolium* and Morex appeared to maintain comparable leaf RWC at the same soil moisture level during the dry-drown. However, Morex already had DEGs on the second day of withholding water, whereas none were detected in *H. erectifolium*. As the leaf RWC dropped, Morex needed structural support due to wilting leaves, while *H. erectifolium* remained erect with its rolled-up leaves (Fig 10C, D). *H. erectifolium's* ability to maintain structural integrity could stem from the increased sclerenchymatous tissue and extensive ribbed/grooved adaxial leaf structure, thereby preventing folding, as the BSE alone does not provide structural support (Barbosa et al., 2019; Guo et al., 2024; Jarvis, 2012; Moulia, 2000). The greater amount and compartmentalization provided by BSE and the higher density of major veins could have provided stabilization of water availability in the mesophyll while the vasculature and BSE reduced (Buckley et al., 2011; Nikolopoulos et al., 2002; Terashima, 1992).

Transcriptional effects were detected later and recovered faster in *H. erectifolium*

On the second day of dry-down, no DEGs were detected in *H. erectifolium,* but Morex was already showing effects of stress at the same level of reduced leaf RWC. Furthermore, *H. erectifolium* appeared to respond in a more synchronized way, upregulating pathways involved in stress responses, cellular reorganization, and transport while downregulating processes involved with photosynthesis and biosynthesis as drought intensified. *H. erectifolium* reversed these pathways during recovery, and

most DEGs had already reached control levels 24 hours after rewatering (Fig. 12, Fig. 13, Fig. 14). However, many DEGs in Morex did not reach control levels after 24 hours of recovery like *H. erectifolium,* even though leaf RWC reached control levels (Fig. 12, Fig. 13, Fig. 14). This pointed towards Morex being more sensitive to decreasing leaf RWC and potentially not being able to mitigate the effects of drought stress, thereby not reaching a baseline transcriptional level within 24 hours as *H. erectifolium*.

H. erectifolium had a much higher number of DEGs that were transiently expressed on DOT5 and 6, and these appeared to have a clearer pattern of enriched functions than Morex. The patterns in *H. erectifolium* were the downregulation of photosynthesis and reactions to reactive oxygen species (ROS) during drought, as potentially less ROS was produced as photosynthetic processes were downregulated and then during recovery initiating metabolic activity (Foyer & Shigeoka, 2010). Morex, on the other hand, had an upregulation of cyclins early on, but genes involved in DNA replication were upregulated only during recovery. Possible explanations could be that damage to cyclin-dependent kinases caused their upregulation or not integrating stress signals appropriately with the continual upregulation of RNA modification-related genes (Qi & Zhang, 2020; H. Zhang et al., 2020). We also saw this in the time series DEGs, where *H. erectifolium* had a cluster of salicylic acid-activated pathways such as glutathione to mitigate ROS (Hasanuzzaman et al., 2017; Liting et al., 2015; Shan et al., 2024). *H. erectifolium* down-regulated cytokinin and its pathways, which could indicate a slowing down of growth, as keeping cytokinin pathways active during short-term drought has been shown to have short-term benefits but is likely detrimental as growth is maintained at the expanse of water use (Prerostova et al., 2018; Reguera et al., 2013). There were no such enriched hormonal pathways evident in Morex. The upward trend seen in expression Cluster 2 in Fig. 12B and its functional enrichment in Fig. 13B supports the idea that Morex increasingly upregulated protein biosynthesis during drought; one additional reason could be initial protein degradation of various causes like denaturation or ROS damage due to desiccation (Fig. 12B, Fig. 13B) (Heinemann et al., 2021). *H. erectifolium* showed overall a more coordinated response to stress and recovery, quick up-and-down-regulation of pathways associated with drought tolerance, and rapid recovery. Morex showed an earlier expression response to drought and slower transcriptome recovery. Morex's significant pathways were reminiscent of drought escape by increasing growth to finish its growth cycle and possibly increasing intracellular damage by lower expression of desiccation tolerance genes.

Differentially expressed single-copy orthologs, a direct cross-species comparison

By exploring the differential gene expression response in relation to only differentially expressed single-copy (SC) genes, we can infer cross-species reactions of a common gene set. We could quickly see a very dissimilar response to drought between *H. erectifolium* and Morex, as only a quarter of all discovered SC DEGs were shared (Fig. 15A, B). Only a few base functions were shared, e.g., amide, carboxylic acid metabolic processes, and photosynthesis. *H. erectifolium*'s response could be explained as preparation for stress by internal cell reorganization, vesicle-mediated transport, detoxification, and ROS mitigation, all functions related to increased osmotic stress tolerance (Jarzyniak & Jasiński, 2014; Mazel et al., 2004; Nguyen et al., 2019; Noctor et al., 2014).We saw a very dynamic response of pathways in SC DEGs unique to *H. erectifolium,* further supporting a drought tolerance response. We found that the pathways of SC DEGs unique to Morex were limited to carbohydrate, polysaccharide metabolic processes, and RNA modification-related (Fig. 15).

Morex's response could have been an attempt to build up cell walls to reduce water loss or due to cell wall damage as a result of leaf wilting (Balsamo et al., 2015; Hou et al., 2024; Piro et al., 2003). This could again potentially explain the constant upregulation of protein and other biosynthesis processes during drought stress. Overall, we can say that *H. erectifolium* shows hallmarks of drought tolerance, whereas Morex struggles at the same leaf RWC.

The expanded gene families of ELIPs and LEAs show drought-specific expression

A good example of *H. erectifolium's* adaption to drought-prone environments was the ELIPs and LEAs gene family expansion we found and whose rapid and strong activation we could verify during desiccation and subsequent deactivation at recovery (Fig. 15D) (Marks et al., 2024). In this study, we utilized the logFC to find differences in gene expression levels. Therefore, it is possible that there was was a constitutive base-level expression of ELIPs or LEAs, which contributed to a later onset of DEGs in *H. erectifolium.* In addition, there were other LEAs present in the genomes which we did not explore in the current context but should be explored further. We are fairly confident that we captured most of the ELIPs within the expanded HOG as there were 25 copies in it and only 26 to 31 could be identified further in the gene annotation of *H. erectifolium,* but this would need further validations. An expected number of ELIPs is 1-5 in drought susceptible plants, but can reach up to 74 copies as is the case for *Selaginella tamariscina*,. LEAs have been reported up to 180 in *Malus domestica* (Artur et al., 2019; Marks et al., 2024). If any of the LEAs or ELIPs during further validation are constitutively expressed in *H. erectifolium* they could be a target for promoter region targeting in barley to improvephotosynthesis stability at the onset of transient drought.

The differences in responses to the onset of drought between the two species were interesting and would need further exploration. Nonetheless, *H. erectifolium* shows far greater potential to increase our understanding of drought tolerance mechanisms, which could be used to improve our modern barley and other drought-susceptible crops (Palmgren et al., 2015).

Conclusions

We found characteristics of xeromorphic leaf adaptation in *H. erectifolium*, such as leaf rolling, increased vein density and larger BSE, and higher density and increased trichomes. We also found genetic signatures of gene copy number gain associated with desiccation, salinity, and cold tolerance. Experimental analysis showed a contrasting transcriptomic effect of reduced soil moisture availability between *H. erectifolium* and Morex. The leaves of *H. erectifolium* rolled up and remained erect, while Morex wilted and lost structural integrity during desiccation. The transcriptomic responses diverged substantially: *H. erectifolium* expressed pathways of desiccation tolerance and growth reduction, whereas Morex expressed mainly genes involved in biosynthesis and genes related to growth, possibly a response to an intracellular disequilibrium and cellular damage due to desiccation. *H. erectifolium's* response displayed pathway responses reminiscent of drought tolerance, while Morex appeared sensitive and less able to quickly recover from drought after rewatering. Taken together, these results provide support for *H. erectifolium* as a promising model for drought tolerance in cereals, a species that has adapted to harsher environments, providing valuable xeromorphic and genetic resources for future crop improvements.

5. Figures

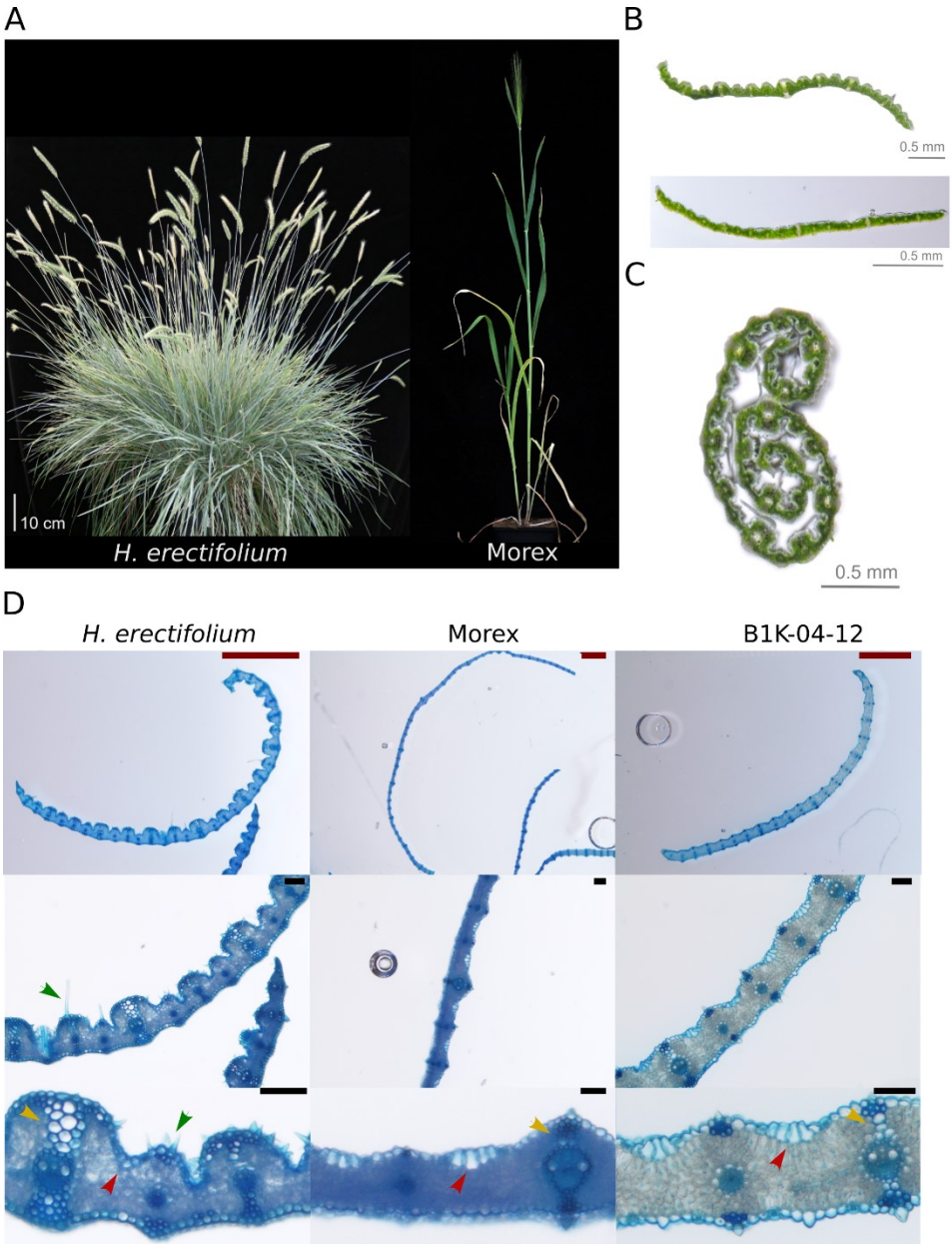

Figure 1: *H. erectifolium* and leaf morphology of *H. erectifolium* and cultivated and wild barley. (**A**) A representative of *Hordeum erectifolium* (left), accession NGB 6816, from which all genetic and transcriptomic data was collected, and an example of *H. vulgare cv.* Morex (right). (**B**) Transverse cuts of a fully turgid *H. erectifolium* leaf (top) and of *H. v. spontaneum acc.* B1K-04-12 (bottom). (**C**) *H. erectifolium* leaves roll inward towards the midriff as the turgor is lost and become rigid while remaining erect. **(D)** Transverse cuts of *H. erectifolium*, Morex, and B1K-04-12, lignin of fixated tissue was stained with toluidine blue. Red arrows point at bulliform cells in Morex and B1K-04-12, and the expected location in *H. erectifolium*. Trichomes are indicated by green arrows in *H. erectifolium*. Yellow arrows point at the adaxial bundle sheath extensions (BSE) on a major vein; the BSE, as well as on the abaxial side of the vein. Scale bars for 1000 µm are indicated with red bars and 100 µm in black.

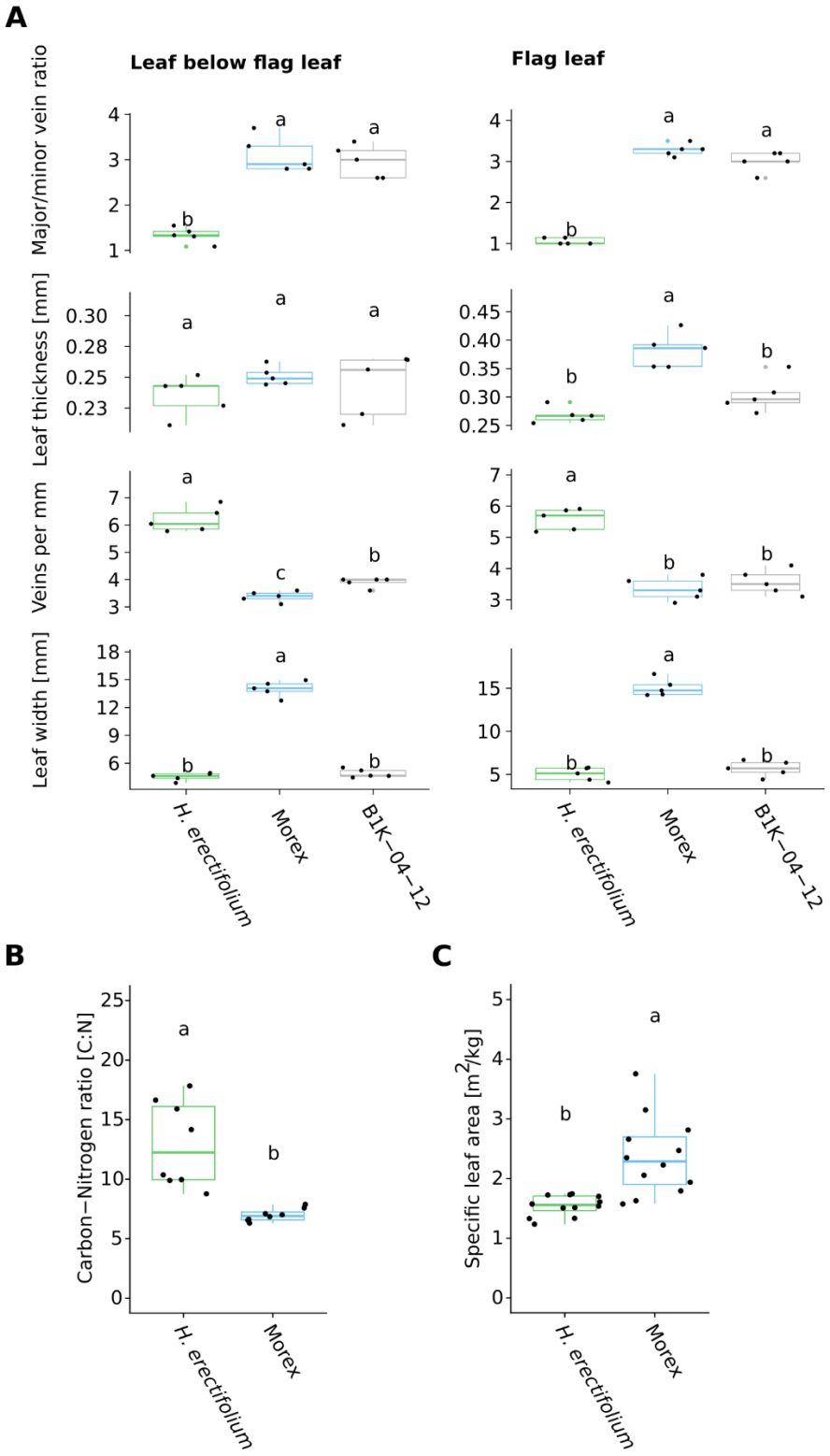

Figure 2: Quantitative leaf characteristics of *H. erectifolium*, cultivated and wild barley.
(A) Leaf morphology of the first leaf below the flag leaf (LBF) and the flag leaf (FL) in *H. erectifolium,* Morex, and B1K-04-12. Different letters indicate significantly differing groups, ANOVA with post-hoc Tukey HSD, $p < 0.05$, $n = 5$. **(B)** Ratio of elemental carbon and nitrogen in the FL of *H. erectifolium* and Morex. **(C)** Specific leaf area in FL of *H. erectifolium* and Morex, n=8. ANOVA with post-hoc Tukey HSD, $p < 0.05$.

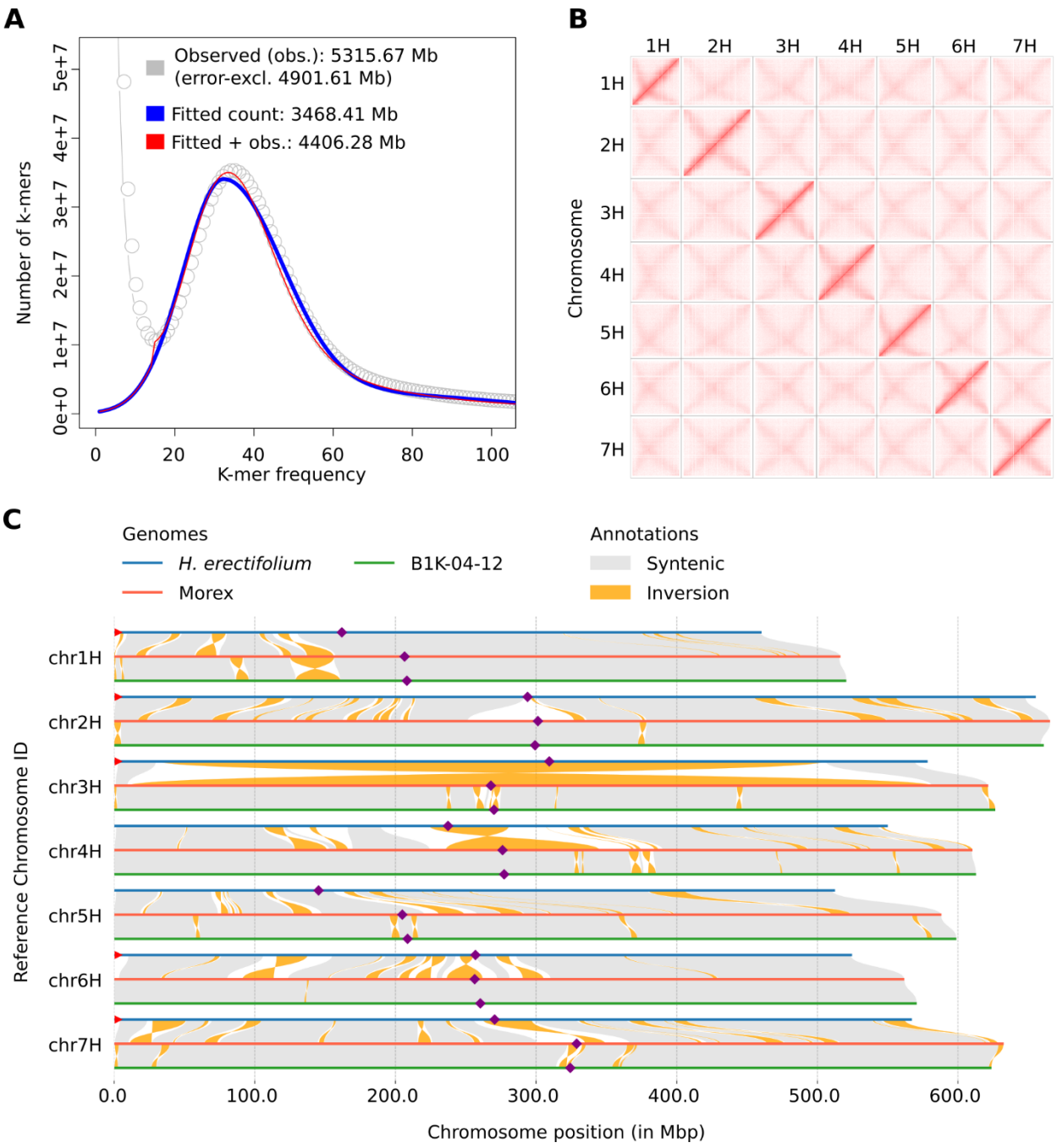

Figure 3: Genome characteristics, interchromosomal contact matrix, and chromosomal synteny between genomes.

(A) K-mer spectra of 21-mers calculated with Jellyfish and findGSE using Illumina data. A smooth single peak is a feature of a homozygous genome. **(B)** Interchomosomal contact matrix of the seven assembled chromosomes. Pixel intensity represents Hi-C link counts normalized over a 1 Mb window on a logarithmic scale. **(C)** Whole chromosomal synteny between *H. erectifolium*, Morex, and B1K-04-12. Inversions smaller than 1 Mb were excluded for visualization. Putative centromeres for all chromosomes are indicated by purple diamonds and identified telomeric sequences on the short arm of five chromosomes in *H. erectifolium* by red triangles.

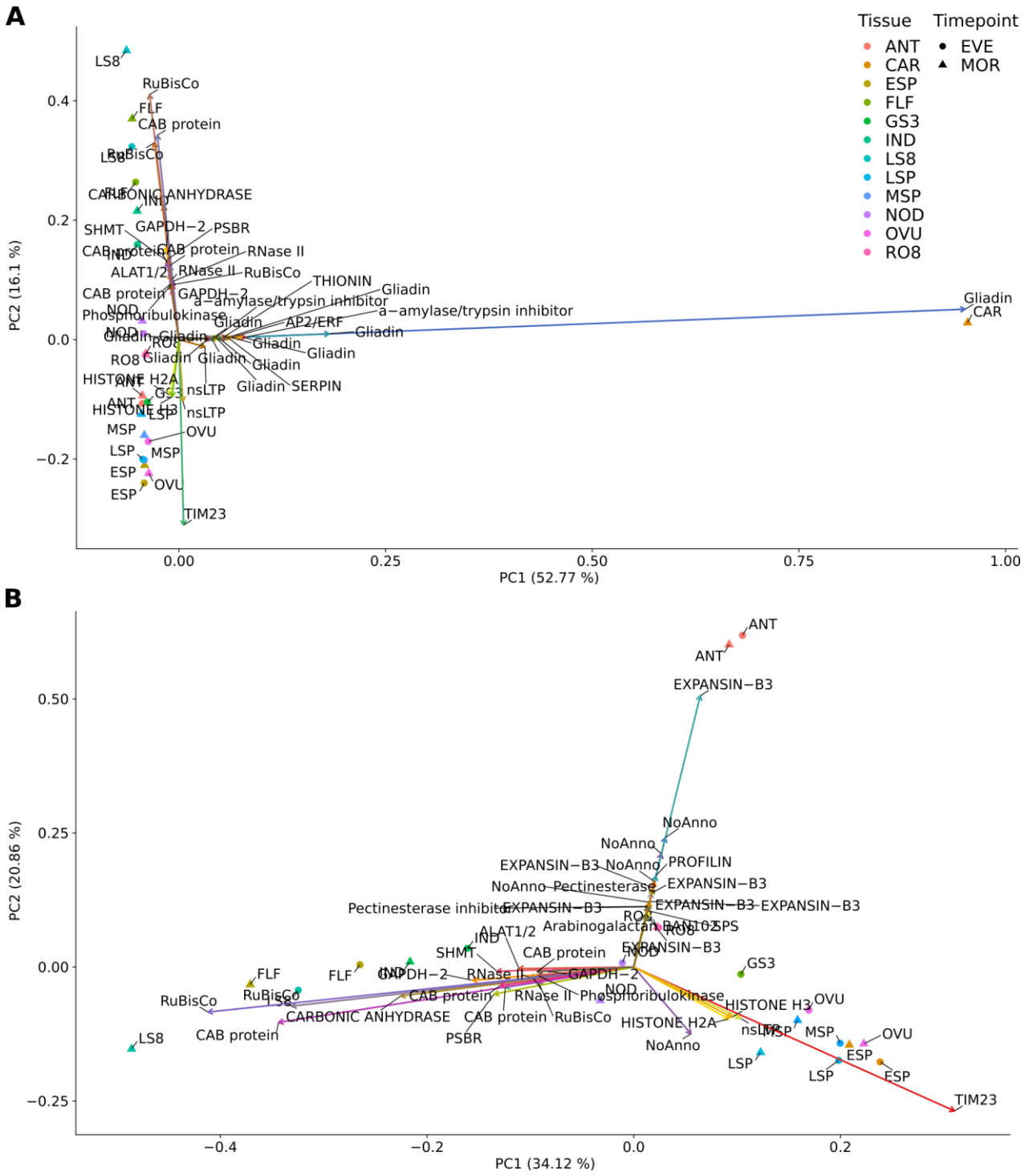

Figure 4: Principle component analysis (PCA) of tissue-specific expression profiles.
PCA of PacBio IsoSeq transcript abundance in all 22 sampled tissues of *H. erectifolium*, among 12 individual tissues of which ten were sampled both in the morning (MOR, ZT 1-3) and evening (EVE, ZT 13-15). **(A)** PCA plot of all 22 tissues and the trajectory of the top 20 highest loading genes for PC1 and PC2. Three main trajectories and influential genes were identified. Lower left: spike development and reproductive tissues: Translocase of the Inner Mitochondrial Membrane 23 (TIM23) and histones were prominent. Upper left: vegetative tissues, influenced by photosynthesis and carbon metabolism-related genes: *CHLOROPHYLL A-B BINDING PROTEIN* (CAB protein), *RIBULOSE BISPHOSPHATE CARBOXYLASE/OXYGENASE (RUBISCO)*, and *CARBONIC ANHYDRASE*. Right: The greatest loading and contributing to 52.77 % of the variance on PC1 were from multiple

and high expression of Gliadin genes in CAR_MOR (caryopsis, 10 days post anthesis), which synthesize seed storage proteins. **(B)** PCA without the CAR_MOR sample, with the opposite trajectories of vegetative versus reproductive tissues along PC1 and a third trajectory on PC2 contributed by anthers (ANT) and to a lesser extent, roots (RO8), this trajectory was influenced by high expression of *EXPANSIN* and *PROFILIN*, both involved in growth by the restructuring of the cell wall and actin cytoskeleton.

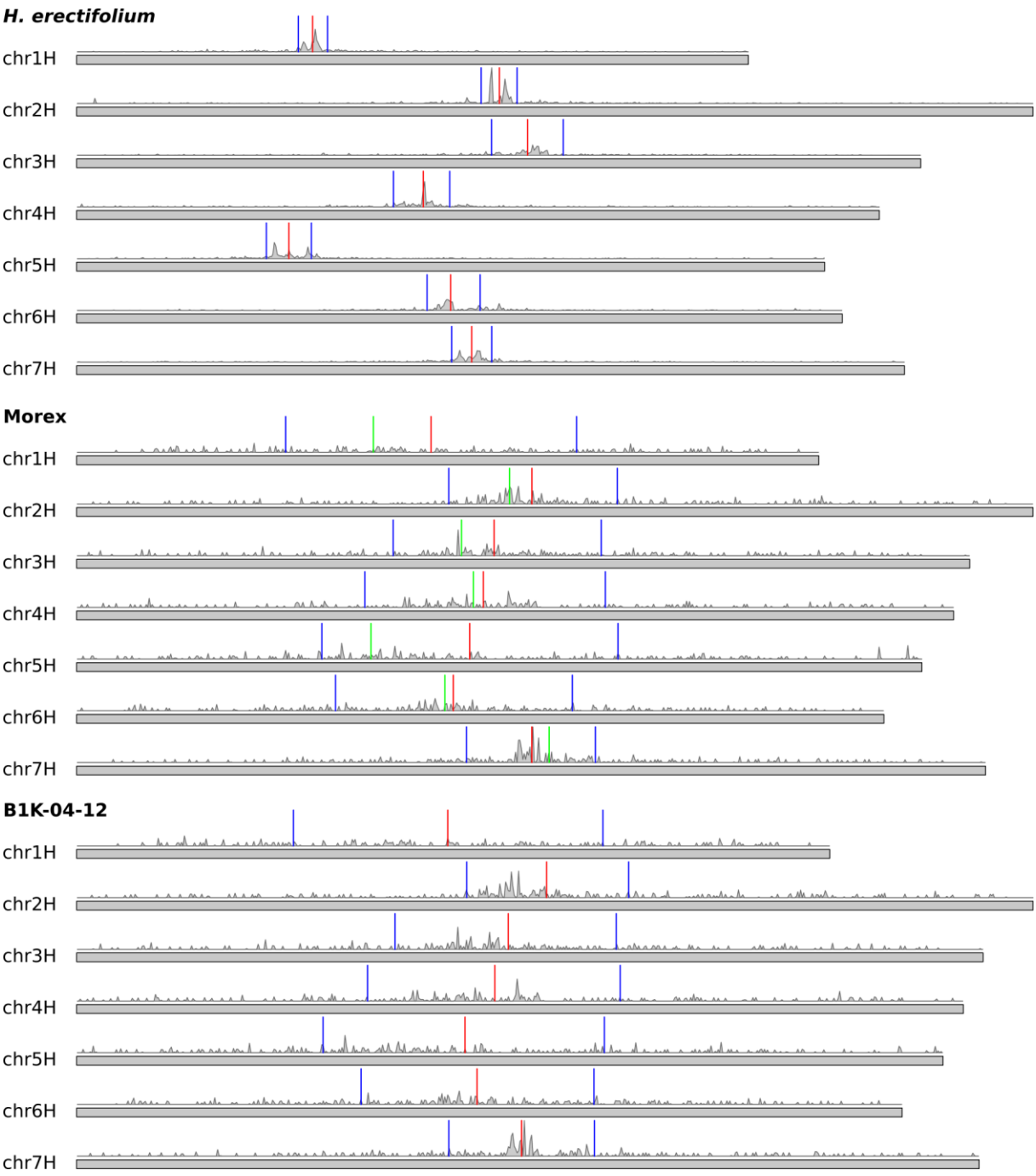

Figure 5: Putative centromere locations and centromere sizes.
Predicted centromeric locations in *H. erectifolium*, Morex, and B1K-04-12. Density of aligned CRM long terminal repeat (LTR) retrotransposons sequences in 1 Mb windows across chromosomes. The red line indicates the predicted midpoint of the CRM LTR clade density at the putative centromere midpoint. Blue lines are the 50 % confidence limits, here used as an estimate of centromere boundaries. The green lines indicate previously published centromere locations for Morex.

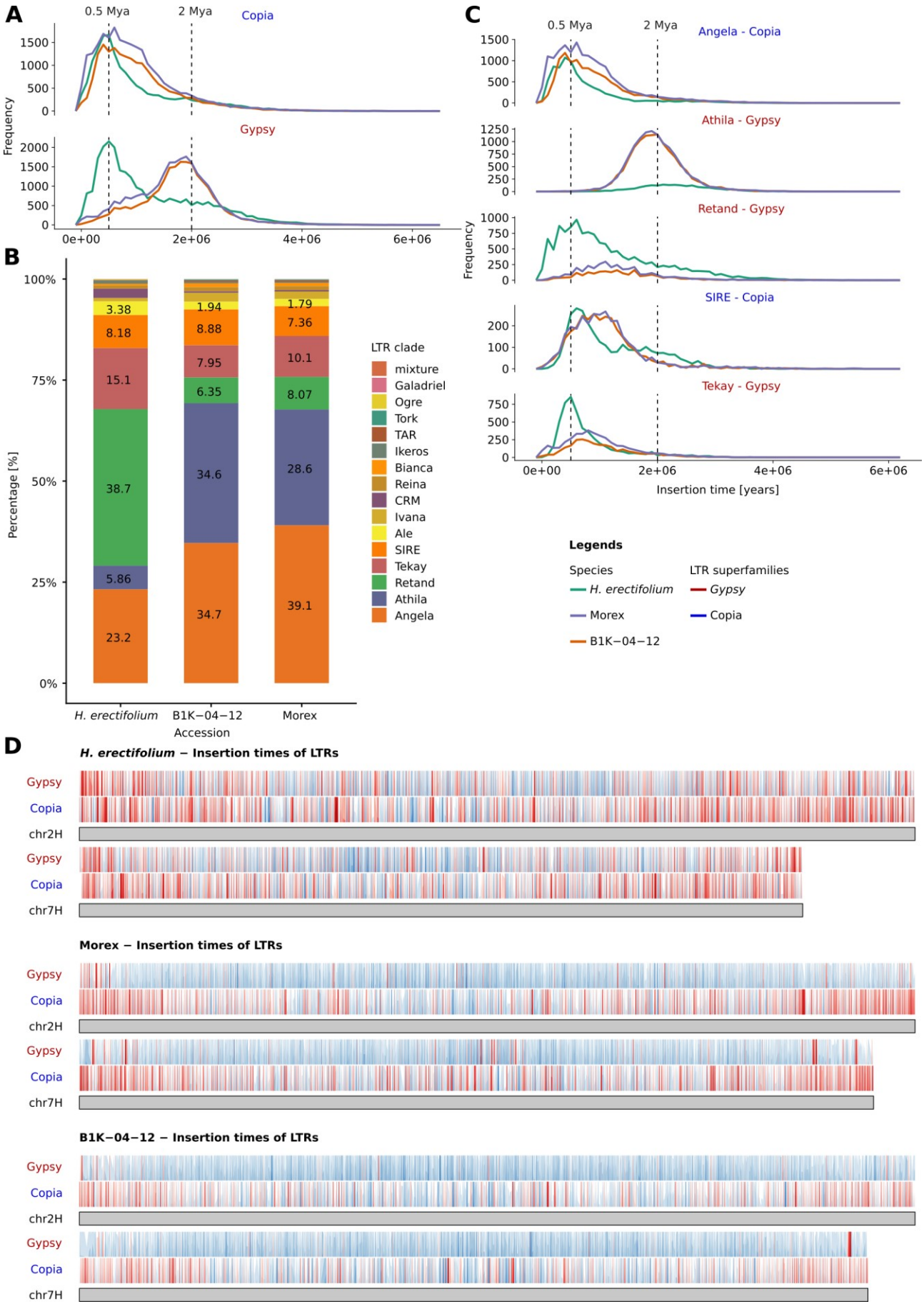
A
0.5 Mya
2 Mya
Copia
Gypsy
Frequency
0e+00
2e+06
4e+06
6e+06
B
100%
75%
50%
25%
0%
Percentage [%]
3.38
8.18
15.1
38.7
5.86
23.2
1.94
8.88
7.95
6.35
34.6
34.7
1.79
7.36
10.1
8.07
28.6
39.1
H. erectifolium
B1K−04−12
Morex
Accession
LTR clade
mixture
Galadriel
Ogre
Tork
TAR
Ikeros
Bianca
Reina
CRM
Ivana
Ale
SIRE
Tekay
Retand
Athila
Angela
C
Angela - Copia
Athila - Gypsy
Retand - Gypsy
SIRE - Copia
Tekay - Gypsy
Insertion time [years]
Legends
Species
H. erectifolium
Morex
B1K−04−12
LTR superfamilies
Gypsy
Copia
D
H. erectifolium − Insertion times of LTRs
Morex − Insertion times of LTRs
B1K−04−12 − Insertion times of LTRs
chr2H
chr7H

Figure 6: Transposable elements composition, long terminal repeat (LTR) retrotransposon profiles, and frequency of predicted insertion times.
(A) Frequency of estimated insertion times for the LTR superfamilies, Gypsy (red) and Copia (blue), insertion times calculated based on the mutation rate in rice for the annotated LTR superfamilies in *H. erectifolium*, Morex, and B1K-04-12. Dotted lines mark a peak, million years ago (Mya), age of a recent burst of Copia insertions at ~0.5 Mya, during the Chibanian period, in all genomes and *H. erectifolium* had an additional Gypsy peak at the same time. A second Gypsy peak was found in Morex and B1K-04-12 at an earlier period ~1.8-2 Mya, the transition of Gelasian to the Calabrian period. **(B)** Composition landscape of intact LTRs representing the total LTRs in *H. erectifolium*, Morex, and B1K-04-12. The percentage of intact LTRs was normalized as total intact LTRs within a genome. **(C)** Intact LTR insertion frequency over time by clade for the five largest LTR clades in the genomes; Copia: Angela and SIRE (blue), Gypsy: Athila, Retand, and Tekay (red). The black dotted lines mark 0.5 Mya and 2 Mya, respectively. **(D)** LTR insertion times were normalized and scaled to show the relative time of the most recent insertions of Copia and Gypsy superfamily elements across two example chromosomes 2H and 7H. There were greater frequencies of recent Copia insertions at the chromosomal ends of all three genomes. *H. erectifolium* had Gypsy insertions that are spread across the entire chromosomes, but in Morex and B1K-04-12, there were few insertions and mainly towards the far ends.

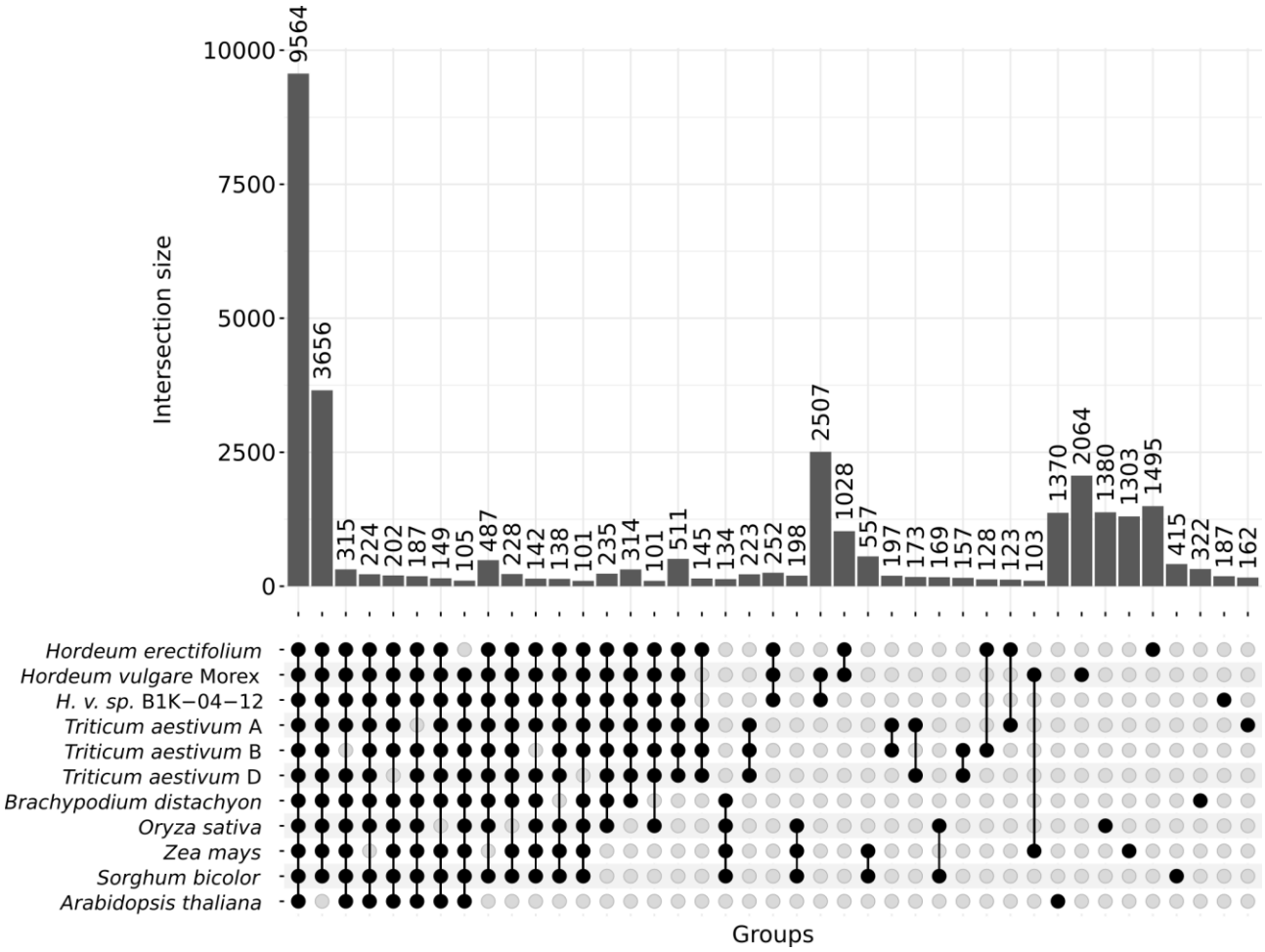

Figure 7: Shared and unique orthologs of *H. erectifolium* with Poaceae and *A. thaliana.*
Shared and unique hierarchical phylogenetic orthologs (HOGs) between nine genomes of eight species; eight monocots and one dicot. Wheat (*T. aestivum*) was divided into its A, B, and D subgenomes. Proteins from unanchored contigs were excluded. There were 9,564 shared HOGs between all eight species, with 3,656 unique to the *Poaceae* family. 1,495 HOGs were only associated with *H. erectifolium*.

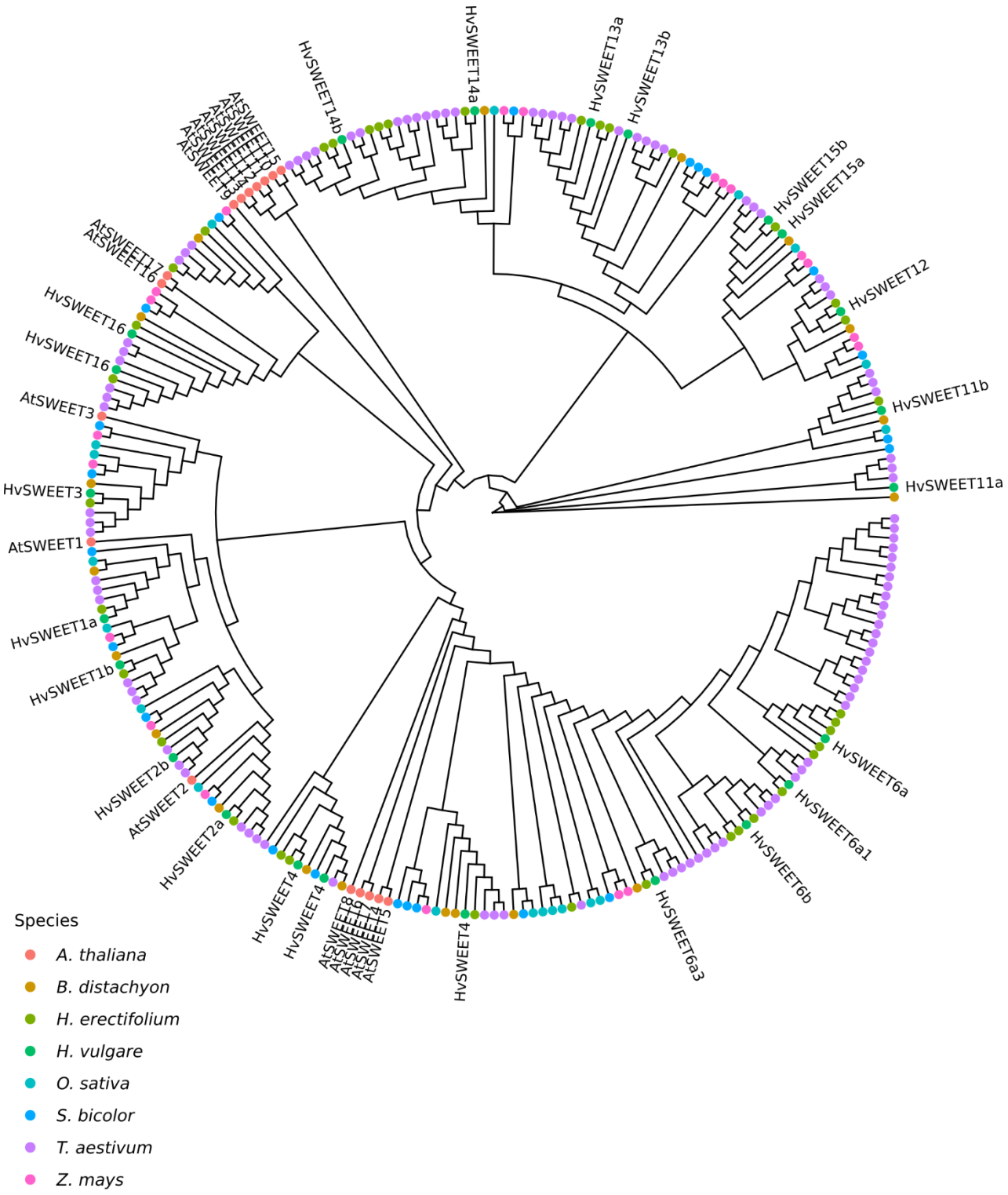

Figure 8: Phylogenetic reconstruction of annotated SWEET proteins.
Phylogeny relationship of 258 SWEET proteins, total number per species in brackets; *Arabidopsis thaliana* (17), *Sorghum bicolor* (23), *Zea mays* (22), *Oryza sativa* (19), *Brachypodium distachyon* (19), *Triticum aestivum* (100), *Hordeum vulgare cv.* Morex (23), and *H. erectifolium* (37).

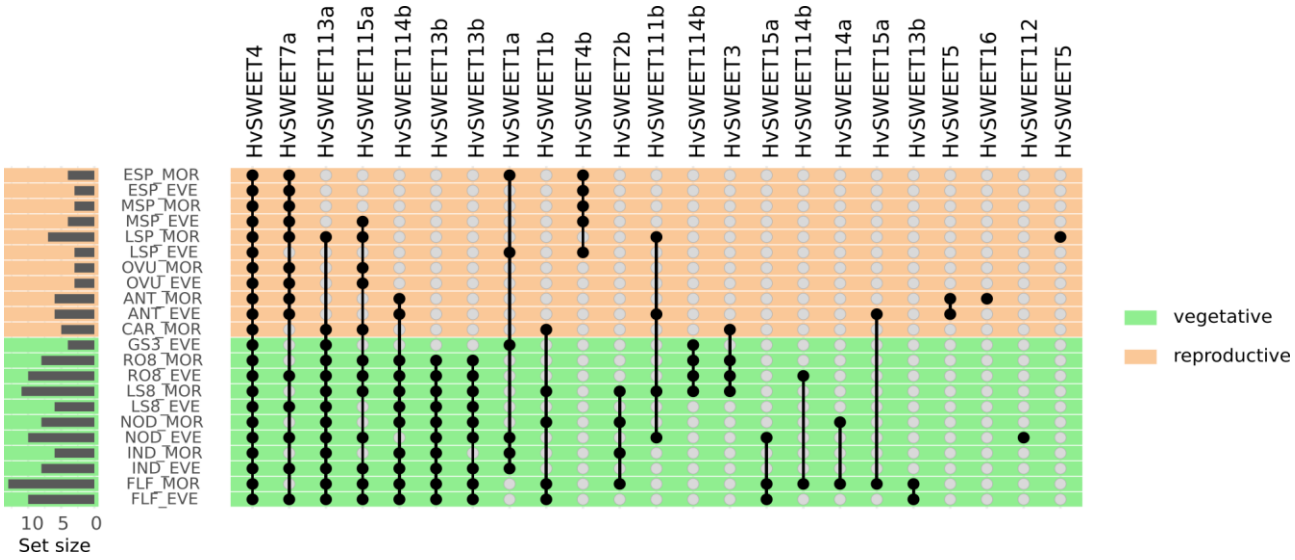

Figure 9: Tissue and time-specific expression of SWEETs captured with PacBio IsoSeq.
Intersection matrix of captured SWEET transcripts from all 22 PacBio IsoSeq sequenced tissue samples in *H. erectifolium*, 12 individual tissues with ten tissues sampled both in the morning (MOR, ZT 1-3) and evening (EVE, ZT 13-15). HvSWEET4 (Herectifolium_NGB6816_ONT-6HG53985) was ubiquitously expressed in every sample, while homologs of HvSWEET3 (Herectifolium_NGB6816_ONT-3HG9439), HvSWEET5 (Herectifolium_NGB6816_ONT-1HG46935), and HvSWEET13b (Herectifolium_NGB6816_ONT-6HG56972) were only found in the shoot apical meristems (ESP, MSP, LSP), anthers (ANT), and flagleaf (FLF), respectively. A homologue of HvSWEET7a (Herectifolium_NGB6816_ONT-7HG38920) was only found in vegetative tissues during evenings (EVE) but found in reproductive tissue during both morning (MOR) and evening (EVE).

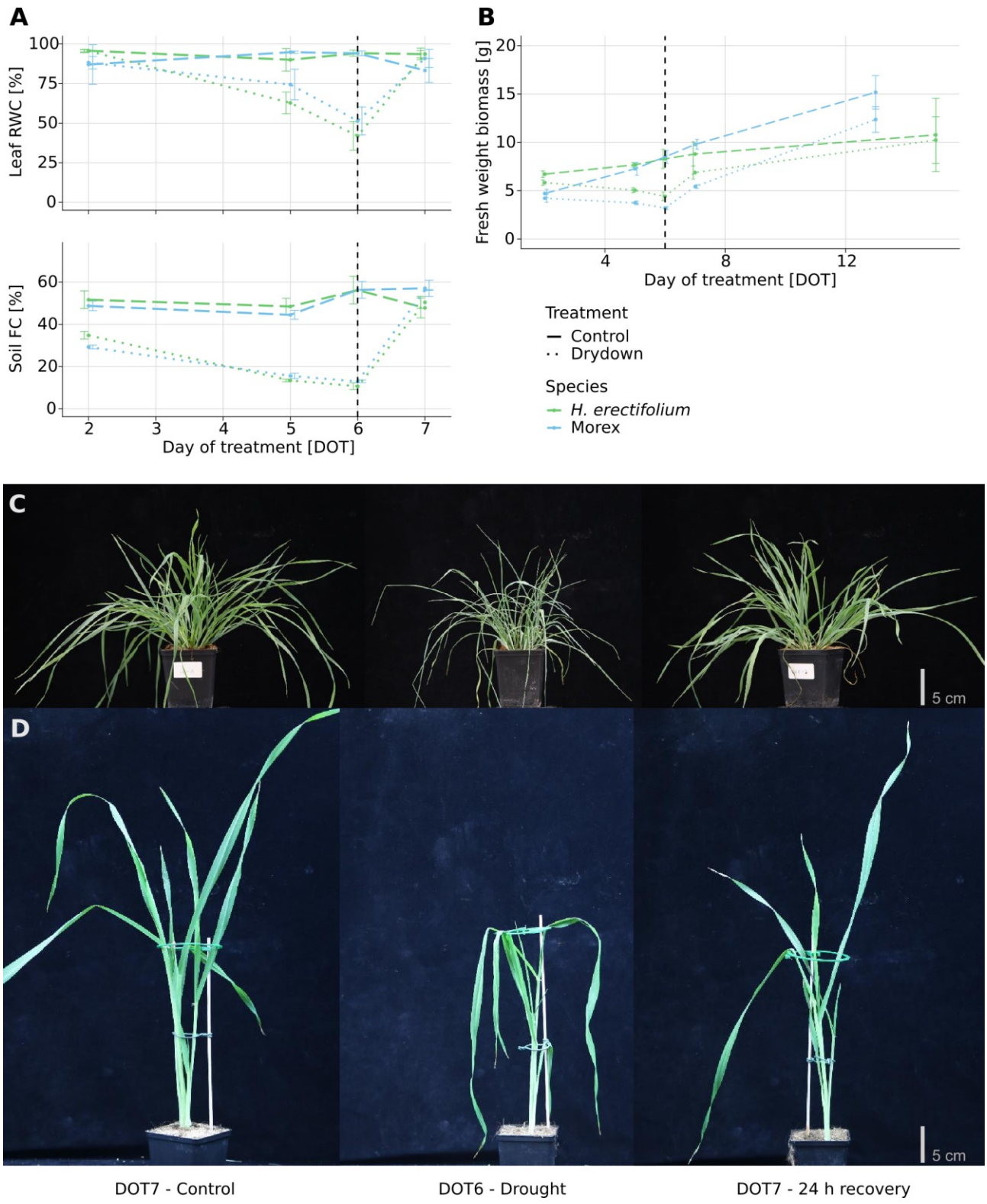

Figure 10: Relative water content and plant morphology during dry-down and recovery.
(A) The control group was maintained at 50 % soil field capacity (FC, dashed line), while for drought treatment, water was withheld for six days after adjusting soil FC to 50 % and rewatered to 50 % FC on the sixth day of treatment (DOT), green dotted line. Soil FC decreased evenly between species, both reaching ~13 % soil FC on DOT6. Leaf relative water content (RWC) also decreased at even rates between species, starting at ~100 % and ending at ~50 % on DOT6, and 24 hours after rewatering, they recovered to ~100 % on DOT7. Dotted lines – drought, dashed line – control, blue – *H. erectifolium*, orange – Morex, n = 4, error bars are standard deviation, two plants were pooled at

each timepoint and treatment. **(B)** Progression of fresh weight biomass during and after recovery of drought treatment at DOT15 and DOT13 for *H. erectifolium* and Morex, respectively. (**C,D)** Drought morphology of *H. erectifolium* and Morex, with control on DOT7 (left), drought on DOT6 (middle) and DOT7 recovery (right). Leaves of *H. erectifolium* rolled inward and maintained erectness (DOT6), while Morex leaves wilted and needed to be supported during treatment.

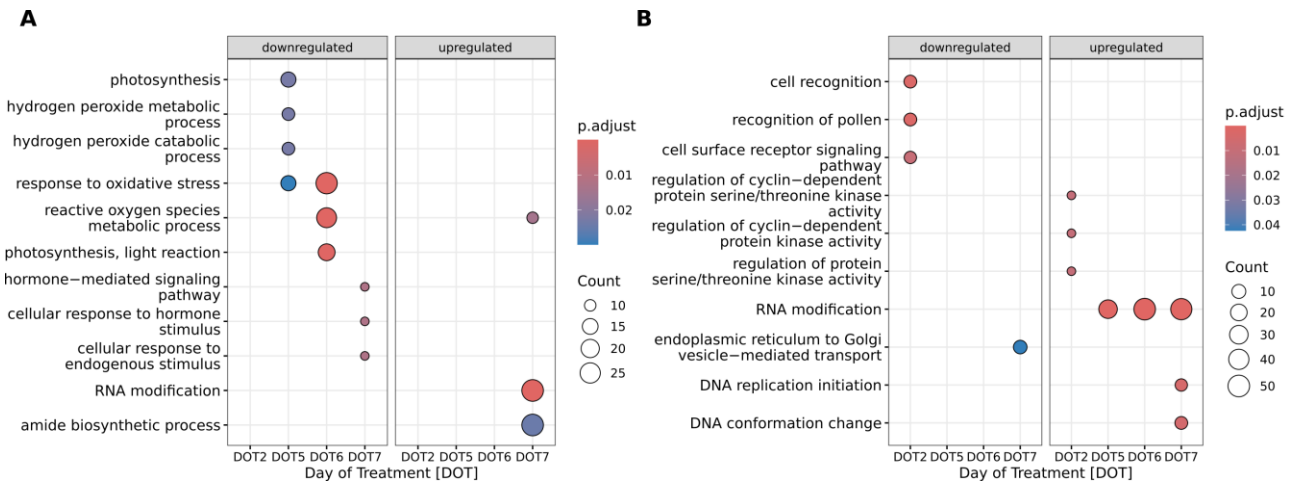

Figure 11: Functional enrichment of transient differentially expressed genes (DEG).
Functional enrichment profiles of up-and-down regulated transient DEGs, which were captured by pairwise comparison at each time point between control and drought with edgeR, these were DEGs not captured through regression analysis by maSigPro. **(A)** *H. erectifolium* showed differentiation of functionally enriched up-down patterns from DOT5/6 to DOT7 involving a downregulation of genes involved in oxidative stress and hormone signaling. There were no DEGs at DOT2. **(B)** Morex presented a pattern of downregulating cell signaling and upregulation of cyclins (DOT2), RNA modification (DOT5-DOT7), and DNA replication on DOT7.

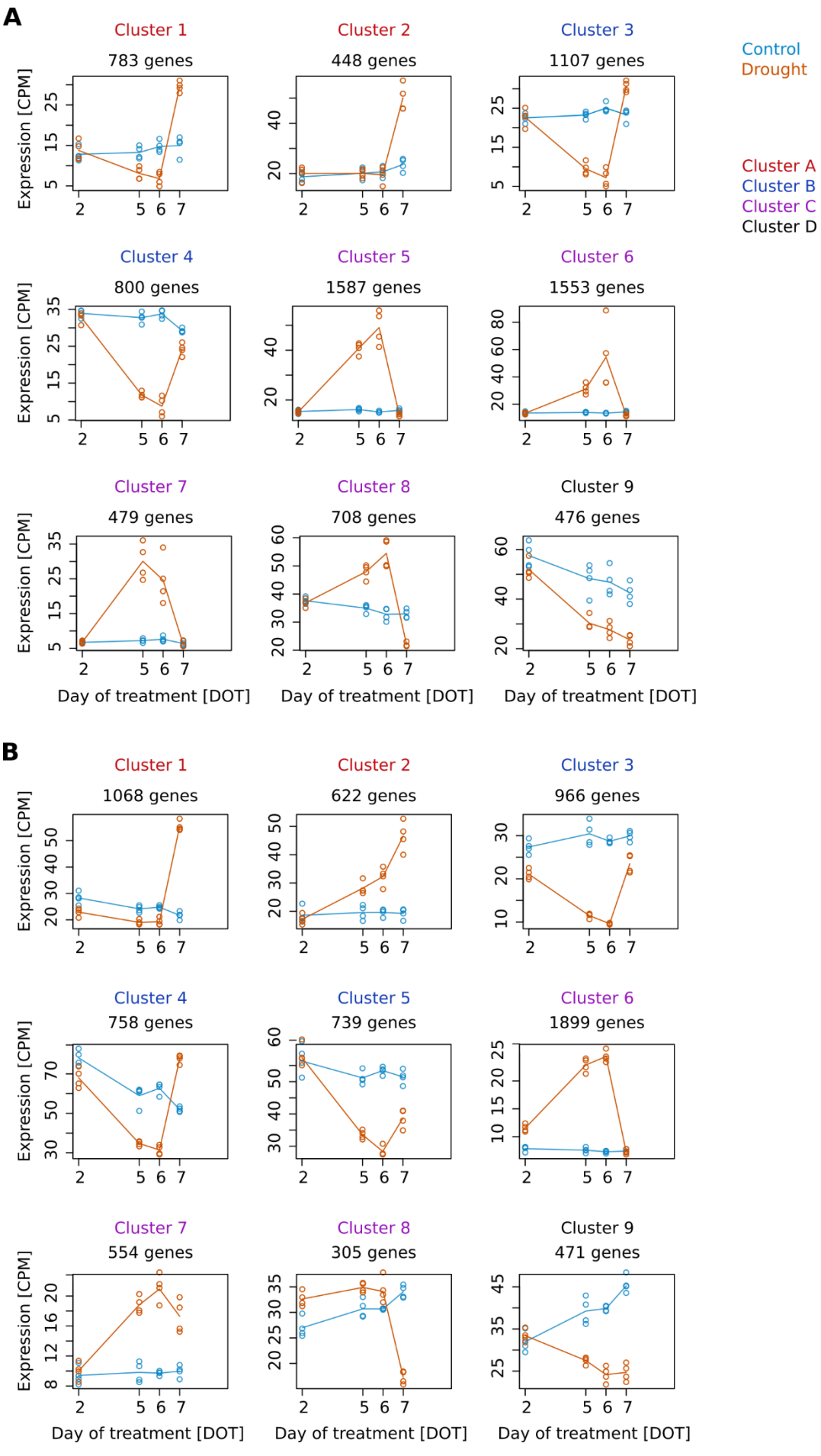
A
Cluster 1
783 genes
Cluster 2
448 genes
Cluster 3
1107 genes
Cluster 4
800 genes
Cluster 5
1587 genes
Cluster 6
1553 genes
Cluster 7
479 genes
Cluster 8
708 genes
Cluster 9
476 genes
Expression [CPM]
Day of treatment [DOT]
Control
Drought
Cluster A
Cluster B
Cluster C
Cluster D
B
Cluster 1
1068 genes
Cluster 2
622 genes
Cluster 3
966 genes
Cluster 4
758 genes
Cluster 5
739 genes
Cluster 6
1899 genes
Cluster 7
554 genes
Cluster 8
305 genes
Cluster 9
471 genes
Expression [CPM]
Day of treatment [DOT]

Figure 12: Transcriptome changes over time in response to drought, regression analysis in maSigPro.

Differentially expressed genes (DEG) over time X drought treatment transcriptome analysis of RNAseq data with maSigPro. **(A)** In *H. erectifolium,* 7,941 DEGs were found showing a time X treatment fit. Expression profile clusters were grouped into A) 1, 2 (red); B) 3, 4 (blue); C) 5, 6, 7, 8 (violet); 9 (black). ***(*B)** In Morex, there were 7,382 DEGs found. Expression profile clusters were grouped into A) 1, 2 (red); B) 3, 4, 5 (blue); C) 6, 7, 8 (violet); 9 (black). DEGs were selected with an R^2 fit of >= 0.7 and assigned to nine expression profile clusters with hclust with normalized read counts (CPM).

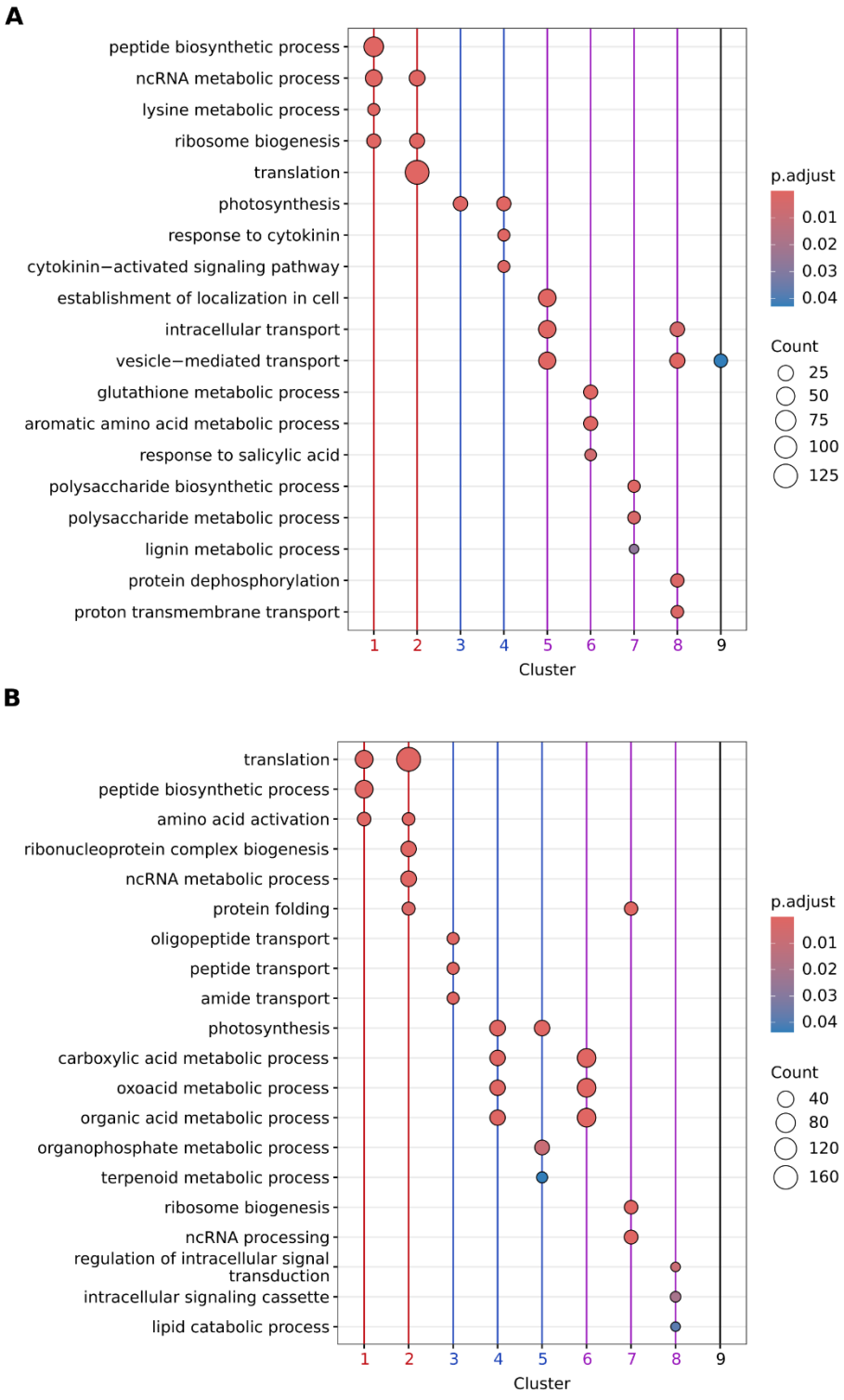

Figure 13: Transcriptome changes over time in response to drought, cluster functional enrichment.

Functional enrichment of Biological Processes (GO-BP) of time X drought treatment expression clusters from transcriptome analysis of RNAseq data with maSigPro. **(A)** *H. erectifolium*, functional enrichment of grouped clusters where involved in 1, 2 (red), peptide biosynthesis and translation; 3, 4 (blue), photosynthesis and cytokinin signaling; 5, 6, 7, 8 (violet), intracellular reorganization, transport, response to salicylic acid, polysaccharide metabolism, and protein dephosphorylation; 9 (black) vesicle-mediated transport. **(B)** Morex, functional enrichment of grouped clusters where involved in 1, 2 (red), peptide biosynthesis, translation, and folding; 3, 4, 5 (blue) peptide transport,

organic acid metabolism, and photosynthesis; 6, 7, 8 (violet), organic acid metabolism, intracellular signaling, and protein synthesis; 9 (violet), no functional enrichment.

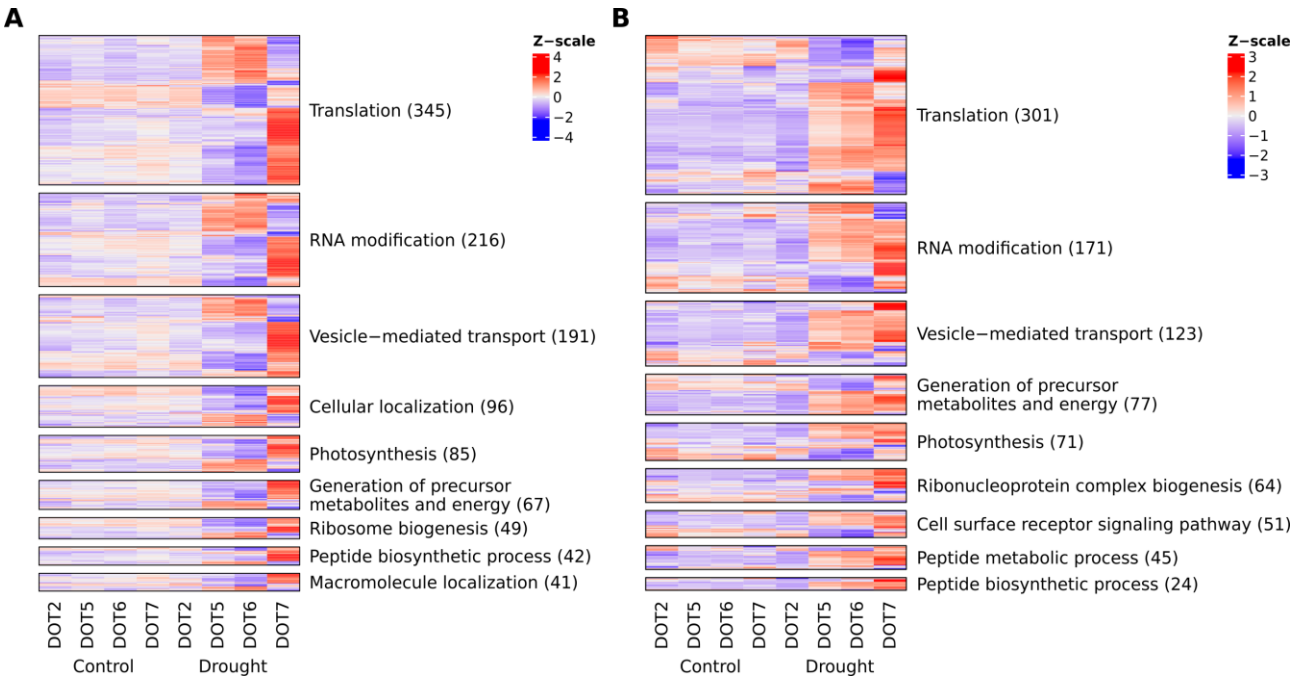

Figure 14: Gene set enrichment analysis (GSEA), the top nine enrichments in *H. erectifolium* and Morex.

Heatmap of the top nine functionally enriched Biological Processes (GO-BP) terms from GSEA across all time X treatment groups, showing normalized RNAseq reads (CPM) and averaged across sample replicates.

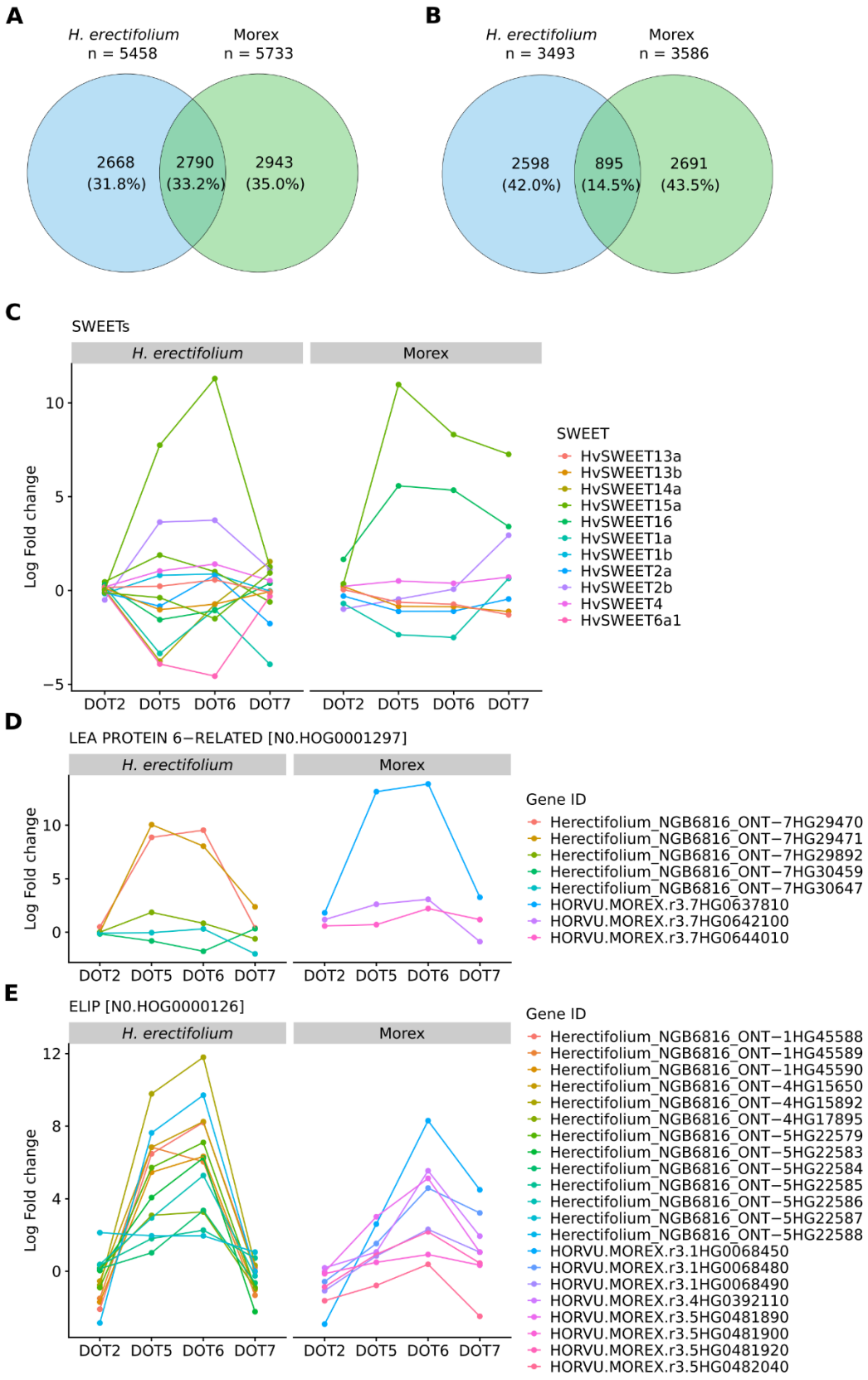

Figure 15: Single Copy (SC) orthologs, shared and unique SC DEGs, and expanded gene family expression.

(A) Shared and unique SC ortholog DEGs between *H. erectifolium* and Morex, which were found in time X treatment regression analysis with maSigPro. **(B)** Shared and unique SC ortholog DEGs between *H. erectifolium* and Morex, which were found transiently expressed by pairwise expression

analysis in edgeR. **(C)** Differential expression of all annotated SWEET genes during drought and recovery in *H. erectifolium* and Morex, nine out of 37 in *H. erectifolium* and eight out of 23 in Morex. **(D)** DEGs found in the respective hierarchical phylogenetic orthologs of expanded gene families of late embryogenesis abundant (LEA) protein (N0.HOG0001297) and **(E)** early light-induced proteins (ELIP) (N0.HOG0000126) which had expanded in on the phylogenetic branch of *H. erectifolium*.

6. Materials and methods

Leaf transverse cutting and staining

Seeds of *H. erectifolium* acc. NGB6816 (Nordic Genetic Resource Center, Sweden), *H. vulgare cv.* Morex and *H. v. spontaneum acc.* B1K-04-12 were sown in a soil mixture of 93% (v/v) Einheitserde ED73 (Einheitserde Werkverband e.V., Sinntal_Altengronau, Germany), 6.6% (v/v) sand, and 0.4% (v/v) Osmocote exact standard 3-4M (Scotts Company LLC). Stratified at 4 °C before being placed in a growth chamber with long day conditions (16h light, 8h dark, at 20°C day/16°C night, 60% relative humidity) for germination. Ten days after germination they were then vernalized for 8 weeks at 4 °C under short day conditions, 8 hours light, before being transferred back to the long day, 16 hours light, growth chamber until flowering. Flag leaf and leaf below flag leaf were collected and 1 cm section at the midpoint of the leaf was sampled. The sample was cut transversely with a razor blade by hand and sections placed in a 1.5 mL tube with fixing solution of Ethanol:Acetic acid (6:1 v/v), the tubes were then placed on top of a rotary shaker for two hours at 20-50 RPM. After two hours, the fixing solution was removed and 85 % (v/v) ethanol was added and stored until microscopy. The fixed sections were washed three times with dH_2O and stained in 0.5 % (w/v) toluidine blue for 10 seconds. The staining solution was removed by washing three times with dH_2O and sections transferred on a slide for imaging. Images of leaf sections were obtained using a Nikon stereo microscope (Nikon SMZ18), Nikon DS-U3 controller unit, and a Nikon DS-Fi2 digital camera. Nikon NIS-Elements software was used for image acquisition (Nikon Corporation, Tokyo, Japan).

H. erectifolium cultivation for DNA and RNA sampling

A single plant of *H. erectifolium* accession NGB 6816 was grown in Conviron ADAPTIS (Conviron Europe Ltd., United Kingdom), 16h light, 8h dark, 20/16 °C day/night. Soil was a mixture of 93% (v/v) Einheitserde ED73 (Einheitserde Werkverband e.V., Sinntal_Altengronau, Germany), 6.6% (v/v) sand, and 0.4% (v/v) Osmocote exact standard 3-4M (Scotts Company LLC). All DNA and mature plant tissues for RNA were sampled from this plant.

DNA extraction and Oxford Nanopore Technology (ONT) DNA sequencing

High molecular weight (HMW) DNA was extracted from one gram of young leaf material, the leaves were ground in liquid nitrogen to a fine powder with pestle and mortar. HMW DNA was extracted in 20 mL of a modified Carlson lysis buffer (100 mM Tris-HCl, pH 9.5, 2% CTAB, 1.4 M NaCl, 2% PVP-40, 20 mM EDTA, 3mM EGTA, 0.25% beta-mercaptoethanol, 0.25 mg Rnase A), followed by purification using the Qiagen Genomic-tip 100/G (Qiagen, Cat. No: 10243) based on Oxford Nanopore Technology (ONT) HMW plant DNA extraction protocol(*Fever Tree (Cinchona Pubescens) Leaf DNA*, 2021). Purified HMW DNA was eluted in 500 uL EB and concentrations and purity measured on a Nanophotometer NP80 (IMPLEN, Germany). ONT DNA sequencing was made at two sequencing centers. There 21 libraries prepared with kit SQK-LSK109 and three libraries with SQK-RAD004, and each library was sequencing on an individual GridION R9.4.1 (FLO-MIN106) flowcell at the Max Planck-Genome-Centre Cologne (MP-GC) (Cologne, Germany). While three PromethION R9.4.1 (FLO-PRO002) flowcells prepared with library kit SQK-LSK110 were sequenced at the Genomics & Transcriptomics Laboratory, HHU (Düsseldorf, Germany).

Germinating seeds and seedling growth for RNAseq

Seeds of *H. erectifolium* harvested of the same plant as DNA and mature RNA samples were collected from were cleaned and only the main central grain was selected, thereafter the seeds were soaked in water overnight at RT in a 2 mL tube. Water was removed and the seeds were sterilized with 1 mL of 0.5% (v/v) sodium hypochlorite solution added, the seeds were incubated for 20 minutes and the tube was inverted every four minutes. The sodium hypochlorite solution was removed and the seeds washed four times with deionized water, before being plated on filter paper in a plastic Petri dish with moisture was added with dH_2O. Plates were sealed with Parafilm, covered in aluminium foil and place in 4°C for 5 days for stratification, thereafter placed in a growth chamber for 3 days. Germinating seeds were then transplanted into 0.7% (w/v) Phyto agar (Prod. No: P1003.1000, Duchefa Biochemie Haarlem, The Netherlands).

RNA sampling, extraction and PacBio IsoSeq sequencing

All mature RNA plant tissue samples were collected from the same plant as was previously harvested for DNA, seedlings and germinating seeds were from seeds of that same plant. In total 12 different tissues were sampled at two different time points, ZT 1-3 and ZT 13-15; shoot 8 days after germination (DAG), root 8 DAG, anthers, ovules, three developmental pools of spikes by their Waddington stage (W3-4.5, W5-6.5, W7-8) (Waddington et al., 1983), third internode, fourth node, flagleaf, caryops 10 days post anthesis (DPA), germinating seed. Two tissues were only sampled at one time point, the caryops and germinating seeds, in total 22 tissue samples were collected. Total RNA was extracted with Qiagen RNeasy Plant Mini Kit (Qiagen, Hilden, Germany, Cat. No. / ID: 74904), with addition of 0.2 % (v/v) beta-mercaptoethanol. The total RNA concentrations and purity was measured with Nanophotometer NP80 (IMPLEN, Germany). PacBio (Pacific Biosciences of California, Inc., USA) IsoSeq sequencing was made at the Genomics & Transcriptomics Laboratory, HHU Düsseldorf (Germany). The RNA samples had to have a RIN >= 8 before library preparation. Library preparations of the 22 RNA samples were prepared with TeloPrime (Lexogen GmbH, Vienna, Austria) 3'-prime and 5'-prime cap full length transcript capture and each of the samples was individually barcoded before sequencing.

10x Genomics and Illumina sequencing

HMW DNA was sent to Novogene (Novogene (UK) Company Limited, Cambridge, UK). For 10x Genomics linked read sequencing. Raw barcoded reads were processed with LongRanger (version 2.2.2) "longranger basic" with default parameters.

Genome size estimation with jellyfish and findGSE

We estimated the genome size, ploidy level, and heterozygosity with findGSE (version 1.94), first Jellyfish (version 2.3.0) was used to count the 21-mers of the processed Illumina short-reads (Marçais & Kingsford, 2011; H. Sun et al., 2018). Parameters used were; Jellyfish: "jellyfish count *fastq -C -m 21 -s 20G -o 21mer ; jellyfish histo -h 3000000 -o 21mer.histo", and findGSE: "findGSE(findGSE(histo="21mer.histo", sizek=21)"

ONT long-read data processing and assembly with Flye

The raw sequencing singal fast5 data files were basecalled with Guppy 5.0.7 (ONT, United Kingdom) using the Super Accuracy Model and using the appropriate configuration file for each flowcell and

library kit combination. Parameters used: “guppy_basecaller -c ${CONFIG} -min_qscore 7 -device cuda:0 -recursive -calib_detect”. Read quality and length distribution was visualized with NanoPlot (version 1.32.1) “-fastq *fastq.gz -loglength -N50” (De Coster & Rademakers, 2023). ONT long-reads were further processed with porechop (version 0.2.4): “-check_reads 1000 -discard_middle” (Wick et al., 2017). Porechopped reads were then assembled with Flye (version 2.9b1774): “-g 4.4g -m 10000 -nano-hq -extra-params max_bubble_length=300000” (Kolmogorov et al., 2019). As part of the Flye’s internal pipeline it did the first round of assembly polishing with long-reads.

Assembly polishing with ONT long-read and Illumina short-read data

The assembled contigs from Flye were further polished and the first long-read polishing steps were performed as recommended by ONT. All porechopped ONT long-reads were mapped to the Flye assembled contigs with Minimap2 (version 2.22-r1110-dirty): “-ax map-ont -2 -I 10G -K 50G -secondary=no” (Li, 2018). The assembly was then polished with Racon (version 1.4.21): “-m 8 -x -6 -g -8 -w 500” and then with Medaka (version 1.4.3): “-model r941_prom_sup_g507” (*Nanoporetech/Medaka*, 2017/2024; Vaser et al., 2017). Finally the 10X Genomics Illumina short-reads were mapped to the long-read polished genome with BWA-MEM2 (version 2.2.1) default settings and BAM file curated with Samtools (version 1.15) “samtools view - -Sb -F 256 | samtools sort -” (Danecek et al., 2021; Vasimuddin et al., 2019). Two rounds of short-read polishing were performed with Hapo-G (version 1.1) “-genome $asm -b $bam -o $out -u”, 10X Genomics Illumina short-reads were re-mapped as before to the output of first round of short-read polishing (Aury & Istace, 2021).

Scaffolding of the assembled and polished contigs

After final polishing of the assembled contigs, the 10x Genomics linked reads were used to correct and scaffold the polished contigs using Tigmint (version 1.2.4)-ARCS (version 1.2.2) pipeline with default parameters: “tigmint-make arcs “ (Jackman et al., 2018). A clone of the sequenced *H. erectifolium* plant was send to Hana Šimková, Centre of Plant Structural and Functional Genomics, Olomouc, Czech Republic. Where her group did the Bionano hybrid-scaffolding of the corrected assembly. The hybrid-scaffolded assembly we received back was finally arranged to pseudomolecules scale with Hi-C chromosome conformation capture and the TRITEX pipeline was used and the final results manual curated (Monat et al., 2019). Seeds of *H. erectifolium* were sent to the sequencing center of IPK Gatersleben (Germany). There Hi-C chromosomal conformation capture libraries were generated and sequenced with PE150 Illumina short-reads sequencing.

Assembly quality benchmarks

Estimation of assembly quality, completeness after each polishing step of the assembled genome were performed with the Merqury toolkit (Rhie et al., 2020). The 10x Genomics Illumina PE150 reads were used to build the kmer database with meryl (version 1.4), “meryl k=21 count Herectifolium_R*.fq.gz output Herectifolium.meryl”. Merqury was then used to evaluated each step of the assembly, “merqury.sh db.meryl $asm $out”. We used BUSCO (version 5.4.7) along with poales_odb10 dataset, (2020-08-05), to estimate genespace completeness of the assembly “-m genome” and transcriptomes “-m transcriptome” (Manni et al., 2021). QUAST (version 5.2.0) was used to collect genome assembly statistics, “quast.py -no-icarus -large” of the assemblies at each step of polishing and scaffolding (Mikheenko et al., 2018).

PacBio IsoSeq data processing and gene structural annotation

The PacBio IsoSeq sequencing data from the 22 samples were merged together with Samtools merge (version 1.16.1) before mapping to the finished genome assembly. We trimmed the ploy-A tails and removed concatenated transcripts with the isoseq3 (version 3.8.2) pipline "refine -require-polya -min-polya-length 12 teloprime.fasta" (*PacBio - IsoSeq3*, 2018/2024). Reads were then mapped to the genome with pbmm2 (version 1.10.0) "align -preset ISOSEQ -sort -bam-index CSI" and redundant transcripts collapsed with isoseq3 collapse " -do-not-collapse-extra-5exons" as samples were treated as bulk sequenced. To predict open reading frames (ORF) of collapsed IsoSeq sequencing reads TransDecoder (version 5.7.0) was used " -m 30 -S -complete_orfs_only", along with Diamond (version 2.1.5) "-very-sensitive -outfmt 6 -evalue 1e-5 -max-target-seqs 1" using UniProt90 2023_01 database and hmmscan (HMMER version 3.3.2) "-domtblout" with Pfam v35 database for the final ORF prediction selection, " -single_best_only" (Blum et al., 2021; Buchfink et al., 2021; *GitHub - TransDecoder/TransDecoder: TransDecoder Source*, 2023; The UniProt Consortium et al., 2023). Finally, Helixer (version 0.3.1) "-lineage land_plant" model land_plant_v0.3_a_0080.h5, was used to *de novo* structurally predict genes in the genome (Holst et al., 2023). Predictions from IsoSeq-TransDecoder and Helixer were compared for redundancy, with preference towards IsoSeq-TransDecoder. If there were overlapping CDS predictions for a transcript but UTRs were different, IsoSeq-TransDecoder transcripts were selected over Helixer predictions. (Custom script). Both predictions were then merged with AGAT (version 1.2.0) (Jacques Dainat et al., 2024).

lncRNA annotation pipeline

Nine tools were used to predict lncRNA for each transcript in the IsoSeq data; RNAsamba (v. 0.2.4), CPAT (v. 3.0.4), RNAplonc (v. 1.1), PlncPRO (v. 1.2.2), LncADeep (v. 1.0), CPPred (v. 2018-05-17), CPC2 (v. 0.1), CNCI (v. 2 Feb 28, 2014), PlncDB_V2.0 (Camargo et al., 2020; Jin et al., 2021; Kang et al., 2017; Negri et al., 2019; Singh et al., 2017; L. Sun et al., 2013; Tong & Liu, 2019; Wang et al., 2013; Yang et al., 2018). In short, if a transcript of a gene was predicted noncoding in seven out of nine predictors and that gene had other transcripts with two or less out of nine predicted as protein coding, no hit of evalue <= 10e-5 and subject cover less than 25 % in UniRef90 (2023_2) protein database after alignment with Diamond (v. 2.1.8), and had no domains predicted by InterProScan (v. 5.62-94.0) for that gene it was assigned as Putative_lncRNA (Jones et al., 2014).

Functional gene annotation

Protein coding transcripts were functionally annotated and GO terms assigned with InterProScan-5.67-99.0 "-goterms -f tsv -dp", and additionally proteins were annotated with Mercator4 (v6.0) (Bolger et al., 2021). Protein coding genes and their isoforms were classified as high (HC) or low confidence (LC) predictions. The protein-coding transcriptome was aligned with Diamond (v. 2.1.8) "blastx -outfmt 6 qseqid sseqid pident length mismatch gapopen qstart qend sstart send evalue bitscore qlen slen qcovhsp scovhsp positive-very-sensitive -masking 0" to the UniRef100 (2024_04) reference protein database. High confidence was assigned to genes that had a match >= 80 % similarity otherwise they were assigned as low confidence.

Representative gene sequence and representative isoform per gene

There were multiple transcripts per gene that coded for the same amino acid sequence (CDS) but differed only in their UTR lengths. We removed redundant transcripts with CD-HIT (v. 4.8.1): "-c

0.99 -n 5 -G 0 -d 0 -s 0.99 -aS 0.99 -AS 1 -AL 1" and selected a representative of identical isoform CDSs using a custom script (Fu et al., 2012). A representative isoform per gene was selected by aligning each protein-coding transcript against the UniRef90 (2023_02) protein database with Diamond (v. 2.1.8) "blastx -outfmt 6 qseqid sseqid pident length mismatch gapopen qstart qend sstart send evalue bitscore qlen slen qcovhsp scovhsp -ultra-sensitive -masking 0 -evalue 1e-05". The isoform with the highest alignment score (based on bitscore, evalue, qcovhsp) was chosen as the representative isoform for that gene. For genes that did not have any hit in the reference database and putative lncRNAs we selected the longest transcript as the representative.

Transposable element annotation with EDTA

Annotations of Transposable elements (TE) and repetitive regions were made with EDTA (v. 2.2.0) (Ou et al., 2019), "EDTA.pl -anno 1 -cds libCDS.fa". A curated library of CDSs, libCDS.fa, was generated for EDTA from a combined non-redundant library of high confidence CDSs from *H. erectifolium* and Morex gene annotations with CD-HIT (v. 4.8.1) "-c 0.95 -n 5 -d 0". We used TEsorter (v. 1.4.6) to further classify unknown LTR superfamilies found by EDTA with a higher sensitivity threshold into either Gypsy or Copia using "-db rexdb-plant -rule 70-30-80" (Zhang et al., 2022).

Estimating telomeric ends and predicting centromeric positions

We identified the telomeres by aligning the sequence TTTAGGGn8 to the genomes of *H. erectifolium* acc. NGB6816, *H. vulgare* cv. Morex and *H. v. spontaneum* acc. B1K-04-12 with BLAST+ 2.15.0: "blastn -task blastn-short" (Camacho et al., 2009). We merged the alignments and joined interval gaps smaller than 1000 bp with bedtools (v2.31.0) : "bedtools merge -i -d 1000". We extracted the protein coding domains of annotated and complete CRM LTR sequences from from the EDTA annotation of the genomes of *H. erectifolium* acc. NGB6816 and *H. vulgare* cv. Morex. The CRM sequences were then aligned to the genomes including *H. v. spontaneum* acc. B1K-04-12 with BLAST+ 2.15.0: " blastn -task blastn -dust no". We merged the alignments and joined interval gaps smaller than 1000 bp with bedtools (v2.31.0) : "bedtools merge -i -d 1000". The identified merged CRM segments were then divided into fragments of 100 bp with bedtools "bedtools makewindows -b $file -w 100" before importing into R (v. 4.4.1) (Quinlan & Hall, 2010; R Core Team, 2024). The fragment density regions of CRM alignments were calculated with hdrcde (v. 3.4) in R and the 50 % confidence interval was chosen as a representative border of the centromere size (Hyndman et al., 2023).

Chromosomal synteny analyzed with SyRI and plotsr

Chromosomal synteny was calculated and visualized by mapping the *H. erectifolium* acc. NGB6816 against *H. vulgare* cv. Morex, and then *H. vulgare* cv. Morex against *H. v. spontaneum* acc. B1K-04-12 with minimap2 (v. 2.28-r1209); "-K 5G -f 0.005 -eqx -c -x asm5" (Li, 2018). Chromosomal alignments were first calculated with Synteny and Rearrangement Identifier (SyRI) (v. 1.6.3) and then inversions >= 1 Mb, syntenic regions, telomeric ends, and centromeres were plotted with plotsr (v. 1.1.0) "-s 1000000 -markers markers_cen_telo.txt -R -nodup -notr" (Goel et al., 2019; Goel & Schneeberger, 2022).

Quantitatification of PacBio IsoSeq data and tissue specific expression with IsoQuant

We further quantified transcript levels of the 22 plant tissue samples sequenced with PacBio IsoSeq and were initially used for structural gene annotation. Here we used IsoQuant (v. 3.4.1) "-data_type

pacbio_ccs -fl_data -normalization_method usable_reads" to map and quantify the full length PacBio IsoSeq transcripts against the annotated *H. erectifolium* acc. NGB6816 genome (Prjibelski et al., 2023). We used the normalized transcripts per million (TPM) output of IsoQuant for Principal component analysis (PCA) in R with the built-in function prcomp. We selected and visualized the top 20 genes contributing the most to principal component 1 (PC1) and 2 (PC2).

Gene family evolution analysis with Orthofinder and CAFE5

All proteomes except *H. erectifolium* and *H. vulgare* cv. Morex, (Hv_Morex.pgsb.Jul2020), were retrived from the JGI Phytozome database; Athaliana_447_Araport11, Bdistachyon_556_v3.2, Osativa_323_v7.0, Sbicolor_730_v5.1, Taestivumcv_ChineseSpring_725_v2.1, Zmays_833_Zm-B73-REFERENCE-NAM-5.0.55 (Goodstein et al., 2012). The "primaryTranscriptOnly" protein annotation files curated by JGI assemblies were used. The primary transcript of *H. erectifolium* gene annotation was selected and the longest transcript form *H. vulgare* cv. Morex annotation. The curated protein annotations of the nine species were assigned to Phylogenetic Hierarchical Orthogroups (HOG) with Orthofinder (v. 2.5.5): "-M msa" (Emms & Kelly, 2019). The rooted species tree generated by Orthofinder was converted to ultrametric "make_ultrametric.py -r 160000000 SpeciesTree_rooted.txt" by providing a species separation date of 160 Mya between *H. erectifolium* and *A. thaliana,* retrived from TimeTree 5 (Kumar et al., 2022). We calculated the gene family evolution using the gene count "orthogroup_gene_count.py N0.tsv" at the root, N0, of HOGs, with CAFE5 (v. 1.1): "-p -k 7" (Mendes et al., 2021). Finally we used CafePlotter (v. 0.2.0): "-ignore_branch_length" to summarize and visualize the results from CAFE5 (moshi, 2023/2024). Functional analysis of genes unique to *H. erectifolium* was made with Clusterprofiler (v. 4.12.6) and rrvgo (v. 1.16.0) (Sayols, 2023; Xu et al., 2024).

Annotation of SWEETs and phylogenetic reconstruction

The proteomes used in the gene family evolution analysis were additionally re-annotated with InterProScan (v. 5.67-99.0). Genes which were annotated as containing two Sugar transporter SWEET repeat (IPR004316) domains had their amino acid sequence extracted. The identified sequences were aligned against each other with MUSCLE (v. 5.1): "-align $file -diversified ; -disperse ; -maxcc" and a phylogenetic tree built with IQ-TREE (v. multicore version 2.3.0 COVID-edition): "iqtree -s $file -B 1000 -alrt 1000 -mset JTT -bnni -wsplits" (Edgar, 2022; Minh et al., 2020). Visualization of the SWEET tree was made in R with ggtree (v. 3.12.0). Classification of SWEET gene homology assignment was made by aligning the *H. erectifolium* sequnces against a manually curated SWEET annotations form Yue et al., 2023 (Yue et al., 2023).We searched for additional genes annotated as belonging to the SWEET family (IPR047664) and as generally eukaryotic SWEET genes contain two MtN3/saliva or SWEET_rpt domains (IPR004316), we excluded single domain genes.

Experimental setup for cross-species dry-down experiment

Experiments were performed in a controlled-environment Fitotron SGC Weiss Technik (Reiskirchen, Germany) growth chambers. Individual seeds were sown in 7×7×8 cm black plastic pots; 40 pots (5×8 rows) per tray. Each pot was filled with exactly 150 g of soil mixture. A mixture of 93% (v/v) Einheitserde ED73 (Einheitserde Werkverband e.V., Sinntal_Altengronau, Germany), 6.6% (v/v) sand, and 0.4% (v/v) Osmocote exact standard 3-4M (Scotts Company LLC), was freshly prepared before sowing. Seeds were stratified in well-watered soil at 4 °C in the dark for at least 4 days. The

plants of the two species plants were grown for different periods until start of drought initiation so that they would have similar biomass. The spring barley Morex was grown for two weeks under 12h photoperiod conditions (12h light, 12h dark, at 20°C day/16°C night, 60% relative humidity, photosynthetically active radiation ~300 µM m-2 s-1) before the start of the dry-down to make sure that the plants remained in the vegetative stage. By contrast, *H. erectifolium* plants were grown for seven weeks under long day conditions, 16 hours light so that they develop a comparable amount of biomass, but remain vegetative as *H. erectifolium* requires vernalization to transition to reproductive growth. We then transferred the *H. erectifolium* plants for five days to 12h photoperiod conditions (12h light, 12h dark, at 20°C day/16°C night, 60% relative humidity, photosynthetically active radiation ~300 µM m-2 s-1) to synchronize the diurnal patterns of Morex and *H. erectifolium* plants before the start of dry-down.

Soil field capacity (FC) was gravimetrically calculated at each sowing, 100 % FC was set as fully hydrated soil and then it was dried at 70 °C for 3 days which was then 0 % FC. Soil FC was adjusted to 50 %, before withholding water for six days for the dry-down treatment, while control plants were maintained at 50 % soil FC. On the 6th day of treatment (DOT6), drought-treated plants were re-watered to 50 % soil FC. Replicate samples were collected from both control and drought treatments at three time points during dry-down on DOT 2, 5, and 6, the final sample was taken on DOT 7, 24 hours after re-watering. At each time-point, four replicate samples were collected from the second leaf at ZT 8 for transcriptomic analyses per treatment consisting of a pool of two plants per sample and frozen in liquid nitrogen. Leaf relative water content (RWC) was measured during each sampling as leaf fresh weight, then leaves soaked overnight at 4 °C in the dark for turgid weight and then dry weight after drying at 70 °C. Calculated as: (fresh weight - dry weight)/(turgid weight - dry weight = RWC) (Smart and Bingham, 1974).

Total RNA was extracted with Qiagen RNeasy Plant Mini Kit (Qiagen, Hilden, Germany, Cat. No. / ID: 74904), with addition of 0.2 % (v/v) beta-mercaptoethanol. RNA quantity and quality was assessed with NanoPhotometer NP80 (IMPLEN, Germany) and on a 1 % agarose gel. Purified total RNA samples were sequenced at Novogene UK (Cambridge, UK). RNA paired-end (PE) libraries were prepared by poly-A tail capture and Illumina PE150 sequenced.

Dry-down experiment RNAseq and differential gene expression with maSigPro and edgeR

The raw reads of the Illumina PE150 sequenced RNA libraries were quality controlled with FastQC (v. 0.12.1) and MulitQC (v. 1.12) to collate the reports (Andrews, 2010; Ewels et al., 2016). STAR (v. 2.7.11a) was used to map the RNAseq reads to their respective genome "Genome index: STAR -runMode genomeGenerate -genomeFastaFiles $genome -sjdbGTFfile $gtf -sjdbOverhang 149; RNAseq alignment: STAR -outSAMtype BAM SortedByCoordinate -quantMode TranscriptomeSAM GeneCounts" (Dobin et al., 2013). Read quantification was done with featureCounts (subread v. 2.0.6) "featureCounts -O -countReadPairs -p -G $genome -J -a $gtf" (Liao et al., 2014). Quantified reads were normalized with edgeR (v. 4.2.1) with experimental setup as groups (Chen et al., 2024). Normalized reads from edgeR were used in time-course analysis with maSigPro (v. 1.76.0) were transcriptomic changes in response to drought over time was analyzed (Nueda et al., 2014). edgeR was further used to quantify DEGs at individual time-points. Clusterprofiler (v. 4.12.6) was used for GO enrichment analyses and ComplexHeatmap (v. 2.20.0) for visualization of top 9 functional enriched terms in GSEA (Gu, 2022). Single copy orthologs between

H. erectifolium and Morex were retrieved from the Phylogenetic Hierarchical Orthogroups (HOG) analyses in Orthofinder and were further restricted by belonging to the same chromosome.

7. Supplemental data

Supplemental data: https://doi.org/10.60507/FK2/DDQAA0

S1_Sequencing_data.xlsx

S2_Assembly_stats_scaffolding.xlsx

S3_Polishing_Merqury.xlsx

S4_Herectifolium_NGB6816_ONT_Gene.Annotation.stats.xlsx

S5_EDTA.xlsx

S6_DEGs_pairwise_and_timeseries_r0.7.xlsx

S7_HOGs_CAFE5_analysis.xlsx

S8_Single_copy_DEG_orthologs.xlsx

S9_Expressed_SWEETs_PacBio_IsoSeq.xlsx

8. References

Akakpo, R., Carpentier, M.-C., Ie Hsing, Y., & Panaud, O. (2020). The impact of transposable elements on the structure, evolution and function of the rice genome. *New Phytologist*, *226*(1), 44–49. https://doi.org/10.1111/nph.16356

Andrews, S. (2010). *FastQC: a quality control tool for high throughout sequence data.* https://www.bioinformatics.babraham.ac.uk/projects/fastqc/

Artur, M. A. S., Zhao, T., Ligterink, W., Schranz, E., & Hilhorst, H. W. M. (2019). Dissecting the Genomic Diversification of Late Embryogenesis Abundant (LEA) Protein Gene Families in Plants. *Genome Biology and Evolution*, *11*(2), 459–471. https://doi.org/10.1093/gbe/evy248

Aury, J.-M., & Istace, B. (2021). Hapo-G, haplotype-aware polishing of genome assemblies with accurate reads. *NAR Genomics and Bioinformatics*, *3*(2), lqab034. https://doi.org/10.1093/nargab/lqab034

Balsamo, R., Boak, M., Nagle, K., Peethambaran, B., & Layton, B. (2015). Leaf biomechanical properties in *Arabidopsis thaliana* polysaccharide mutants affect drought survival. *Journal of Biomechanics*, *48*(15), 4124–4129. https://doi.org/10.1016/j.jbiomech.2015.10.016

Barbosa, M. A. M., Chitwood, D. H., Azevedo, A. A., Araújo, W. L., Ribeiro, D. M., Peres, L. E. P., Martins, S. C. V., & Zsögön, A. (2019). Bundle sheath extensions affect leaf structural and physiological plasticity in response to irradiance. *Plant, Cell & Environment*, *42*(5), 1575–1589. https://doi.org/10.1111/pce.13495

Bariah, I., Keidar-Friedman, D., & Kashkush, K. (2020). Where the Wild Things Are: Transposable Elements as Drivers of Structural and Functional Variations in the Wheat Genome. *Frontiers in Plant Science*, *11*. https://doi.org/10.3389/fpls.2020.585515

Basu, S., Ramegowda, V., Kumar, A., & Pereira, A. (2016). *Plant adaptation to drought stress* (No. 5:1554). F1000Research. https://doi.org/10.12688/f1000research.7678.1

Bennetzen, J. L., Ma, J., & Devos, K. M. (2005). Mechanisms of Recent Genome Size Variation in Flowering Plants. *Annals of Botany*, *95*(1), 127–132. https://doi.org/10.1093/aob/mci008

Berry, Z. C., Emery, N. C., Gotsch, S. G., & Goldsmith, G. R. (2019). Foliar water uptake: Processes, pathways, and integration into plant water budgets. *Plant, Cell & Environment*, *42*(2), 410–423. https://doi.org/10.1111/pce.13439

Blattner, F. R. (2006). Multiple intercontinental dispersals shaped the distribution area of Hordeum (Poaceae). *New Phytologist*, *169*(3), 603–614. https://doi.org/10.1111/j.1469-8137.2005.01610.x

Blum, M., Chang, H.-Y., Chuguransky, S., Grego, T., Kandasaamy, S., Mitchell, A., Nuka, G., Paysan-Lafosse, T., Qureshi, M., Raj, S., Richardson, L., Salazar, G. A., Williams, L., Bork, P., Bridge, A., Gough, J., Haft, D. H., Letunic, I., Marchler-Bauer, A., … Finn, R. D. (2021). The InterPro protein families and domains database: 20 years on. *Nucleic Acids Research*, *49*(D1), D344–D354. https://doi.org/10.1093/nar/gkaa977

Bolger, M., Schwacke, R., & Usadel, B. (2021). MapManMapMan Visualization of RNA-Seq Data Using Mercator4Mercator4 Functional Annotations. In D. Dobnik, K. Gruden, Ž. Ramšak,

& A. Coll (Eds.), *Solanum tuberosum: Methods and Protocols* (pp. 195–212). Springer US. https://doi.org/10.1007/978-1-0716-1609-3_9

Bothmer, R. von, Jacobsen, N., & Jørgensen, R. B. (1985). Two New American Species of Hordeum (Poaceae). *Willdenowia*, *15*(1), 85–90.

Bothmer, R. von, Jacobsen, N., Baden, C., Jorgensen, R. B., & Linde-Laursen, I. (1995). *An ecogeographical study of the genus Hordeum (2nd edition)*. https://hdl.handle.net/10568/104311

Bothmer, R. von, Jacobsen, N., & Jørgensen, R. B. (1985). Two New American Species of Hordeum (Poaceae). *Willdenowia*, *15*(1), 85–90.

Brassac, J., & Blattner, F. R. (2015). Species-Level Phylogeny and Polyploid Relationships in Hordeum (Poaceae) Inferred by Next-Generation Sequencing and In Silico Cloning of Multiple Nuclear Loci. *Systematic Biology*, *64*(5), 792–808. https://doi.org/10.1093/sysbio/syv035

Buchfink, B., Reuter, K., & Drost, H.-G. (2021). Sensitive protein alignments at tree-of-life scale using DIAMOND. *Nature Methods*, *18*(4), 366–368. https://doi.org/10.1038/s41592-021-01101-x

Buckley, T. N. (2005). The control of stomata by water balance. *New Phytologist*, *168*(2), 275–292. https://doi.org/10.1111/j.1469-8137.2005.01543.x

Buckley, T. N., Sack, L., & Gilbert, M. E. (2011). The Role of Bundle Sheath Extensions and Life Form in Stomatal Responses to Leaf Water Status. *Plant Physiology*, *156*(2), 962–973. https://doi.org/10.1104/pp.111.175638

Butlin, R. K., & Faria, R. (2024). Local adaptation and reproductive isolation: When does speciation start? *Evolutionary Journal of the Linnean Society*, *3*(1), kzae003. https://doi.org/10.1093/evolinnean/kzae003

Cai, W., McPhaden, M. J., Grimm, A. M., Rodrigues, R. R., Taschetto, A. S., Garreaud, R. D., Dewitte, B., Poveda, G., Ham, Y.-G., Santoso, A., Ng, B., Anderson, W., Wang, G., Geng, T., Jo, H.-S., Marengo, J. A., Alves, L. M., Osman, M., Li, S., … Vera, C. (2020). Climate impacts of the El Niño–Southern Oscillation on South America. *Nature Reviews Earth & Environment*, *1*(4), 215–231. https://doi.org/10.1038/s43017-020-0040-3

Camacho, C., Coulouris, G., Avagyan, V., Ma, N., Papadopoulos, J., Bealer, K., & Madden, T. L. (2009). BLAST+: Architecture and applications. *BMC Bioinformatics*, *10*(1), Article 1. https://doi.org/10.1186/1471-2105-10-421

Camargo, A. P., Sourkov, V., Pereira, G. A. G., & Carazzolle, M. F. (2020). RNAsamba: Neural network-based assessment of the protein-coding potential of RNA sequences. *NAR Genomics and Bioinformatics*, *2*(1), lqz024. https://doi.org/10.1093/nargab/lqz024

Candat, A., Paszkiewicz, G., Neveu, M., Gautier, R., Logan, D. C., Avelange-Macherel, M.-H., & Macherel, D. (2014). The Ubiquitous Distribution of Late Embryogenesis Abundant Proteins across Cell Compartments in Arabidopsis Offers Tailored Protection against Abiotic Stress. *The Plant Cell*, *26*(7), 3148–3166. https://doi.org/10.1105/tpc.114.127316

Chandra, A. K., Jha, S. K., Agarwal, P., Mallick, N., Niranjana, M., & Vinod. (2022). Leaf rolling in bread wheat (Triticum aestivum L.) is controlled by the upregulation of a pair of closely

linked/duplicate zinc finger homeodomain class transcription factors during moisture stress conditions. *Frontiers in Plant Science*, *13*. https://doi.org/10.3389/fpls.2022.1038881

Chen, Q., Hu, T., Li, X., Song, C.-P., Zhu, J.-K., Chen, L., & Zhao, Y. (2022). Phosphorylation of SWEET sucrose transporters regulates plant root:shoot ratio under drought. *Nature Plants*, *8*(1), 68–77. https://doi.org/10.1038/s41477-021-01040-7

Chen, Y., Chen, L., Lun, A. T. L., Baldoni, P. L., & Smyth, G. K. (2024). *edgeR 4.0: Powerful differential analysis of sequencing data with expanded functionality and improved support for small counts and larger datasets* (p. 2024.01.21.576131). bioRxiv. https://doi.org/10.1101/2024.01.21.576131

Chapman, E. A., Thomsen, H. C., Tulloch, S., Correia, P. M. P., Luo, G., Najafi, J., DeHaan, L. R., Crews, T. E., Olsson, L., Lundquist, P.-O., Westerbergh, A., Pedas, P. R., Knudsen, S., & Palmgren, M. (2022). Perennials as Future Grain Crops: Opportunities and Challenges. *Frontiers in Plant Science*, *13*. https://doi.org/10.3389/fpls.2022.898769

Danecek, P., Bonfield, J. K., Liddle, J., Marshall, J., Ohan, V., Pollard, M. O., Whitwham, A., Keane, T., McCarthy, S. A., Davies, R. M., & Li, H. (2021). Twelve years of SAMtools and BCFtools. *GigaScience*, *10*(2), giab008. https://doi.org/10.1093/gigascience/giab008

Dar, A. A., Choudhury, A. R., Kancharla, P. K., & Arumugam, N. (2017). The FAD2 Gene in Plants: Occurrence, Regulation, and Role. *Frontiers in Plant Science*, *8*. https://doi.org/10.3389/fpls.2017.01789

Dassanayake, M., Oh, D., Hong, H., Bohnert, H. J., & Cheeseman, J. M. (2011). Transcription strength and halophytic lifestyle. *Trends in Plant Science*, *16*(1), 1–3. https://doi.org/10.1016/j.tplants.2010.10.006

Dawson, I. K., Russell, J., Powell, W., Steffenson, B., Thomas, W. T. B., & Waugh, R. (2015). Barley: A translational model for adaptation to climate change. *New Phytologist*, *206*(3), 913–931. https://doi.org/10.1111/nph.13266

De Coster, W., & Rademakers, R. (2023). NanoPack2: Population-scale evaluation of long-read sequencing data. *Bioinformatics*, *39*(5), btad311. https://doi.org/10.1093/bioinformatics/btad311

Deneweth, J., Van de Peer, Y., & Vermeirssen, V. (2022). Nearby transposable elements impact plant stress gene regulatory networks: A meta-analysis in A. thaliana and S. lycopersicum. *BMC Genomics*, *23*(1), Article 1. https://doi.org/10.1186/s12864-021-08215-8

Dobin, A., Davis, C. A., Schlesinger, F., Drenkow, J., Zaleski, C., Jha, S., Batut, P., Chaisson, M., & Gingeras, T. R. (2013). STAR: Ultrafast universal RNA-seq aligner. *Bioinformatics*, *29*(1), 15–21. https://doi.org/10.1093/bioinformatics/bts635

Edgar, R. C. (2022). Muscle5: High-accuracy alignment ensembles enable unbiased assessments of sequence homology and phylogeny. *Nature Communications*, *13*(1), 6968. https://doi.org/10.1038/s41467-022-34630-w

Emms, D. M., & Kelly, S. (2019). OrthoFinder: Phylogenetic orthology inference for comparative genomics. *Genome Biology*, *20*(1), Article 1. https://doi.org/10.1186/s13059-019-1832-y

Ewels, P., Magnusson, M., Lundin, S., & Käller, M. (2016). MultiQC: Summarize analysis results for multiple tools and samples in a single report. *Bioinformatics*, *32*(19), 3047–3048. https://doi.org/10.1093/bioinformatics/btw354

FAOSTAT. (2024). FAOSTAT. https://www.fao.org/faostat/en/#data/QCL

Feuillet, C., Langridge, P., & Waugh, R. (2008). Cereal breeding takes a walk on the wild side. *Trends in Genetics*, *24*(1), 24–32. https://doi.org/10.1016/j.tig.2007.11.001

Fever tree (Cinchona pubescens) leaf DNA. (2021, September 10). Oxford Nanopore Technologies. https://nanoporetech.com/document/extraction-method/fever-tree-gdna

Foyer, C. H., & Shigeoka, S. (2010). Understanding Oxidative Stress and Antioxidant Functions to Enhance Photosynthesis. *Plant Physiology*, *155*(1), 93. https://doi.org/10.1104/pp.110.166181

Franks, S. J., Sim, S., & Weis, A. E. (2007). Rapid evolution of flowering time by an annual plant in response to a climate fluctuation. *Proceedings of the National Academy of Sciences*, *104*(4), 1278–1282. https://doi.org/10.1073/pnas.0608379104

Fu, L., Niu, B., Zhu, Z., Wu, S., & Li, W. (2012). CD-HIT: Accelerated for clustering the next-generation sequencing data. *Bioinformatics*, *28*(23), 3150–3152. https://doi.org/10.1093/bioinformatics/bts565

Galdon-Armero, J., Fullana-Pericas, M., Mulet, P. A., Conesa, M. A., Martin, C., & Galmes, J. (2018). The ratio of trichomes to stomata is associated with water use efficiency in Solanum lycopersicum (tomato). *The Plant Journal*, *96*(3), 607–619. https://doi.org/10.1111/tpj.14055

Garay-Arroyo, A., Colmenero-Flores, J. M., Garciarrubio, A., & Covarrubias, A. A. (2000). Highly Hydrophilic Proteins in Prokaryotes and Eukaryotes Are Common during Conditions of Water Deficit*. *Journal of Biological Chemistry*, *275*(8), 5668–5674. https://doi.org/10.1074/jbc.275.8.5668

Gautam, T., Saripalli, G., Gahlaut, V., Kumar, A., Sharma, P. K., Balyan, H. S., & Gupta, P. K. (2019). Further studies on sugar transporter (SWEET) genes in wheat (Triticum aestivum L.). *Molecular Biology Reports*, *46*(2), 2327–2353. https://doi.org/10.1007/s11033-019-04691-0

GitHub—TransDecoder/TransDecoder: TransDecoder source. (2023). TransDecoder. https://github.com/TransDecoder/TransDecoder

Goel, M., & Schneeberger, K. (2022). plotsr: Visualizing structural similarities and rearrangements between multiple genomes. *Bioinformatics*, *38*(10), 2922–2926. https://doi.org/10.1093/bioinformatics/btac196

Goel, M., Sun, H., Jiao, W.-B., & Schneeberger, K. (2019). SyRI: Finding genomic rearrangements and local sequence differences from whole-genome assemblies. *Genome Biology*, *20*(1), 277. https://doi.org/10.1186/s13059-019-1911-0

Gong, X., Wang, F., Chen, H., Liu, X., Zhang, S., Zhao, J., & Yi, J. (2022). Genetic Mapping and Transcriptomic Analysis Revealed the Molecular Mechanism Underlying Leaf-Rolling and a Candidate Protein Phosphatase Gene for the Rolled Leaf-Dominant (RL-D) Mutant in Rice. *Plant Molecular Biology Reporter*, *40*(2), 256–270. https://doi.org/10.1007/s11105-021-01318-2

Goodstein, D. M., Shu, S., Howson, R., Neupane, R., Hayes, R. D., Fazo, J., Mitros, T., Dirks, W., Hellsten, U., Putnam, N., & Rokhsar, D. S. (2012). Phytozome: A comparative platform for green plant genomics. *Nucleic Acids Research*, *40*(D1), D1178–D1186. https://doi.org/10.1093/nar/gkr944

Groen, S. C., Ćalić, I., Joly-Lopez, Z., Platts, A. E., Choi, J. Y., Natividad, M., Dorph, K., Mauck, W. M., Bracken, B., Cabral, C. L. U., Kumar, A., Torres, R. O., Satija, R., Vergara, G., Henry, A., Franks, S. J., & Purugganan, M. D. (2020). The strength and pattern of natural selection on gene expression in rice. *Nature*, *578*(7796), 572–576. https://doi.org/10.1038/s41586-020-1997-2

Grünhofer, P., Schreiber, L., & Kreszies, T. (2021). Suberin in Monocotyledonous Crop Plants: Structure and Function in Response to Abiotic Stresses. In S. Mukherjee & F. Baluška (Eds.), *Rhizobiology: Molecular Physiology of Plant Roots* (pp. 333–378). Springer International Publishing. https://doi.org/10.1007/978-3-030-84985-6_19

Gu, Z. (2022). Complex heatmap visualization. *iMeta*, *1*(3), e43. https://doi.org/10.1002/imt2.43

Guo, K., Liu, M., Vella, D., Suresh, S., & Hsia, K. J. (2024). Dehydration-induced corrugated folding in Rhapis excelsa plant leaves. *Proceedings of the National Academy of Sciences*, *121*(17), e2320259121. https://doi.org/10.1073/pnas.2320259121

Hand, S. C., Menze, M. A., Toner, M., Boswell, L., & Moore, D. (2011). LEA Proteins During Water Stress: Not Just for Plants Anymore. *Annual Review of Physiology*, *73*(Volume 73, 2011), 115–134. https://doi.org/10.1146/annurev-physiol-012110-142203

Hakeem, S., Ali, Z., Saddique, M. A. B., Habib-ur-Rahman, M., & Trethowan, R. (2021). Leaf prickle hairs and longitudinal grooves help wheat plants capture air moisture as a water-smart strategy for a changing climate. *Planta*, *254*(1), 18. https://doi.org/10.1007/s00425-021-03645-w

Hasanuzzaman, M., Nahar, K., Anee, T. I., & Fujita, M. (2017). Glutathione in plants: Biosynthesis and physiological role in environmental stress tolerance. *Physiology and Molecular Biology of Plants*, *23*(2), 249–268. https://doi.org/10.1007/s12298-017-0422-2

Hassan, A. H., Mokhtar, M. M., & El Allali, A. (2024). Transposable elements: Multifunctional players in the plant genome. *Frontiers in Plant Science*, *14*. https://doi.org/10.3389/fpls.2023.1330127

Haworth, M., & McElwain, J. (2008). Hot, dry, wet, cold or toxic? Revisiting the ecological significance of leaf and cuticular micromorphology. *Palaeogeography, Palaeoclimatology, Palaeoecology*, *262*(1), 79–90. https://doi.org/10.1016/j.palaeo.2008.02.009

Heinemann, B., Künzler, P., Eubel, H., Braun, H.-P., & Hildebrandt, T. M. (2021). Estimating the number of protein molecules in a plant cell: Protein and amino acid homeostasis during drought. *Plant Physiology*, *185*(2), 385–404. https://doi.org/10.1093/plphys/kiaa050

Hernández-Sánchez, I. E., Maruri-López, I., Martinez-Martinez, C., Janis, B., Jiménez-Bremont, J. F., Covarrubias, A. A., Menze, M. A., Graether, S. P., & Thalhammer, A. (2022). LEAfing through literature: Late embryogenesis abundant proteins coming of age—achievements and perspectives. *Journal of Experimental Botany*, *73*(19), 6525–6546. https://doi.org/10.1093/jxb/erac293

Holst, F., Bolger, A., Günther, C., Maß, J., Triesch, S., Kindel, F., Kiel, N., Saadat, N., Ebenhöh, O., Usadel, B., Schwacke, R., Bolger, M., Weber, A. P. M., & Denton, A. K. (2023). *Helixer–de novo Prediction of Primary Eukaryotic Gene Models Combining Deep Learning and a Hidden Markov Model* (p. 2023.02.06.527280). bioRxiv. https://doi.org/10.1101/2023.02.06.527280

Hou, H., Wu, J., Zhang, Y., Lu, C., Jiang, W., Shen, Y., Pan, L., Shao, Q., & Lv, A. (2024). The cellulose synthase-like G3 (CslG3) gene mediates polysaccharide synthesis and drought stress response in *Dendrobium catenatum*. *Scientia Horticulturae*, *338*, 113514. https://doi.org/10.1016/j.scienta.2024.113514

Hübner, S., Höffken, M., Oren, E., Haseneyer, G., Stein, N., Graner, A., Schmid, K., & Fridman, E. (2009). Strong correlation of wild barley (Hordeum spontaneum) population structure with temperature and precipitation variation. *Molecular Ecology*, *18*(7), 1523–1536. https://doi.org/10.1111/j.1365-294X.2009.04106.x

Hyndman, R. J., Einbeck, J., & Wand, M. P. (2023). *hdrcde: Highest Density Regions and Conditional Density Estimation*. https://pkg.robjhyndman.com/hdrcde/

Isoda, R., Palmai, Z., Yoshinari, A., Chen, L.-Q., Tama, F., Frommer, W. B., & Nakamura, M. (2022). SWEET13 transport of sucrose, but not gibberellin, restores male fertility in Arabidopsis sweet13;14. *Proceedings of the National Academy of Sciences*, *119*(42), e2207558119. https://doi.org/10.1073/pnas.2207558119

Jackman, S. D., Coombe, L., Chu, J., Warren, R. L., Vandervalk, B. P., Yeo, S., Xue, Z., Mohamadi, H., Bohlmann, J., Jones, S. J. M., & Birol, I. (2018). Tigmint: Correcting assembly errors using linked reads from large molecules. *BMC Bioinformatics*, *19*(1), Article 1. https://doi.org/10.1186/s12859-018-2425-6

Jakob, S. S., Meister, A., & Blattner, F. R. (2004). The Considerable Genome Size Variation of Hordeum Species (Poaceae) Is Linked to Phylogeny, Life Form, Ecology, and Speciation Rates. *Molecular Biology and Evolution*, *21*(5), 860–869. https://doi.org/10.1093/molbev/msh092

Dainat, J., Hereñú, D., Murray, Dr. K. D., Davis, E., Ugrin, I., Crouch, K., Nuno Agostinho, L., pascal-git, Zollman, Z., & tayyrov. (2024). *NBISweden/AGAT: AGAT-v1.4.1* (Version v1.4.1) [Computer software]. Zenodo. https://doi.org/10.5281/ZENODO.3552717

Jarvis, M. C. (2012). Sclerenchyma. In *eLS*. John Wiley & Sons, Ltd. https://doi.org/10.1002/9780470015902.a0002082.pub2

Jarzyniak, K. M., & Jasiński, M. (2014). Membrane transporters and drought resistance – a complex issue. *Frontiers in Plant Science*, *5*. https://doi.org/10.3389/fpls.2014.00687

Jayakodi, M., Padmarasu, S., Haberer, G., Bonthala, V. S., Gundlach, H., Monat, C., Lux, T., Kamal, N., Lang, D., Himmelbach, A., Ens, J., Zhang, X.-Q., Angessa, T. T., Zhou, G., Tan, C., Hill, C., Wang, P., Schreiber, M., Boston, L. B., … Stein, N. (2020). The barley pan-genome reveals the hidden legacy of mutation breeding. *Nature*, *588*(7837), 284–289. https://doi.org/10.1038/s41586-020-2947-8

Jin, J., Lu, P., Xu, Y., Li, Z., Yu, S., Liu, J., Wang, H., Chua, N.-H., & Cao, P. (2021). PLncDB V2.0: A comprehensive encyclopedia of plant long noncoding RNAs. *Nucleic Acids Research*, *49*(D1), D1489–D1495. https://doi.org/10.1093/nar/gkaa910

Jones, P., Binns, D., Chang, H.-Y., Fraser, M., Li, W., McAnulla, C., McWilliam, H., Maslen, J., Mitchell, A., Nuka, G., Pesseat, S., Quinn, A. F., Sangrador-Vegas, A., Scheremetjew, M., Yong, S.-Y., Lopez, R., & Hunter, S. (2014). InterProScan 5: Genome-scale protein function classification. *Bioinformatics*, *30*(9), 1236–1240. https://doi.org/10.1093/bioinformatics/btu031

Kadioglu, A., & Terzi, R. (2007). A Dehydration Avoidance Mechanism: Leaf Rolling. *Botanical Review*, *73*(4), 290–302.

Kang, Y.-J., Yang, D.-C., Kong, L., Hou, M., Meng, Y.-Q., Wei, L., & Gao, G. (2017). CPC2: A fast and accurate coding potential calculator based on sequence intrinsic features. *Nucleic Acids Research*, *45*(W1), W12–W16. https://doi.org/10.1093/nar/gkx428

Kargiotidou, A., Deli, D., Galanopoulou, D., Tsaftaris, A., & Farmaki, T. (2008). Low temperature and light regulate delta 12 fatty acid desaturases (FAD2) at a transcriptional level in cotton (Gossypium hirsutum). *Journal of Experimental Botany*, *59*(8), 2043–2056. https://doi.org/10.1093/jxb/ern065

Karitter, P., March-Salas, M., Ensslin, A., Rauschkolb, R., Godefroid, S., & Scheepens, J. F. (2024). Combining the resurrection approach with transplant experiments to investigate adaptation of plant populations to environmental change. *Perspectives in Plant Ecology, Evolution and Systematics*, *62*, 125773. https://doi.org/10.1016/j.ppees.2023.125773

Kasapligil, B. (1961). Foliar Xeromorphy of Certain Geophytic Monocotyledons. *Madroño*, *16*(2), 43–70.

Kreszies, T., Eggels, S., Kreszies, V., Osthoff, A., Shellakkutti, N., Baldauf, J. A., Zeisler-Diehl, V. V., Hochholdinger, F., Ranathunge, K., & Schreiber, L. (2020). Seminal roots of wild and cultivated barley differentially respond to osmotic stress in gene expression, suberization, and hydraulic conductivity. *Plant, Cell & Environment*, *43*(2), 344–357. https://doi.org/10.1111/pce.13675

Kolmogorov, M., Yuan, J., Lin, Y., & Pevzner, P. A. (2019). Assembly of long, error-prone reads using repeat graphs. *Nature Biotechnology*, *37*(5), 540–546. https://doi.org/10.1038/s41587-019-0072-8

Kreszies, T., Eggels, S., Kreszies, V., Osthoff, A., Shellakkutti, N., Baldauf, J. A., Zeisler-Diehl, V. V., Hochholdinger, F., Ranathunge, K., & Schreiber, L. (2020). Seminal roots of wild and cultivated barley differentially respond to osmotic stress in gene expression, suberization, and hydraulic conductivity. *Plant, Cell & Environment*, *43*(2), 344–357. https://doi.org/10.1111/pce.13675

Kumar, S., Suleski, M., Craig, J. M., Kasprowicz, A. E., Sanderford, M., Li, M., Stecher, G., & Hedges, S. B. (2022). TimeTree 5: An Expanded Resource for Species Divergence Times. *Molecular Biology and Evolution*, *39*(8), msac174. https://doi.org/10.1093/molbev/msac174

Lee, S. B., & Suh, M. C. (2015). Advances in the understanding of cuticular waxes in Arabidopsis thaliana and crop species. *Plant Cell Reports*, *34*(4), 557–572. https://doi.org/10.1007/s00299-015-1772-2

Lei, L., Gordon, S. P., Liu, L., Sade, N., Lovell, J. T., Rubio Wilhelmi, M. D. M., Singan, V., Sreedasyam, A., Hestrin, R., Phillips, J., Hernandez, B. T., Barry, K., Shu, S., Jenkins, J., Schmutz, J., Goodstein, D. M., Thilmony, R., Blumwald, E., & Vogel, J. P. (2024). The

reference genome and abiotic stress responses of the model perennial grass Brachypodium sylvaticum. *G3 Genes|Genomes|Genetics*, *14*(1), jkad245. https://doi.org/10.1093/g3journal/jkad245

Lesk, C., Anderson, W., Rigden, A., Coast, O., Jägermeyr, J., McDermid, S., Davis, K. F., & Konar, M. (2022). Compound heat and moisture extreme impacts on global crop yields under climate change. *Nature Reviews Earth & Environment*, *3*(12), 872–889. https://doi.org/10.1038/s43017-022-00368-8

Li, H. (2018). Minimap2: Pairwise alignment for nucleotide sequences. *Bioinformatics*, *34*(18), 3094–3100. https://doi.org/10.1093/bioinformatics/bty191

Li, P., Yang, H., Wang, L., Liu, H., Huo, H., Zhang, C., Liu, A., Zhu, A., Hu, J., Lin, Y., & Liu, L. (2019). Physiological and Transcriptome Analyses Reveal Short-Term Responses and Formation of Memory Under Drought Stress in Rice. *Frontiers in Genetics*, *10*. https://doi.org/10.3389/fgene.2019.00055

Li, G., Wang, Y., Liu, H., Qin, S., Sui, F., Fu, H., Duan, R., Li, C., & Zhao, P. (2022). A comparison study of physiological response and *TaZIPs* expression in seedlings of two wheat (*Triticum aestivum* L.) cultivars with contrasting grain zinc accumulation. *Plant Science*, *318*, 111237. https://doi.org/10.1016/j.plantsci.2022.111237

Liakoura, V., Stefanou, M., Manetas, Y., Cholevas, C., & Karabourniotis, G. (1997). Trichome density and its UV-B protective potential are affected by shading and leaf position on the canopy. *Environmental and Experimental Botany*, *38*(3), 223–229. https://doi.org/10.1016/S0098-8472(97)00005-1

Liao, Y., Smyth, G. K., & Shi, W. (2014). featureCounts: An efficient general purpose program for assigning sequence reads to genomic features. *Bioinformatics*, *30*(7), 923–930. https://doi.org/10.1093/bioinformatics/btt656

Liting, W., Lina, W., Yang, Y., Pengfei, W., Tiancai, G., & Guozhang, K. (2015). Abscisic acid enhances tolerance of wheat seedlings to drought and regulates transcript levels of genes encoding ascorbate-glutathione biosynthesis. *Frontiers in Plant Science*, *6*. https://doi.org/10.3389/fpls.2015.00458

Liu, X., Wang, H., Tang, H., Du, X., He, F., Ren, M., & Bao, Y. (2022). *TaSWEET14* confers low cadmium accumulation in wheat and is regulated by TaMYB41. *Environmental and Experimental Botany*, *201*, 104992. https://doi.org/10.1016/j.envexpbot.2022.104992

Lynch, D. J., McInerney, F. A., Kouwenberg, L. L. R., & Gonzalez-Meler, M. A. (2012). Plasticity in bundle sheath extensions of heterobaric leaves. *American Journal of Botany*, *99*(7), 1197–1206. https://doi.org/10.3732/ajb.1100525

Manni, M., Berkeley, M. R., Seppey, M., Simão, F. A., & Zdobnov, E. M. (2021). BUSCO Update: Novel and Streamlined Workflows along with Broader and Deeper Phylogenetic Coverage for Scoring of Eukaryotic, Prokaryotic, and Viral Genomes. *Molecular Biology and Evolution*, *38*(10), 4647–4654. https://doi.org/10.1093/molbev/msab199

Marçais, G., & Kingsford, C. (2011). A fast, lock-free approach for efficient parallel counting of occurrences of k-mers. *Bioinformatics*, *27*(6), 764–770. https://doi.org/10.1093/bioinformatics/btr011

Marks, R. A., Van Der Pas, L., Schuster, J., Gilman, I. S., & VanBuren, R. (2024). Convergent evolution of desiccation tolerance in grasses. *Nature Plants*, *10*(7), 1112–1125. https://doi.org/10.1038/s41477-024-01729-5

Mascher, M., Gundlach, H., Himmelbach, A., Beier, S., Twardziok, S. O., Wicker, T., Radchuk, V., Dockter, C., Hedley, P. E., Russell, J., Bayer, M., Ramsay, L., Liu, H., Haberer, G., Zhang, X.-Q., Zhang, Q., Barrero, R. A., Li, L., Taudien, S., … Stein, N. (2017). A chromosome conformation capture ordered sequence of the barley genome. *Nature*, *544*(7651), 427–433. https://doi.org/10.1038/nature22043

Mascher, M., Wicker, T., Jenkins, J., Plott, C., Lux, T., Koh, C. S., Ens, J., Gundlach, H., Boston, L. B., Tulpová, Z., Holden, S., Hernández-Pinzón, I., Scholz, U., Mayer, K. F. X., Spannagl, M., Pozniak, C. J., Sharpe, A. G., Šimková, H., Moscou, M. J., … Stein, N. (2021). Long-read sequence assembly: A technical evaluation in barley. *The Plant Cell*, *33*(6), 1888–1906. https://doi.org/10.1093/plcell/koab077

Mazel, A., Leshem, Y., Tiwari, B. S., & Levine, A. (2004). Induction of Salt and Osmotic Stress Tolerance by Overexpression of an Intracellular Vesicle Trafficking Protein AtRab7 (AtRabG3e). *Plant Physiology*, *134*(1), 118–128. https://doi.org/10.1104/pp.103.025379

Mendes, F. K., Vanderpool, D., Fulton, B., & Hahn, M. W. (2021). CAFE 5 models variation in evolutionary rates among gene families. *Bioinformatics*, *36*(22–23), 5516–5518. https://doi.org/10.1093/bioinformatics/btaa1022

Metz, J., Lampei, C., Bäumler, L., Bocherens, H., Dittberner, H., Henneberg, L., de Meaux, J., & Tielbörger, K. (2020). Rapid adaptive evolution to drought in a subset of plant traits in a large-scale climate change experiment. *Ecology Letters*, *23*(11), 1643–1653. https://doi.org/10.1111/ele.13596

Milner, M. J., Seamon, J., Craft, E., & Kochian, L. V. (2013). Transport properties of members of the ZIP family in plants and their role in Zn and Mn homeostasis. *Journal of Experimental Botany*, *64*(1), 369–381. https://doi.org/10.1093/jxb/ers315

Mikheenko, A., Prjibelski, A., Saveliev, V., Antipov, D., & Gurevich, A. (2018). Versatile genome assembly evaluation with QUAST-LG. *Bioinformatics*, *34*(13), i142–i150. https://doi.org/10.1093/bioinformatics/bty266

Minh, B. Q., Schmidt, H. A., Chernomor, O., Schrempf, D., Woodhams, M. D., von Haeseler, A., & Lanfear, R. (2020). IQ-TREE 2: New Models and Efficient Methods for Phylogenetic Inference in the Genomic Era. *Molecular Biology and Evolution*, *37*(5), 1530–1534. https://doi.org/10.1093/molbev/msaa015

Monat, C., Padmarasu, S., Lux, T., Wicker, T., Gundlach, H., Himmelbach, A., Ens, J., Li, C., Muehlbauer, G. J., Schulman, A. H., Waugh, R., Braumann, I., Pozniak, C., Scholz, U., Mayer, K. F. X., Spannagl, M., Stein, N., & Mascher, M. (2019). TRITEX: Chromosome-scale sequence assembly of Triticeae genomes with open-source tools. *Genome Biology*, *20*(1), Article 1. https://doi.org/10.1186/s13059-019-1899-5

moshi. (2024). *Moshi4/CafePlotter* [Python]. https://github.com/moshi4/CafePlotter (Original work published 2023)

Moulia, B. (2000). Leaves as Shell Structures: Double Curvature, Auto-Stresses, and Minimal Mechanical Energy Constraints on Leaf Rolling in Grasses. *Journal of Plant Growth Regulation*, *19*(1), 19–30. https://doi.org/10.1007/s003440000004

Nanoporetech/medaka. (2024). [Python]. Oxford Nanopore Technologies. https://github.com/nanoporetech/medaka (Original work published 2017)

Naseer, S., Lee, Y., Lapierre, C., Franke, R., Nawrath, C., & Geldner, N. (2012). Casparian strip diffusion barrier in Arabidopsis is made of a lignin polymer without suberin. *Proceedings of the National Academy of Sciences*, *109*(25), 10101–10106. https://doi.org/10.1073/pnas.1205726109

Navrátilová, P., Toegelová, H., Tulpová, Z., Kuo, Y.-T., Stein, N., Doležel, J., Houben, A., Šimková, H., & Mascher, M. (2022). Prospects of telomere-to-telomere assembly in barley: Analysis of sequence gaps in the MorexV3 reference genome. *Plant Biotechnology Journal*, *20*(7), 1373–1386. https://doi.org/10.1111/pbi.13816

Negri, T. da C., Alves, W. A. L., Bugatti, P. H., Saito, P. T. M., Domingues, D. S., & Paschoal, A. R. (2019). Pattern recognition analysis on long noncoding RNAs: A tool for prediction in plants. *Briefings in Bioinformatics*, *20*(2), 682–689. https://doi.org/10.1093/bib/bby034

Nelson, J. M., Lane, B., & Freeling, M. (2002). Expression of a mutant maize gene in the ventral leaf epidermis is sufficient to signal a switch of the leaf's dorsoventral axis. *Development*, *129*(19), 4581–4589. https://doi.org/10.1242/dev.129.19.4581

Neumann, P., Navrátilová, A., Koblížková, A., Kejnovský, E., Hřibová, E., Hobza, R., Widmer, A., Doležel, J., & Macas, J. (2011). Plant centromeric retrotransposons: A structural and cytogenetic perspective. *Mobile DNA*, *2*(1), 4. https://doi.org/10.1186/1759-8753-2-4

Nguyen, K. H., Mostofa, M. G., Watanabe, Y., Tran, C. D., Rahman, Md. M., & Tran, L.-S. P. (2019). Overexpression of *GmNAC085* enhances drought tolerance in *Arabidopsis* by regulating glutathione biosynthesis, redox balance and glutathione-dependent detoxification of reactive oxygen species and methylglyoxal. *Environmental and Experimental Botany*, *161*, 242–254. https://doi.org/10.1016/j.envexpbot.2018.12.021

Nguyen, V. C., Nakamura, Y., & Kanehara, K. (2019). Membrane lipid polyunsaturation mediated by 2 (2) is involved in endoplasmic reticulum stress tolerance in Arabidopsis thaliana. *The Plant Journal*, *99*(3), 478–493. https://doi.org/10.1111/tpj.14338

Nikolopoulos, D., Liakopoulos, G., Drossopoulos, I., & Karabourniotis, G. (2002). The Relationship between Anatomy and Photosynthetic Performance of Heterobaric Leaves. *Plant Physiology*, *129*(1), 235–243. https://doi.org/10.1104/pp.010943

Noctor, G., Mhamdi, A., & Foyer, C. H. (2014). The Roles of Reactive Oxygen Metabolism in Drought: Not So Cut and Dried. *Plant Physiology*, *164*(4), 1636–1648. https://doi.org/10.1104/pp.113.233478

Nueda, M. J., Tarazona, S., & Conesa, A. (2014). Next maSigPro: Updating maSigPro bioconductor package for RNA-seq time series. *Bioinformatics*, *30*(18), 2598–2602. https://doi.org/10.1093/bioinformatics/btu333

Ou, S., Su, W., Liao, Y., Chougule, K., Agda, J. R. A., Hellinga, A. J., Lugo, C. S. B., Elliott, T. A., Ware, D., Peterson, T., Jiang, N., Hirsch, C. N., & Hufford, M. B. (2019). Benchmarking

transposable element annotation methods for creation of a streamlined, comprehensive pipeline. *Genome Biology*, *20*(1), Article 1. https://doi.org/10.1186/s13059-019-1905-y

O'Toole, J. C., & Cruz, R. T. (1980). Response of Leaf Water Potential, Stomatal Resistance, and Leaf Rolling to Water Stress. *Plant Physiology*, *65*(3), 428–432. https://doi.org/10.1104/pp.65.3.428

PacBio—IsoSeq3. (2024). [Computer software]. PacBio. https://github.com/PacificBiosciences/pbbioconda (Original work published 2018)

Palermo, F. H., Fortuna-Perez, A. P., Chain, H. B., Pezzini, F. F., Lewis, G. P., de Oliveira, R. A., & Rodrigues, T. M. (2023). Taxonomic significance and evolution of homobaric and heterobaric leaves in Adesmia clade species (Leguminosae – Papilionoideae). *Perspectives in Plant Ecology, Evolution and Systematics*, *58*, 125714. https://doi.org/10.1016/j.ppees.2022.125714

Palmgren, M. G., Edenbrandt, A. K., Vedel, S. E., Andersen, M. M., Landes, X., Østerberg, J. T., Falhof, J., Olsen, L. I., Christensen, S. B., Sandøe, P., Gamborg, C., Kappel, K., Thorsen, B. J., & Pagh, P. (2015). Are we ready for back-to-nature crop breeding? *Trends in Plant Science*, *20*(3), 155–164. https://doi.org/10.1016/j.tplants.2014.11.003

Paul, M., Tanskanen, J., Jääskeläinen, M., Chang, W., Dalal, A., Moshelion, M., & Schulman, A. H. (2023). Drought and recovery in barley: Key gene networks and retrotransposon response. *Frontiers in Plant Science*, *14*. https://doi.org/10.3389/fpls.2023.1193284

Perico, C., Tan, S., & Langdale, J. A. (2022). Developmental regulation of leaf venation patterns: Monocot versus eudicots and the role of auxin. *New Phytologist*, *234*(3), 783–803. https://doi.org/10.1111/nph.17955

Piro, G., Leucci, M. R., Waldron, K., & Dalessandro, G. (2003). Exposure to water stress causes changes in the biosynthesis of cell wall polysaccharides in roots of wheat cultivars varying in drought tolerance. *Plant Science*, *165*(3), 559–569. https://doi.org/10.1016/S0168-9452(03)00215-2

Poppenwimer, T., Mayrose, I., & DeMalach, N. (2023). Revising the global biogeography of annual and perennial plants. *Nature*, *624*(7990), 109–114. https://doi.org/10.1038/s41586-023-06644-x

Pourkheirandish, M., & Komatsuda, T. (2007). The Importance of Barley Genetics and Domestication in a Global Perspective. *Annals of Botany*, *100*(5), 999–1008. https://doi.org/10.1093/aob/mcm139

Prerostova, S., Dobrev, P. I., Gaudinova, A., Knirsch, V., Körber, N., Pieruschka, R., Fiorani, F., Brzobohatý, B., Černý, M., Spichal, L., Humplik, J., Vanek, T., Schurr, U., & Vankova, R. (2018). Cytokinins: Their Impact on Molecular and Growth Responses to Drought Stress and Recovery in Arabidopsis. *Frontiers in Plant Science*, *9*. https://doi.org/10.3389/fpls.2018.00655

Prjibelski, A. D., Mikheenko, A., Joglekar, A., Smetanin, A., Jarroux, J., Lapidus, A. L., & Tilgner, H. U. (2023). Accurate isoform discovery with IsoQuant using long reads. *Nature Biotechnology*, *41*(7), 915–918. https://doi.org/10.1038/s41587-022-01565-y

Qi, F., & Zhang, F. (2020). Cell Cycle Regulation in the Plant Response to Stress. *Frontiers in Plant Science*, *10*. https://doi.org/10.3389/fpls.2019.01765

Quinlan, A. R., & Hall, I. M. (2010). BEDTools: A flexible suite of utilities for comparing genomic features. *Bioinformatics*, *26*(6), 841–842. https://doi.org/10.1093/bioinformatics/btq033

Rauschkolb, R., Li, Z., Godefroid, S., Dixon, L., Durka, W., Májeková, M., Bossdorf, O., Ensslin, A., & Scheepens, J. F. (2022). Evolution of plant drought strategies and herbivore tolerance after two decades of climate change. *New Phytologist*, *235*(2), 773–785. https://doi.org/10.1111/nph.18125

R Core Team. (2024). *R: A Language and Environment for Statistical Computing*. R Foundation for Statistical Computing. https://www.R-project.org/

Redmann, R. E. (1985). Adaptation of Grasses to Water Stress-Leaf Rolling and Stomate Distribution. *Annals of the Missouri Botanical Garden*, *72*(4), 833–842. https://doi.org/10.2307/2399225

Reguera, M., Peleg, Z., Abdel-Tawab, Y. M., Tumimbang, E. B., Delatorre, C. A., & Blumwald, E. (2013). Stress-Induced Cytokinin Synthesis Increases Drought Tolerance through the Coordinated Regulation of Carbon and Nitrogen Assimilation in Rice. *Plant Physiology*, *163*(4), 1609–1622. https://doi.org/10.1104/pp.113.227702

Rezaei, E. E., Webber, H., Asseng, S., Boote, K., Durand, J. L., Ewert, F., Martre, P., & MacCarthy, D. S. (2023). Climate change impacts on crop yields. *Nature Reviews Earth & Environment*, *4*(12), 831–846. https://doi.org/10.1038/s43017-023-00491-0

Rhie, A., Walenz, B. P., Koren, S., & Phillippy, A. M. (2020). Merqury: Reference-free quality, completeness, and phasing assessment for genome assemblies. *Genome Biology*, *21*(1), Article 1. https://doi.org/10.1186/s13059-020-02134-9

Ribeiro, M., Nunes-Miranda, J. D., Branlard, G., Carrillo, J. M., Rodriguez-Quijano, M., & Igrejas, G. (2013). One Hundred Years of Grain Omics: Identifying the Glutens That Feed the World. *Journal of Proteome Research*, *12*(11), 4702–4716. https://doi.org/10.1021/pr400663t

Roppolo, D., Boeckmann, B., Pfister, A., Boutet, E., Rubio, M. C., Dénervaud-Tendon, V., Vermeer, J. E. M., Gheyselinck, J., Xenarios, I., & Geldner, N. (2014). Functional and Evolutionary Analysis of the CASPARIAN STRIP MEMBRANE DOMAIN PROTEIN Family. *Plant Physiology*, *165*(4), 1709–1722. https://doi.org/10.1104/pp.114.239137

Sack, L., Scoffoni, C., John, G. P., Poorter, H., Mason, C. M., Mendez-Alonzo, R., & Donovan, L. A. (2013a). How do leaf veins influence the worldwide leaf economic spectrum? Review and synthesis. *Journal of Experimental Botany*, *64*(13), 4053–4080. https://doi.org/10.1093/jxb/ert316

Sack, L., & Scoffoni, C. (2013b). Leaf venation: Structure, function, development, evolution, ecology and applications in the past, present and future. *New Phytologist*, *198*(4), 983–1000. https://doi.org/10.1111/nph.12253

Sayols, S. (2023). rrvgo: A Bioconductor package for interpreting lists of Gene Ontology terms. *microPublication Biology*. https://doi.org/10.17912/micropub.biology.000811

Senft, A. D., & Macfarlan, T. S. (2021). Transposable elements shape the evolution of mammalian development. *Nature Reviews Genetics*, *22*(11), 691–711. https://doi.org/10.1038/s41576-021-00385-1

Sgroi, L. C., Lovino, M. A., Berbery, E. H., & Müller, G. V. (2021). Characteristics of droughts in Argentina's core crop region. *Hydrology and Earth System Sciences*, *25*(5), 2475–2490. https://doi.org/10.5194/hess-25-2475-2021

Shan, L., Xu, Y., Wu, D., Hu, J., Yu, T., Dang, C., Fang, Y., Zhang, X., Tian, Q., & Xue, D. (2024). Effects of salicylic acid on growth, physiology, and gene expression in rice seedlings under salt and drought stress. *Plant Stress*, *11*, 100413. https://doi.org/10.1016/j.stress.2024.100413

Shi, Z., Wang, J., Wan, X., Shen, G., Wang, X., & Zhang, J. (2007). Over-expression of rice OsAGO7 gene induces upward curling of the leaf blade that enhanced erect-leaf habit. *Planta*, *226*(1), 99–108. https://doi.org/10.1007/s00425-006-0472-0

Shields, L. M. (1950). Leaf Xeromorphy as Related to Physiological and Structural Influences. *Botanical Review*, *16*(8), 399–447.

Singh, U., Khemka, N., Rajkumar, M. S., Garg, R., & Jain, M. (2017). PLncPRO for prediction of long non-coding RNAs (lncRNAs) in plants and its application for discovery of abiotic stress-responsive lncRNAs in rice and chickpea. *Nucleic Acids Research*, *45*(22), e183. https://doi.org/10.1093/nar/gkx866

Song, C., Yan, Y., Rosado, A., Zhang, Z., & Castellarin, S. D. (2019). ABA Alleviates Uptake and Accumulation of Zinc in Grapevine (Vitis vinifera L.) by Inducing Expression of ZIP and Detoxification-Related Genes. *Frontiers in Plant Science*, *10*. https://doi.org/10.3389/fpls.2019.00872

Sun, L., Luo, H., Bu, D., Zhao, G., Yu, K., Zhang, C., Liu, Y., Chen, R., & Zhao, Y. (2013). Utilizing sequence intrinsic composition to classify protein-coding and long non-coding transcripts. *Nucleic Acids Research*, *41*(17), e166. https://doi.org/10.1093/nar/gkt646

Sun, H., Ding, J., Piednoël, M., & Schneeberger, K. (2018). findGSE: Estimating genome size variation within human and Arabidopsis using k-mer frequencies. *Bioinformatics*, *34*(4), 550–557. https://doi.org/10.1093/bioinformatics/btx637

Sun, J., Cui, X., Teng, S., Kunnong, Z., Wang, Y., Chen, Z., Sun, X., Wu, J., Ai, P., Quick, W. P., Lu, T., & Zhang, Z. (2020). HD-ZIP IV gene Roc8 regulates the size of bulliform cells and lignin content in rice. *Plant Biotechnology Journal*, *18*(12), 2559–2572. https://doi.org/10.1111/pbi.13435

Sun, X., Xiang, Y., Dou, N., Zhang, H., Pei, S., Franco, A. V., Menon, M., Monier, B., Ferebee, T., Liu, T., Liu, S., Gao, Y., Wang, J., Terzaghi, W., Yan, J., Hearne, S., Li, L., Li, F., & Dai, M. (2023). The role of transposon inverted repeats in balancing drought tolerance and yield-related traits in maize. *Nature Biotechnology*, *41*(1), 120–127. https://doi.org/10.1038/s41587-022-01470-4

Terashima, I. (1992). Anatomy of non-uniform leaf photosynthesis. *Photosynthesis Research*, *31*(3), 195–212. https://doi.org/10.1007/BF00035537

The UniProt Consortium, Bateman, A., Martin, M.-J., Orchard, S., Magrane, M., Ahmad, S., Alpi, E., Bowler-Barnett, E. H., Britto, R., Bye-A-Jee, H., Cukura, A., Denny, P., Dogan, T., Ebenezer, T., Fan, J., Garmiri, P., Da Costa Gonzales, L. J., Hatton-Ellis, E., Hussein, A., … Zhang, J. (2023). UniProt: The Universal Protein Knowledgebase in 2023. *Nucleic Acids Research*, *51*(D1), D523–D531. https://doi.org/10.1093/nar/gkac1052

Tong, X., & Liu, S. (2019). CPPred: Coding potential prediction based on the global description of RNA sequence. *Nucleic Acids Research*, *47*(8), e43. https://doi.org/10.1093/nar/gkz087

VanBuren, R., Pardo, J., Man Wai, C., Evans, S., & Bartels, D. (2019). Massive Tandem Proliferation of ELIPs Supports Convergent Evolution of Desiccation Tolerance across Land Plants. *Plant Physiology*, *179*(3), 1040–1049. https://doi.org/10.1104/pp.18.01420

Vaser, R., Sović, I., Nagarajan, N., & Šikić, M. (2017). Fast and accurate de novo genome assembly from long uncorrected reads. *Genome Research*, *27*(5), 737–746. https://doi.org/10.1101/gr.214270.116

Vasimuddin, Md., Misra, S., Li, H., & Aluru, S. (2019). Efficient Architecture-Aware Acceleration of BWA-MEM for Multicore Systems. *2019 IEEE International Parallel and Distributed Processing Symposium (IPDPS)*, 314–324. https://doi.org/10.1109/IPDPS.2019.00041

Vitte, C., Panaud, O., & Quesneville, H. (2007). LTR retrotransposons in rice (Oryza sativa, L.): Recent burst amplifications followed by rapid DNA loss. *BMC Genomics*, *8*(1), Article 1. https://doi.org/10.1186/1471-2164-8-218

Waddington, S. R., Cartwright, P. M., & WALL, P. C. (1983). A Quantitative Scale of Spike Initial and Pistil Development in Barley and Wheat. *Annals of Botany*, *51*(1), 119–130. https://doi.org/10.1093/oxfordjournals.aob.a086434

Wang, Y., Carrie, C., Giraud, E., Elhafez, D., Narsai, R., Duncan, O., Whelan, J., & Murcha, M. W. (2012). Dual Location of the Mitochondrial Preprotein Transporters B14.7 and Tim23-2 in Complex I and the TIM17:23 Complex in Arabidopsis Links Mitochondrial Activity and Biogenesis. *The Plant Cell*, *24*(6), 2675–2695. https://doi.org/10.1105/tpc.112.098731

Wang, L., Park, H. J., Dasari, S., Wang, S., Kocher, J.-P., & Li, W. (2013). CPAT: Coding-Potential Assessment Tool using an alignment-free logistic regression model. *Nucleic Acids Research*, *41*(6), e74. https://doi.org/10.1093/nar/gkt006

Wang, X., Huang, J., Peng, S., & Xiong, D. (2023). Leaf rolling precedes stomatal closure in rice (Oryza sativa) under drought conditions. *Journal of Experimental Botany*, *74*(21), 6650–6661. https://doi.org/10.1093/jxb/erad316

Wells, J. N., & Feschotte, C. (2020). A Field Guide to Eukaryotic Transposable Elements. *Annual Review of Genetics*, *54*, 539–561. https://doi.org/10.1146/annurev-genet-040620-022145

Wei, X., Liu, L., Lu, C., Yuan, F., Han, G., & Wang, B. (2021). SbCASP4 improves salt exclusion by enhancing the root apoplastic barrier. *Planta*, *254*(4), 81. https://doi.org/10.1007/s00425-021-03731-z

White, N. J., Beckerman, A. P., Snook, R. R., Brockhurst, M. A., Butlin, R. K., & Eyres, I. (2022). Experimental evolution of local adaptation under unidimensional and multidimensional selection. *Current Biology*, *32*(6), 1310-1318.e4. https://doi.org/10.1016/j.cub.2022.01.048

Whiting, J. R., Booker, T. R., Rougeux, C., Lind, B. M., Singh, P., Lu, M., Huang, K., Whitlock, M. C., Aitken, S. N., Andrew, R. L., Borevitz, J. O., Bruhl, J. J., Collins, T. L., Fischer, M. C., Hodgins, K. A., Holliday, J. A., Ingvarsson, P. K., Janes, J. K., Khandaker, M., … Yeaman, S. (2024). The genetic architecture of repeated local adaptation to climate in distantly related plants. *Nature Ecology & Evolution*, *8*(10), 1933–1947. https://doi.org/10.1038/s41559-024-02514-5

Wick, R. R., Judd, L. M., Gorrie, C. L., & Holt, K. E. (2017). Completing bacterial genome assemblies with multiplex MinION sequencing. *Microbial Genomics*, *3*(10). https://doi.org/10.1099/mgen.0.000132

WMO. (2020). *WMO Climatological Normals | World Meteorological Organization*. https://community.wmo.int/en/activity-areas/climate-services/climate-products-and-initiatives/wmo-climatological-normals

Wu, H.-J., Zhang, Z., Wang, J.-Y., Oh, D.-H., Dassanayake, M., Liu, B., Huang, Q., Sun, H.-X., Xia, R., Wu, Y., Wang, Y.-N., Yang, Z., Liu, Y., Zhang, W., Zhang, H., Chu, J., Yan, C., Fang, S., Zhang, J., … Xie, Q. (2012). Insights into salt tolerance from the genome of Thellungiella salsuginea. *Proceedings of the National Academy of Sciences*, *109*(30), 12219–12224. https://doi.org/10.1073/pnas.1209954109

Wu, X., Zhang, X., Huang, B., Han, J., & Fang, H. (2023). Advances in biological functions and mechanisms of histone variants in plants. *Frontiers in Genetics*, *14*. https://doi.org/10.3389/fgene.2023.1229782

Xie, W., Xiong, W., Pan, J., Ali, T., Cui, Q., Guan, D., Meng, J., Mueller, N. D., Lin, E., & Davis, S. J. (2018). Decreases in global beer supply due to extreme drought and heat. *Nature Plants*, *4*(11), 964–973. https://doi.org/10.1038/s41477-018-0263-1

Xu, Y., Kong, W., Wang, F., Wang, J., Tao, Y., Li, W., Chen, Z., Fan, F., Jiang, Y., Zhu, Q.-H., & Yang, J. (2021). Heterodimer formed by ROC8 and ROC5 modulates leaf rolling in rice. *Plant Biotechnology Journal*, *19*(12), 2662–2672. https://doi.org/10.1111/pbi.13690

Xu, S., Hu, E., Cai, Y., Xie, Z., Luo, X., Zhan, L., Tang, W., Wang, Q., Liu, B., Wang, R., Xie, W., Wu, T., Xie, L., & Yu, G. (2024). Using clusterProfiler to characterize multiomics data. *Nature Protocols*, *19*(11), 3292–3320. https://doi.org/10.1038/s41596-024-01020-z

Xue, D., Zhang, X., Lu, X., Chen, G., & Chen, Z.-H. (2017). Molecular and Evolutionary Mechanisms of Cuticular Wax for Plant Drought Tolerance. *Frontiers in Plant Science*, *8*. https://www.frontiersin.org/articles/10.3389/fpls.2017.00621

Yan, S., Yan, C.-J., Zeng, X.-H., Yang, Y.-C., Fang, Y.-W., Tian, C.-Y., Sun, Y.-W., Cheng, Z.-K., & Gu, M.-H. (2008). ROLLED LEAF 9, encoding a GARP protein, regulates the leaf abaxial cell fate in rice. *Plant Molecular Biology*, *68*(3), 239–250. https://doi.org/10.1007/s11103-008-9365-x

Yang, Q., Li, Z., Li, W., Ku, L., Wang, C., Ye, J., Li, K., Yang, N., Li, Y., Zhong, T., Li, J., Chen, Y., Yan, J., Yang, X., & Xu, M. (2013). CACTA-like transposable element in ZmCCT attenuated photoperiod sensitivity and accelerated the postdomestication spread of maize. *Proceedings of the National Academy of Sciences*, *110*(42), 16969–16974. https://doi.org/10.1073/pnas.1310949110

Yang, C., Yang, L., Zhou, M., Xie, H., Zhang, C., Wang, M. D., & Zhu, H. (2018). LncADeep: An ab initio lncRNA identification and functional annotation tool based on deep learning. *Bioinformatics*, *34*(22), 3825–3834. https://doi.org/10.1093/bioinformatics/bty428

Ye, Z., Sawada, M., Iwasa, M., Moriyama, R., Dey, D., Furutani, M., Kitao, M., Hara, T., Tanaka, A., Kishimoto, J., Yokono, M., Akimoto, S., Takabayashi, A., & Tanaka, R. (2024). Revisiting the early light-induced protein hypothesis in the sustained thermal dissipation mechanism in yew leaves. *Journal of Experimental Botany*, erae412. https://doi.org/10.1093/jxb/erae412

You, Y., Sawikowska, A., Neumann, M., Posé, D., Capovilla, G., Langenecker, T., Neher, R. A., Krajewski, P., & Schmid, M. (2017). Temporal dynamics of gene expression and histone marks at the Arabidopsis shoot meristem during flowering. *Nature Communications*, *8*(1), 15120. https://doi.org/10.1038/ncomms15120

Yue, W., Cai, K., Xia, X., Liu, L., & Wang, J. (2023). Genome-wide identification, expression pattern and genetic variation analysis of SWEET gene family in barley reveal the artificial selection of HvSWEET1a during domestication and improvement. *Frontiers in Plant Science*, *14*. https://doi.org/10.3389/fpls.2023.1137434

Zhang, G.-H., Xu, Q., Zhu, X.-D., Qian, Q., & Xue, H.-W. (2009). SHALLOT-LIKE1 Is a KANADI Transcription Factor That Modulates Rice Leaf Rolling by Regulating Leaf Abaxial Cell Development. *The Plant Cell*, *21*(3), 719. https://doi.org/10.1105/tpc.108.061457

Zhang, J., Liu, H., Sun, J., Li, B., Zhu, Q., Chen, S., & Zhang, H. (2012). Arabidopsis Fatty Acid Desaturase FAD2 Is Required for Salt Tolerance during Seed Germination and Early Seedling Growth. *PLOS ONE*, *7*(1), e30355. https://doi.org/10.1371/journal.pone.0030355

Zhang, H., Zhao, Y., & Zhu, J.-K. (2020). Thriving under Stress: How Plants Balance Growth and the Stress Response. *Developmental Cell*, *55*(5), 529–543. https://doi.org/10.1016/j.devcel.2020.10.012

Zhang, R.-G., Li, G.-Y., Wang, X.-L., Dainat, J., Wang, Z.-X., Ou, S., & Ma, Y. (2022). TEsorter: An accurate and fast method to classify LTR-retrotransposons in plant genomes. *Horticulture Research*, *9*, uhac017. https://doi.org/10.1093/hr/uhac017

Zhang, S., Huang, G., Zhang, Y., Lv, X., Wan, K., Liang, J., Feng, Y., Dao, J., Wu, S., Zhang, L., Yang, X., Lian, X., Huang, L., Shao, L., Zhang, J., Qin, S., Tao, D., Crews, T. E., Sacks, E. J., … Hu, F. (2023). Sustained productivity and agronomic potential of perennial rice. *Nature Sustainability*, *6*(1), 28–38. https://doi.org/10.1038/s41893-022-00997-3

Zheng, X., Chen, L., & Li, X. (2018). Arabidopsis and rice showed a distinct pattern in ZIPs genes expression profile in response to Cd stress. *Botanical Studies*, *59*(1), Article 1. https://doi.org/10.1186/s40529-018-0238-6

Zhuo, C., Cai, J., & Guo, Z. (2013). Overexpression of Early Light-Induced Protein (ELIP) Gene from Medicago sativa ssp. Falcata Increases Tolerance to Abiotic Stresses. *Agronomy Journal*, *105*(5), 1433–1440. https://doi.org/10.2134/agronj2013.0155

Zsögön, A., Čermák, T., Naves, E. R., Notini, M. M., Edel, K. H., Weinl, S., Freschi, L., Voytas, D. F., Kudla, J., & Peres, L. E. P. (2018). De novo domestication of wild tomato using genome editing. *Nature Biotechnology*, *36*(12), 1211–1216. https://doi.org/10.1038/nbt.4272

9. Abbreviations

RIN	RNA integrity number
RT	Room temperature
RPM	Rounds per minute
DAG	Days after germination
DPA	Days post anthesis
ONT	Oxford Nanopore Technologies
BSE	Bundle sheath extensions
ZT	Zeitgeber time
LTR	Long terminal repeats
EVE	Eveing
MOR	Morning
ANT	Anthers
CAR	Caryopses,10 days post anthesis
ESP	Developing spike W. 3-4.5
FLF	Flagleaf
GS3	Germinating seed, 3 days after germination
IND	3rd internode
LS8	Leaf/shoot, 8 days after germination
LSP	Developing spike W. 7-8
MSP	Developing spike W. 5-6.5
NOD	4th node
OVU	Ovules
RO8	Root, 8 days after germination
EDTA	The Extensive de novo TE Annotator
RWC	Relative water content
FC	Field capacity
HC	High-Confidence
LC	Low-Confidence
Mya	Million years
SLA	Specific leaf area
HMW	High molecular weight
Mbp	Million base pairs
ORF	Open reading frame
TTS	Transcription termination sites
TSS	Transcription start sites
CDS	Coding sequence
UTR	Untranslated region
TIR	Terminal inverted repeats
HOG	Phylogenetic hierarchical orthogroups
DEGs	Differentially expressed genes
DOT	Day of treatment
CPM	Counts per million
GSEA	Gene set enrichment analyses

ZIP	Zinc/iron transport family
LEA	Late embryogenesis abundant
CASP	Casparian strip membrane protein
FAD2	Fatty acid desaturase
ELIPs	Early light-inducible proteins
CWR	Crop wild relatives
SWEET	Sugars Will Eventually be Exported Transporters

10. Acknowledgments

Let me begin by expressing my gratitude to my supervisor Prof. Maria von Korff Schmising, for your continual support and belief in me reaching the final goal. You have allowed me to develop my academic and research skills, and you encouraged me to explore the broader scientific world through conferences and collaborations. I would also like to thank my second supervisor Prof. Peter Dörmann for your honest feedback and help in navigating the bureaucracy of academia.

I am extremely grateful to all my coworkers and the wonderful lab environment that is the Plant Genetics group. A very special thank you to Agatha, Gesa, Thea, Tianyu, and Michael, you been with me through this journey that is the PhD. Sincerely thank you all for all your scientific and humorous contributions during this time. To my lovely and wonderful Master's Crew, Dora, Pinelopi, Simge, and Vadim. For all the good time and the great times. With whom the Covid times would have been even worse, our Skype game and intellectual topic's sessions. To all my long time friends back home, Kristján, Helgi, Jón, Alexander, Guttormur, and Péter who have patiently waited for my return all these years. They welcome me always during my brief and infrequent visits like I had never left. To the close friends I have come to know while in Düsseldorf, Sonja, Benedetta, and Juliana. With whom I have great time with and a lot of walks and talks over the years and countless Meet-Up's, and have supported me through the rough times.

Finally, my heartfelt gratitude to my family who have supported me through the years on my academic journey.